



301 Mission St Perimeter Pile Upgrade

Calculations

Vol 2 – Design for Gravity Load

301 Mission Street
San Francisco, CA

1 November 2018

SGH Project 147041.10

SIMPSON GUMPERTZ & HEGER



Engineering of Structures
and Building Enclosures

PREPARED FOR:

Millennium Tower Association
301 Mission Street
Level B-1
San Francisco, CA 94103

PREPARED BY:

Simpson Gumpertz & Heger Inc.
100 Pine Street, Suite 1600
San Francisco, CA 94111
Tel: 415.495.3700
Fax: 415.495.3550

TABLE OF CONTENTS

1.	ANALYTICAL MODEL: PERFORM 3D	1
1.1	Model Description	1
1.1.1	Geometry	1
1.1.2	Gravity Loads	5
1.1.3	Modal Response	7
1.2	Capacity Calculations	9
1.2.1	Material Properties	10
1.2.2	Shear Walls	12
1.2.3	Reinforced Concrete Columns	21
1.2.4	Reinforced Concrete Beams	27
1.2.5	Pile Cap	31
1.2.6	Pile and Soil Springs	39
1.3	Loading	41
1.4	Substructure Results	42
1.4.1	Results for ENGEO Pile Properties	42
1.4.2	Results for Alternate Pile Properties	44
2.	ANALYTICAL MODEL: SAFE V2016	47
2.1	Description and Screenshots	47
2.1.1	SAFE Model	47
2.1.2	Mat Slab	52
2.1.3	Walls	58
2.1.4	Piles	59
2.1.5	Mesh and Analysis Options	69
2.2	Weight and Assigned Loads Summary	69
2.2.1	Load Combinations	69
2.2.2	Dead Load	70
2.2.3	Live Load	73
2.3	Design Strip Definitions	75
2.4	Nonlinear Immediate Cracked Analysis	77
2.5	Mat Slab Reinforcement Capacity	78
2.6	Analysis Results	80
2.6.1	Flexural Design Checks with ENGEO Spring Definitions	80
2.6.2	Analysis Results with Alternative Spring Definitions	89

1. ANALYTICAL MODEL: PERFORM 3D

We performed nonlinear analyses of the tower structure using the computer program Perform-3D V6.0.1, developed by Computers & Structures Incorporated of Berkeley, California. We constructed an analytical model of the structure, with nonlinear representation of the strength, stiffness, and ductility of the various elements. The properties of the structural elements in our model were based on data presented in ASCE 41-13 Seismic Rehabilitation of Structures. Details of the model properties are described in this section of our calculations, along with results under gravity loading (dead and live loads). Additional details and results for seismic loading are described in Volume 3.

1.1 Model Description

1.1.1 Geometry

Our Perform-3D nonlinear model includes mathematical representation of the tower reinforced concrete shear walls, outriggers and coupling beams, moment frame beams and columns, and the pile cap foundation. Figure 1-1 shows an isometric view of the model. Figure 1-2 and Figure 1-3 show elevations of the shear walls and moment frames, respectively. Figure 1-4 shows a plan view of the pile cap.

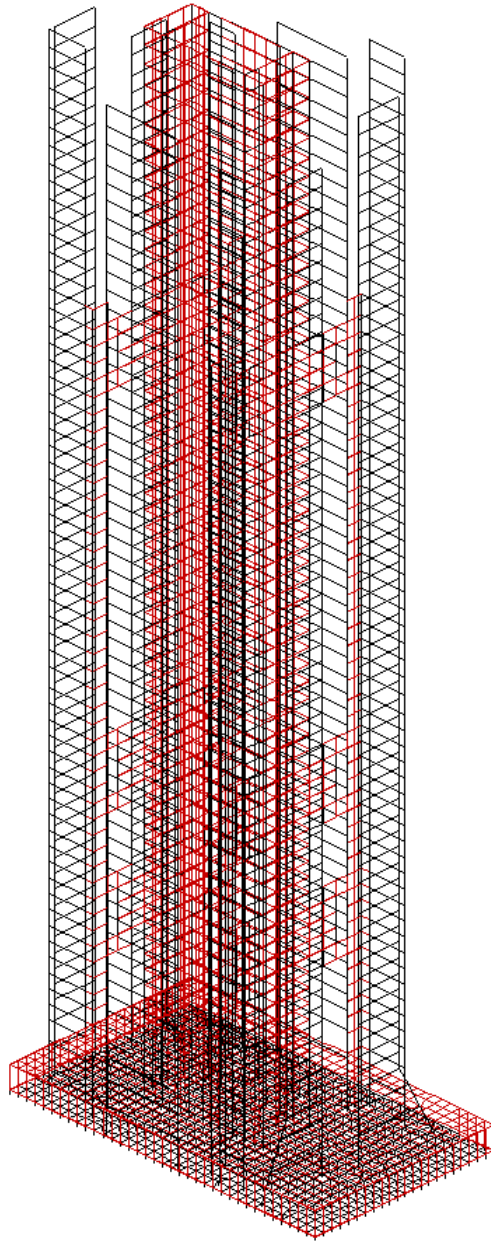


Figure 1-1 – Isometric View of Perform Model

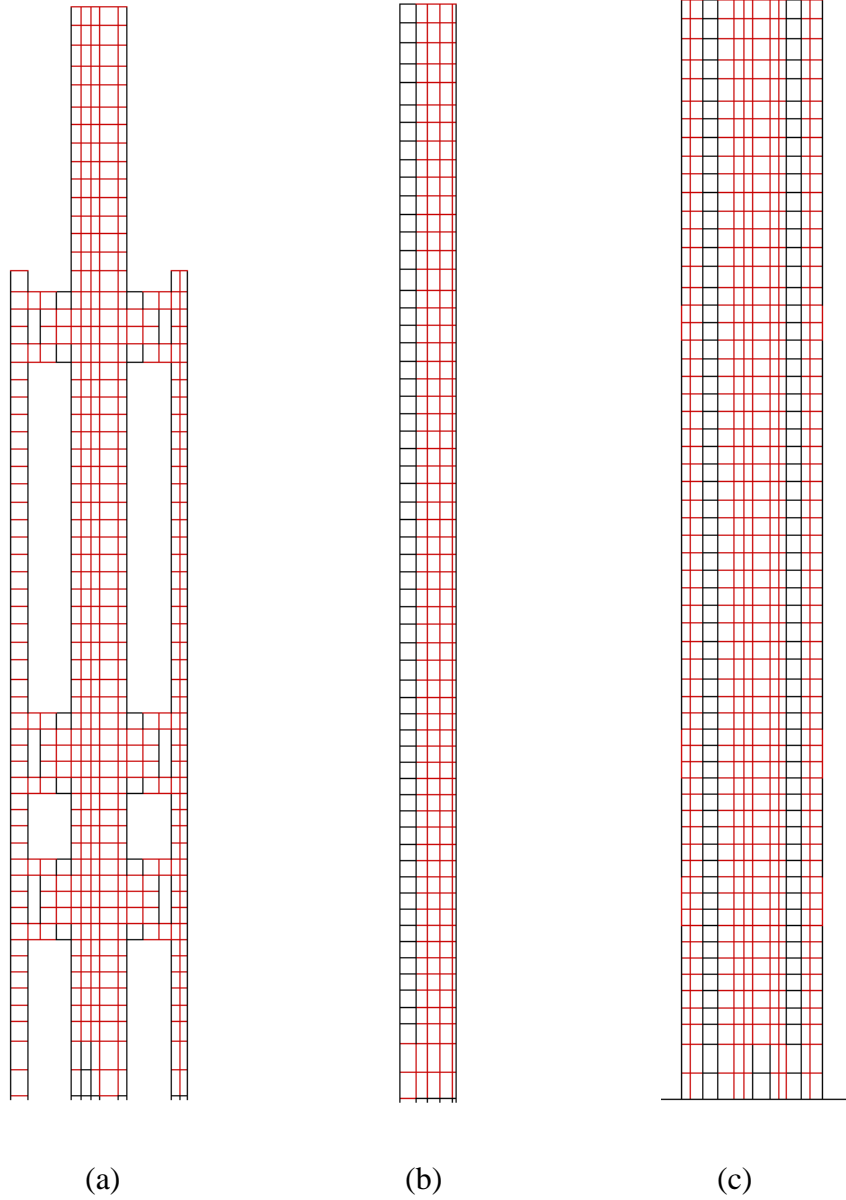


Figure 1-2 – Wall Elevations (a) Lines C, F; (b) Lines C.7, E.3; and (c) Lines 4, 9

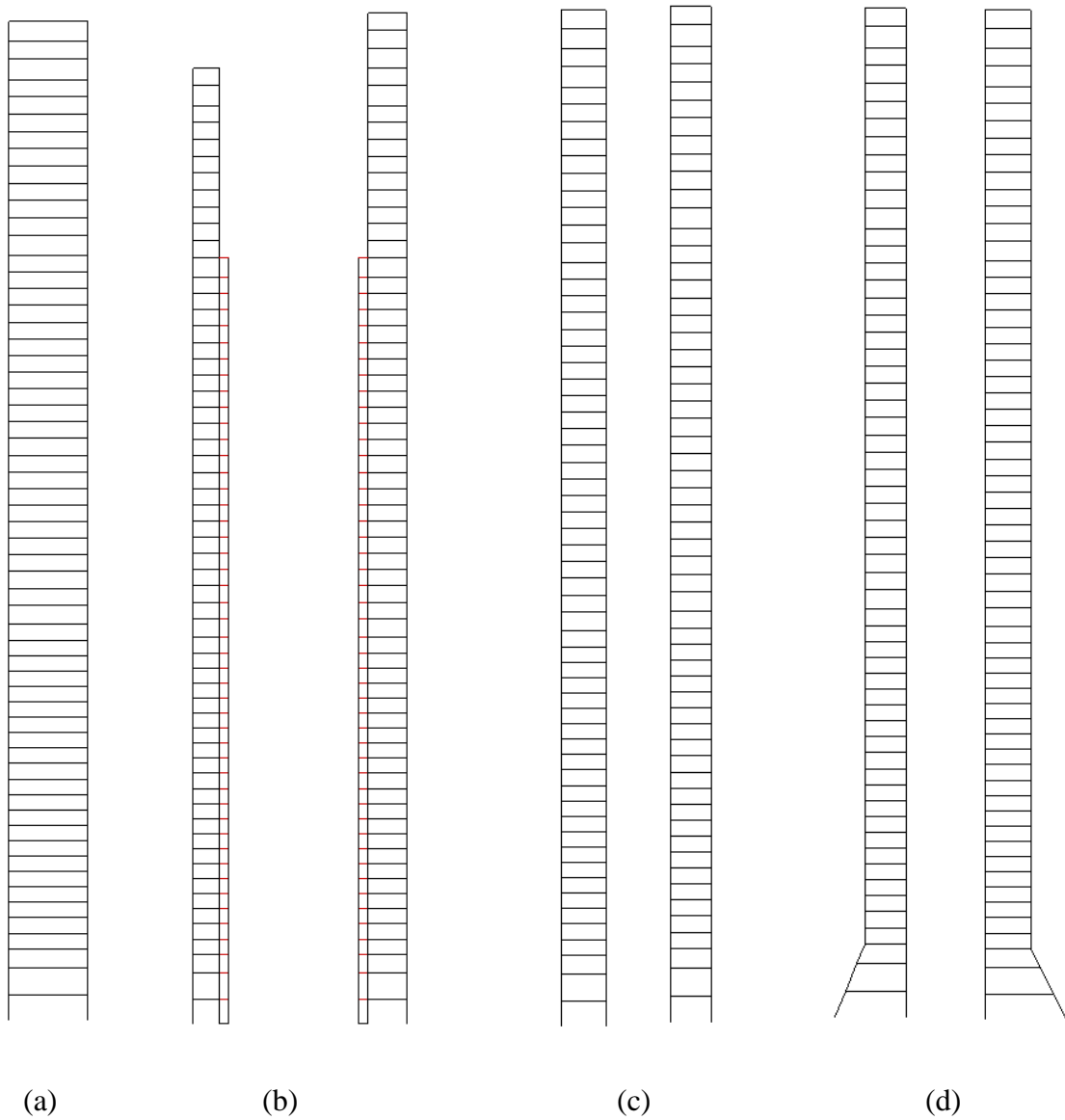


Figure 1-3 – Frames (a) Lines 1, 12; (b) Lines 2, 11; (c) Lines A, A.2; and (d) Lines G.8, H

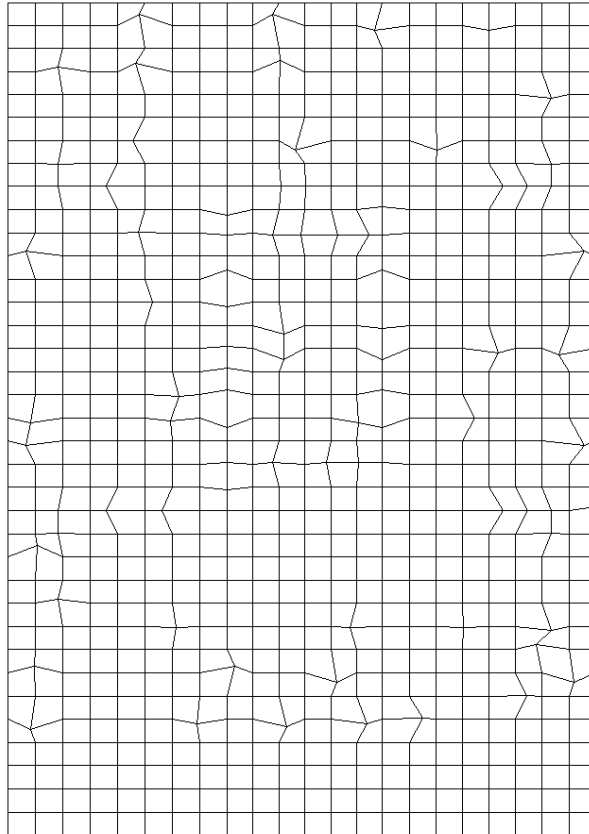


Figure 1-4 – Plan View of Pile Cap

1.1.2 Gravity Loads

The self-weight of the structural elements is calculated directly by the program. We used point and distributed floor loads for super-imposed dead loads and live load. Material unit weights and dead and live load pressures are detailed in description of the ETABS model in Volume 3. Figure 1-5 and Figure 1-6 show dead and live loads, respectively, in the columns and shear wall core at the base of the tower. We applied hydrostatic uplift pressure to the foundation based on a groundwater elevation of 3 feet below grade from the 2005 Treadwell & Rollo geotechnical report for the site.

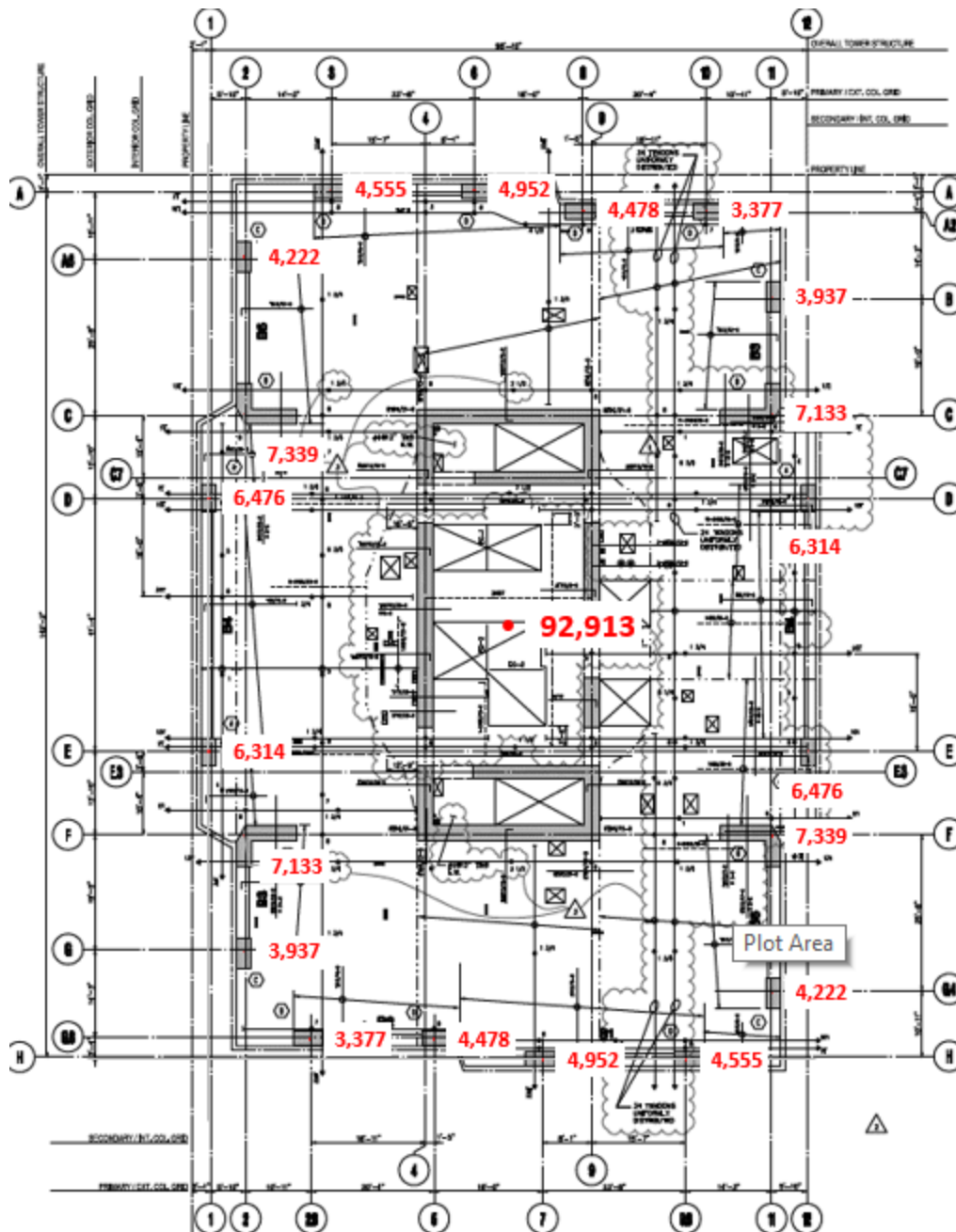


Figure 1-5 – Dead Load Distribution at Base of Tower

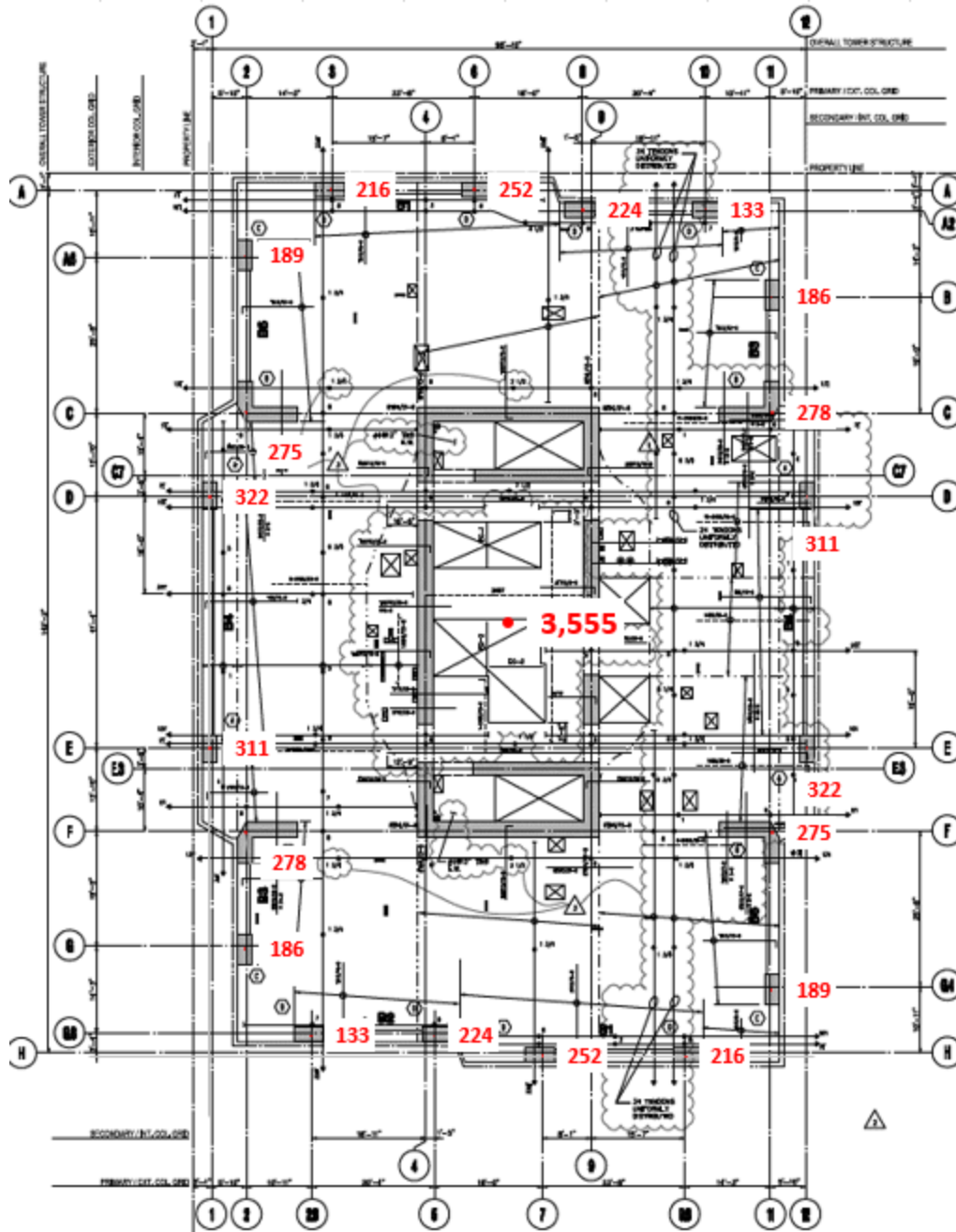
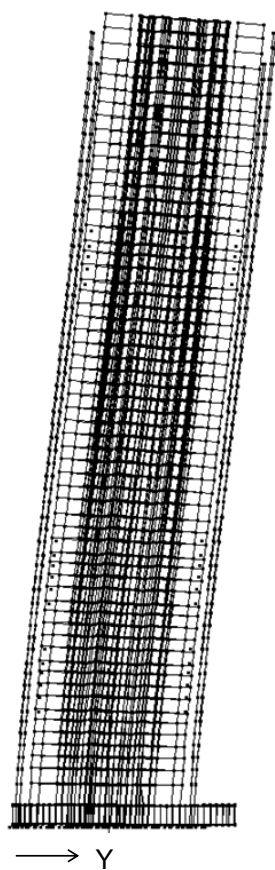


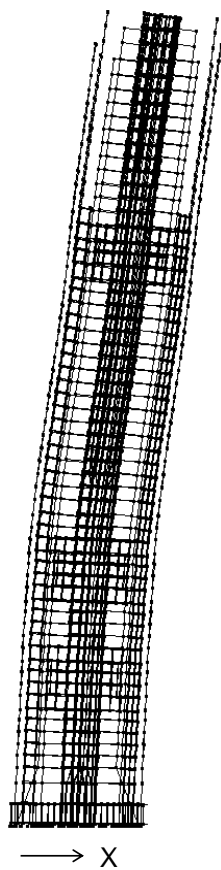
Figure 1-6 – Live Load Distribution at Base of Tower (LLF = 0.25)

1.1.3 Modal Response

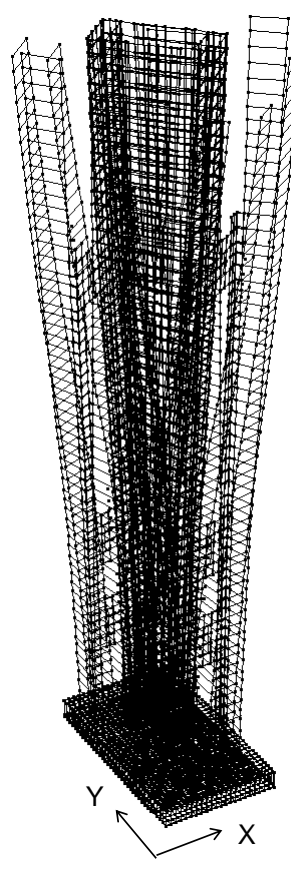
Figure 1-7 shows the first three modes of the structure. Table 1-1 details the period and mass participation for the first 50 modes.



Mode 1
T = 4.79s
Primary UY



Mode 2
T = 4.70s
Primary UX



Mode 3
T = 3.17s
Torsion

Figure 1-7 – First Three Modes

Table 1-1 – Modal Periods and Mass Participation

Mode	T (s)	UX	UY	Sum UX	Sum UY	Mode	T (s)	UX	UY	Sum UX	Sum UY
1	4.65	0.046	0.652	0.046	0.652	26	0.10	0.000	0.001	0.997	0.995
2	4.57	0.579	0.051	0.625	0.703	27	0.10	0.000	0.001	0.997	0.996
3	3.13	0.000	0.001	0.625	0.704	28	0.10	0.000	0.000	0.997	0.996
4	1.44	0.000	0.164	0.625	0.867	29	0.09	0.000	0.000	0.998	0.996
5	1.20	0.221	0.000	0.846	0.867	30	0.09	0.000	0.001	0.998	0.997
6	0.93	0.000	0.000	0.846	0.867	31	0.08	0.000	0.000	0.998	0.997
7	0.74	0.086	0.000	0.932	0.867	32	0.08	0.000	0.001	0.998	0.999
8	0.72	0.000	0.054	0.932	0.922	33	0.08	0.000	0.000	0.998	0.999
9	0.59	0.000	0.000	0.932	0.922	34	0.08	0.000	0.000	0.998	0.999
10	0.45	0.000	0.030	0.932	0.952	35	0.07	0.000	0.001	0.998	0.999
11	0.38	0.026	0.000	0.958	0.952	36	0.07	0.001	0.000	0.999	0.999
12	0.32	0.000	0.002	0.959	0.953	37	0.07	0.000	0.000	0.999	0.999
13	0.31	0.000	0.017	0.959	0.970	38	0.06	0.000	0.000	0.999	1.000
14	0.28	0.018	0.000	0.976	0.970	39	0.06	0.000	0.000	1.000	1.000
15	0.24	0.000	0.004	0.976	0.974	40	0.06	0.000	0.000	1.000	1.000
16	0.23	0.000	0.008	0.976	0.982	41	0.06	0.000	0.000	1.000	1.000
17	0.20	0.007	0.000	0.983	0.982	42	0.06	0.000	0.000	1.000	1.000
18	0.18	0.000	0.005	0.983	0.987	43	0.06	0.000	0.000	1.000	1.000
19	0.18	0.000	0.002	0.983	0.989	44	0.06	0.000	0.000	1.000	1.000
20	0.15	0.006	0.000	0.989	0.989	45	0.05	0.000	0.000	1.000	1.000
21	0.15	0.000	0.004	0.989	0.993	46	0.05	0.000	0.000	1.000	1.000
22	0.14	0.000	0.000	0.989	0.993	47	0.05	0.000	0.000	1.000	1.000
23	0.13	0.008	0.000	0.996	0.993	48	0.05	0.000	0.000	1.000	1.000
24	0.12	0.000	0.002	0.996	0.994	49	0.05	0.000	0.000	1.000	1.000
25	0.11	0.001	0.000	0.997	0.994	50	0.05	0.000	0.000	1.000	1.000

1.2 Capacity Calculations

We modeled the following elements as nonlinear:

- Shear walls at all levels and gridlines (flexure).
- Outrigger coupling beams (shear behavior).
- Reinforced concrete columns at all levels and gridlines (P-M-M hinge).
- Reinforced concrete beams at all levels and gridlines (flexural hinge).
- Embedded steel beams at all levels and gridlines (shear hinge).
- Concrete pile cap modeled as a grillage of beams (flexure and shear hinges).
- Vertical soil springs (axial compression).

We modeled all other elements with linear properties.

Details of the properties and capacities used for each element are provided in the following sections.

1.2.1 Material Properties

All capacities are calculated using expected material properties, rather than design minimum specifications, to best estimate performance of the structure. Expected material properties are shown in Table 1-2.

Table 1-2 – Expected Material Strengths

Element	Nominal	Expected
Existing Mat Foundation		
Concrete f'_c	7,000 psi ¹	9,100 psi
Reinforcing f_y	75 ksi	82 ksi
Shear Walls, Outriggers		
Concrete f'_c	7,000 psi – 10,000 psi	9,100 psi – 13,000 psi
Reinforcing f_y	60 ksi / 75 ksi	69 ksi / 82 ksi
Moment Frame Beams and Columns		
Concrete f'_c	7,000 psi – 10,000 psi	9,100 psi – 13,000 psi
Reinforcing f_y	60 ksi / 75 ksi	69 ksi / 82 ksi
Existing Piles		
Concrete f'_c	7,000 psi	9,100 psi
Reinforcing f_y	60 ksi	70 ksi

¹Calculated based on results from concrete breaks and the provisions of ACI 301-16.

We defined confined concrete materials using the Inelastic 1D Concrete Material with a trilinear curve, strength loss, no tension capacity (zero stiffness and strength), and no cyclic degradation.

We defined reinforcing steel materials using the Inelastic Steel Material, Non-Buckling with different tensile and compressive trilinear curves, strength loss, and no cyclic degradation. We assumed that relatively low residual strength would result from compressive buckling reinforcing steel, while tension strength would not degrade significantly until rebar fracture occurs.

Figure 1-8 and Figure 1-9 show the implementation of the concrete and steel material properties in the model.

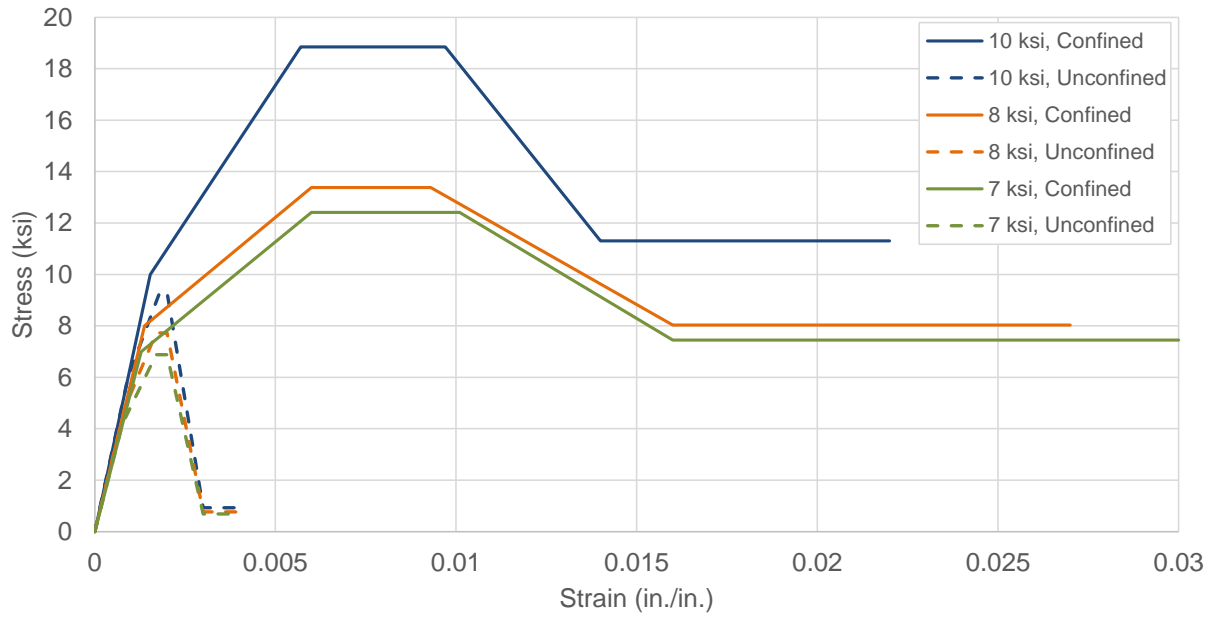


Figure 1-8 – Modeled Concrete Material Properties

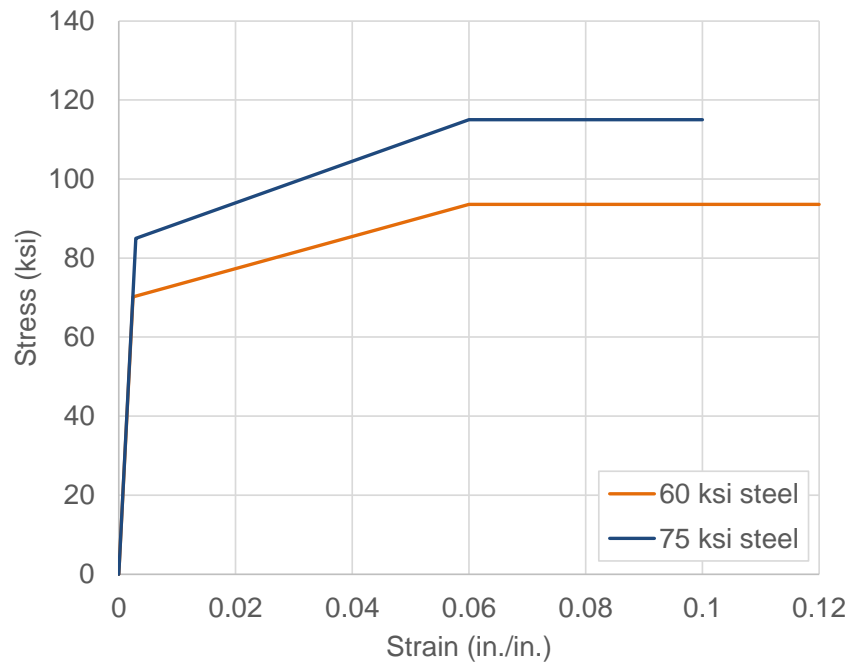


Figure 1-9 – Modeled Steel Material Properties

1.2.2 Shear Walls

We modeled the shear walls as planar sections of wall discretized vertically using a single element per story throughout the entire building height. We discretized the walls horizontally into several elements depending on the wall geometric configuration and discontinuities along the building height, as well as intersecting walls and beams. We generally limited the aspect ratio of the wall elements (in either horizontal or vertical directions) to 1:5. We defined the behavior of shear walls using a compound element which included elastic shear material behavior and a nonlinear fiber model for simulation of wall flexure-axial interaction. We included the self-weight of all walls for mass computation using a concrete density of 150 pcf.

1.2.2.1 In-Plane Shear

We modeled shear behavior as a force-controlled action in accordance with the assumptions listed in our design criteria.

Figure 1-10 shows the locations of shear walls 1-4. Wall E refers to the outrigger columns. Figure 1-11 shows a sample layout of steel reinforcement ratios and shear capacities for Wall 2 between Level 8 and Level 20. A sample shear capacity calculation is provided for the same wall. Appendix A shows reinforcement ratios and shear capacities for all walls.

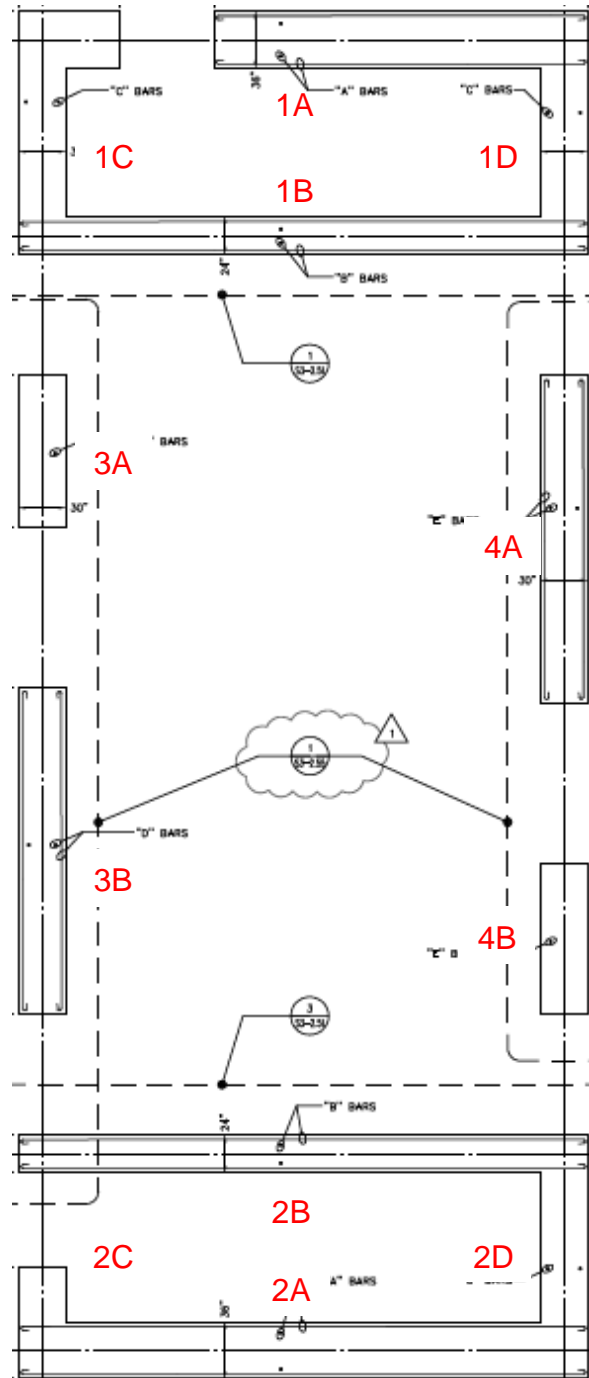


Figure 1-10 – Shear Wall Locations

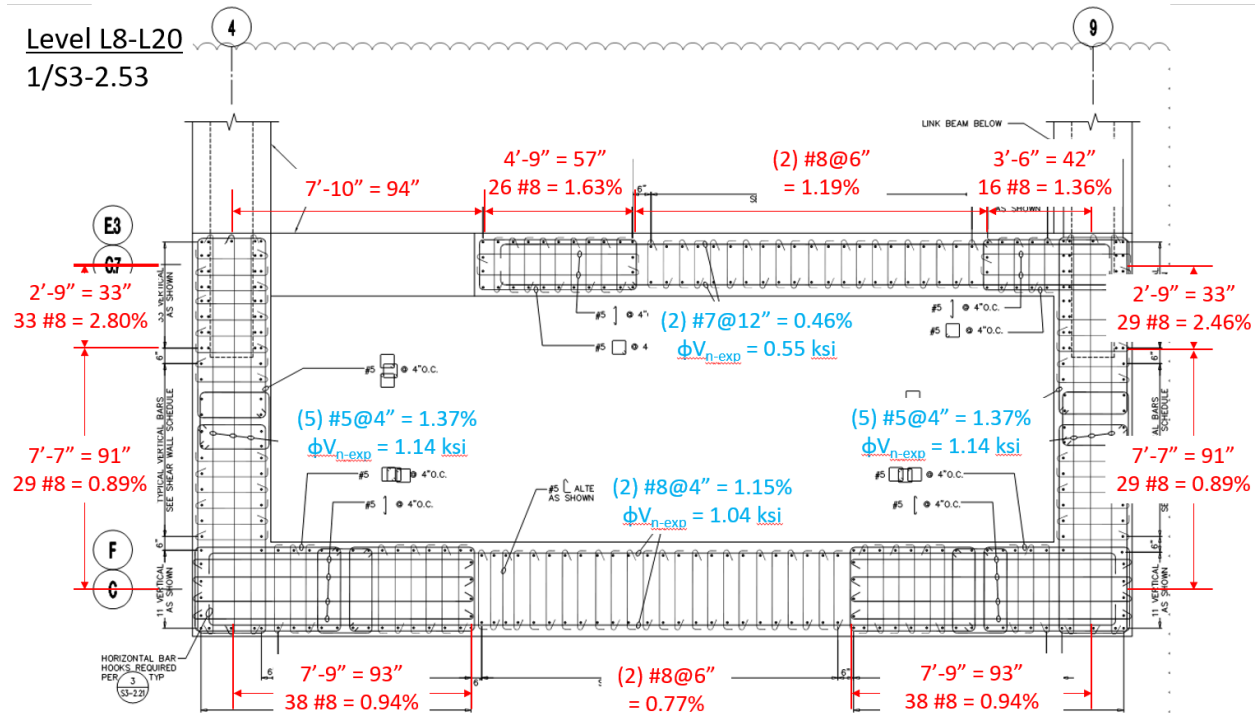


Figure 1-11 – Sample Reinforcement Ratios and Shear Capacities (Wall 2, Levels 8-20)

Expected Shear Capacity of Wall 2A, Level 8-20

Wall thickness $t_w := 34 \text{ in}$

Expected concrete strength $f_c := 13 \text{ ksi}$

Expected rebar strength $f_y := 70.2 \text{ ksi}$

Area of steel $A_s := \frac{2 \cdot 0.79 \text{ in}^2}{4 \text{ in}} = 0.395 \frac{\text{in}^2}{\text{in}}$ 2 layers #8@4

Steel reinforcement ratio $\rho_t := \frac{A_s}{t_w} = 1.162 \%$

Dimensional coefficient $\alpha_c := 2$ $hw/lw > 2$

Expected shear capacity $V_n := \min \left(\alpha_c \cdot \sqrt{\frac{f_c}{\text{psi}}} \cdot \text{psi} + \rho_t \cdot f_y, 10 \cdot \sqrt{\frac{f_c}{\text{psi}}} \cdot \text{psi} \right) = 1.044 \text{ ksi}$

1.2.2.2 Axial-Flexure Interaction

We used nonlinear fiber models to account for axial and flexural effects. Each fiber model includes eight fibers of reinforcing steel and confined concrete with expected material behavior. We specified the vertical reinforcement ratio in the walls based on the original design drawings. Figure 11 shows a sample layout of steel reinforcement ratios for Wall 2 between Level 8 and Level 20. Appendix A shows reinforcement ratios for all walls.

In the out-of-plane direction, the shear walls remain elastic under flexure. We adjusted the concrete modulus by a factor of 0.25 to account for out-of-plane flexural cracking of the shear walls.

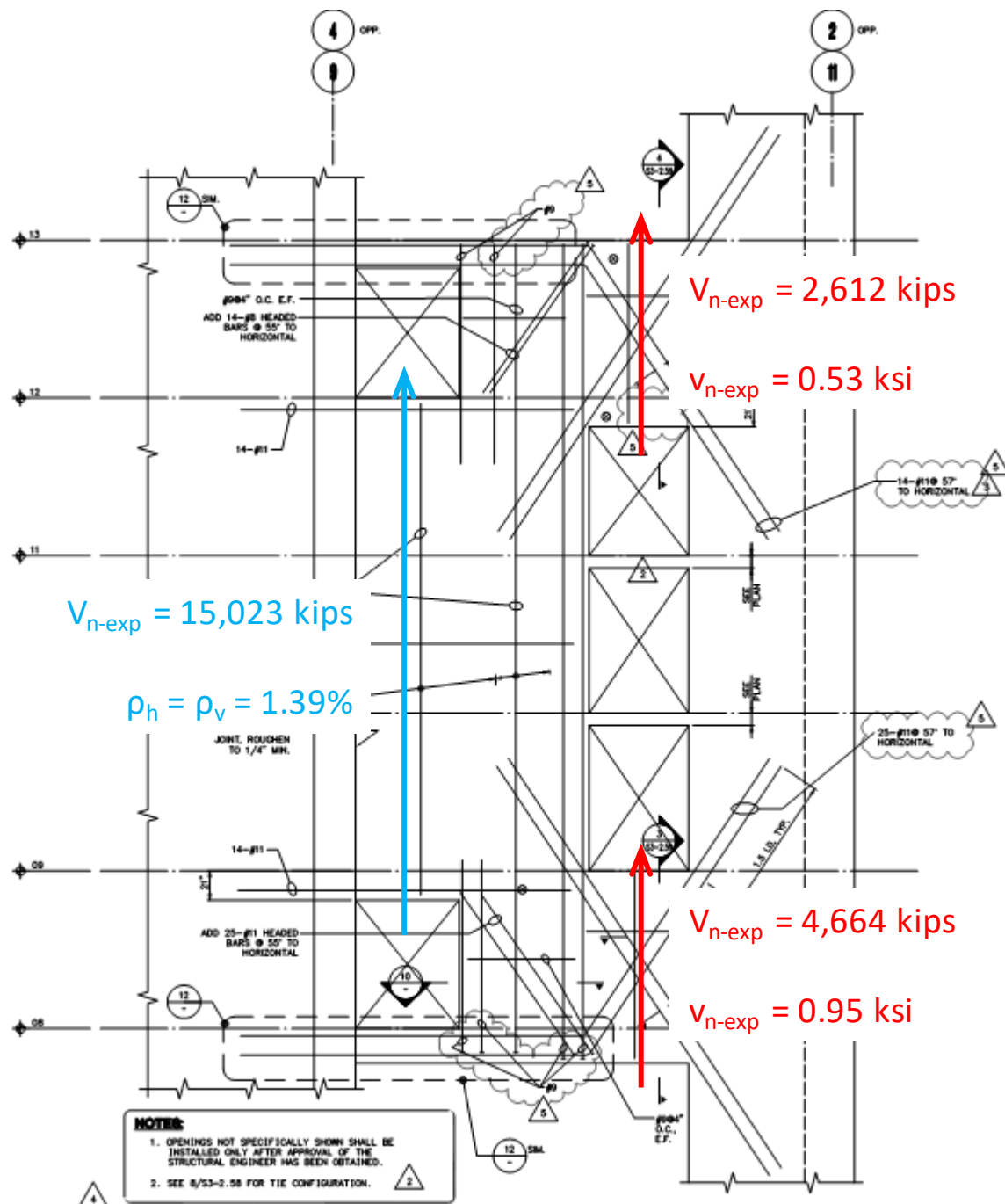
1.2.2.3 Outrigger Coupling Beams

We modeled the outrigger coupling beams on gridlines C and F as shear wall elements with inelastic axial/flexural behavior. We used the same modeling approach for the axial/flexural fiber model of the outrigger coupling beams as the shear walls. We similarly used the Perform Wall Inelastic Shear Material to model the shear backbone curve using a trilinear relationship, strength loss, and no cyclic degradation. However, we modified the shear stress, strain parameters and limit states for these coupling beams to account for the diagonal reinforcement present.

We defined the initial shear stiffness of the coupling beams using a cracked effective stiffness of 0.5 times the shear modulus of the concrete material. We estimated the ultimate shear strength as the added strength due to diagonal reinforcement, shear wall vertical reinforcement, and concrete contribution, not to exceed a limiting shear strength for shear walls of $10\sqrt{f'_c}A_{cv}$. Figure 1-12, Figure 1-13, Figure 1-14 show the calculated shear capacities of the coupling beams. The diagonally-reinforced links on the outrigger side of the beams act as fuses and control the capacity. A sample capacity calculation is shown for Level 12.

The outrigger beams include a degrading hysteretic model based on physical testing by Canbolat et al. The cyclic backbone for this model maintains elastic-perfectly-plastic behavior through a shear deformation of 2% then degrades to a residual strength equal to 25% of the yield strength at a shear deformation of 4%. The model retains this residual displacement through shear

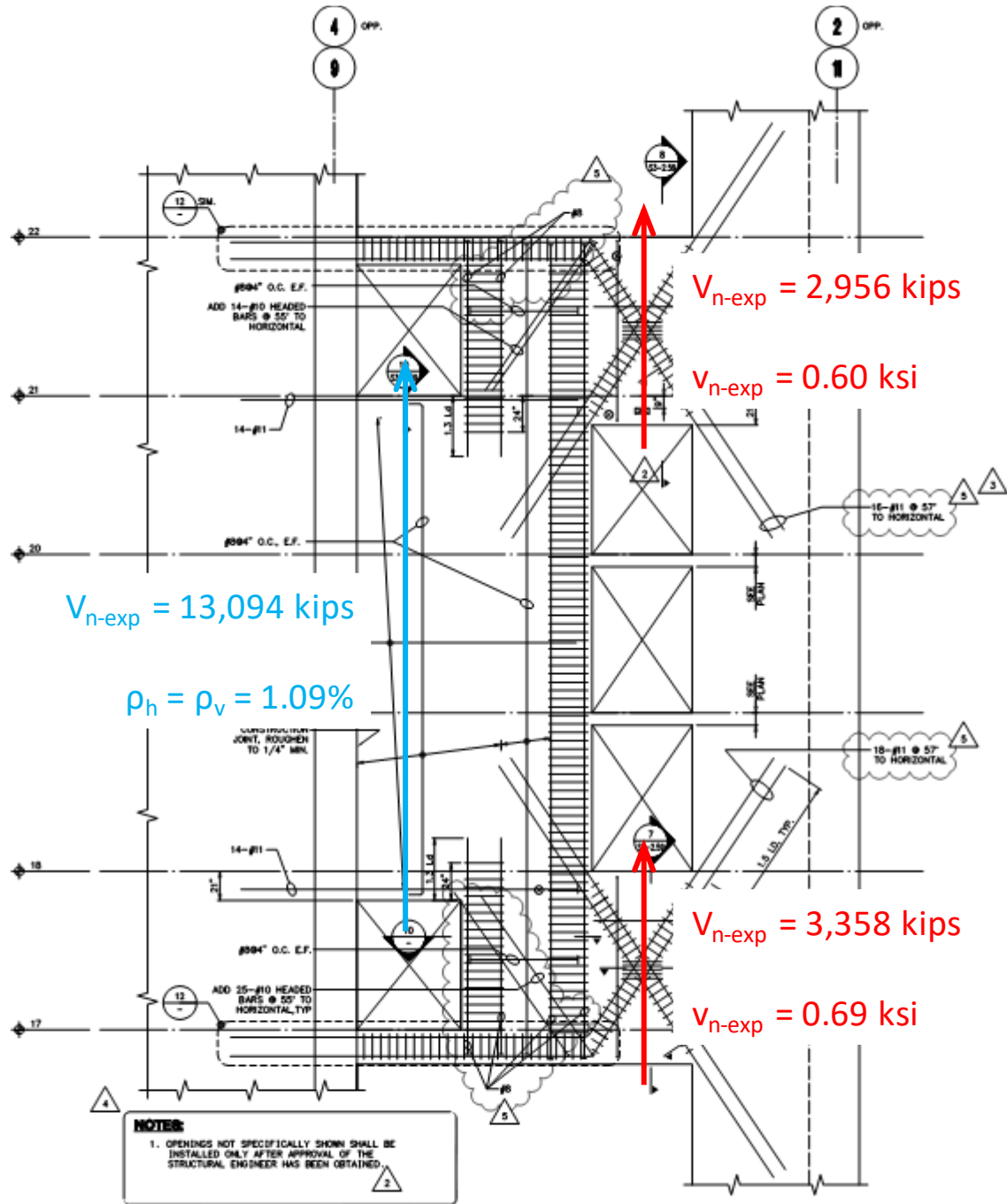
deformation of 6%, after which it has nil residual strength. Figure 1-15 shows the modeled hysteretic behavior of the outrigger coupling beam in red, over the test results in black.



6 OUTRIGGER ELEVATION - LEVEL 06 THROUGH 13

SCALE: 1/4"=1'-0"

Figure 1-12 – Outrigger Coupling Beam Expected Shear Capacity, L8-L13



8 OUTRIGGER ELEVATION - LEVEL 17 THROUGH 22
SCALE: 1/4"=1'-0"

Figure 1-13 – Outrigger Coupling Beam Expected Shear Capacity, L17-L22

Expected Shear Capacity of Outrigger Coupling Beam at Level 12

Coupling Beam Geometry

Length (L_n) =	72 in
Height (h) =	136 in
Width (b_w) =	36 in
CLR Cover H =	1.5 in
CLR Cover V =	1.5 in
CCT =	4.0 in

1.5 in Minimum
1.5 in Minimum

Coupling Beam Properties

Concrete Strength (f'_c) =	13,000 psi
Rebar Strength (f_y) =	70,200 psi

Not all horizontal rebar shown for clarity

Coupling Beam Forces

$V_{u,Analysed}$ =	5,574 kips
M_{uL} =	100 kip-ft
M_{uR} =	100 kip-ft
V_u =	5,574 kips
M_u =	100 kip-in

Requirement of Coupling Beam

L_n/h =	0.53	May require Diagonal Reinforcement
		ACI 318-11 sec. 21.9.7.1 & 21.9.7.2
$4\sqrt{f'_c}A_{cw}$ =	2,233	Diagonal Reinforcement Required
		ACI 318-11 sec. 21.9.7.2

Shear Strength $\phi V_n = \phi(2A_{vt} f_y \sin \alpha \leq 10\sqrt{f'_c} A_{cw})$ (eq. 21-9)

ϕ =	1.00
α =	1.02 radians
	58.4 degrees
$A_{vt \text{ required}}$ =	46.6 total in ²

Diagonal Longitudinal Reinforcement

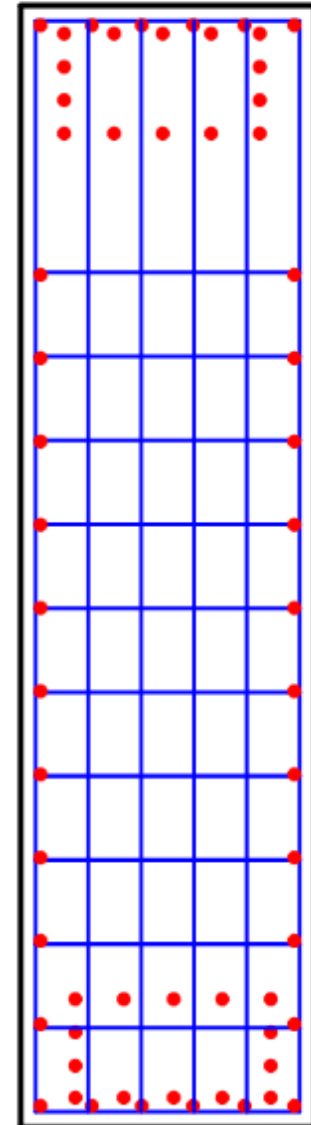
n_{column} =	5 bars	Max. $n = 5$
$s_{diag,h}$ =	6 in	Min. $n = 2$ (2 top and 2 bottom)
n_{add} =	0 bars	OK
$s_{diag,v}$ =	4 in	0 = no fill or 1 = fill
$n_{add \text{ rows}}$ =	2 rows	OK
CCD =	0.00 in	Add Spacing
Bar Size	#11	
$d_{diagonal}$ =	1.41 in	2812.02187
$A_{diagonal}$ =	1.56 in ² /bar	3565.02303
Total n_{bars} =	14	
A_{vt} =	21.8 in ²	$Wt_{st} = 3100 \text{ lbs}$
V_n =	2812.0 kips	$P_{DIAGONAL} \% = 0.89\%$
ϕV_n =	2812.0 kips	ACI 318-11 sec. 21.9.7.4 (a)
DCR =	2.13	NO

Full Section Transverse Reinforcement (Vertical)

n_{legs} =	6	Min. $n = 2$ (1 left & 1 right)
s_{leg} =	5 in	Max. $s = 8$
Bar Size	#5	
$d_{stirrup}$ =	0.6 in	
$A_{stirrup}$ =	0.31 in ² /bar	

Full Section Transverse Reinforcement (Horizontal)

n_{legs} =	14	Min. $n = 2$ (1 left & 1 right)
s_{leg} =	5 in	Max. $s = 8$
Bar Size	#5	
$d_{stirrup}$ =	0.6 in	
$A_{stirrup}$ =	0.31 in ² /bar	$Wt_{transv} = 1777 \text{ lbs}$



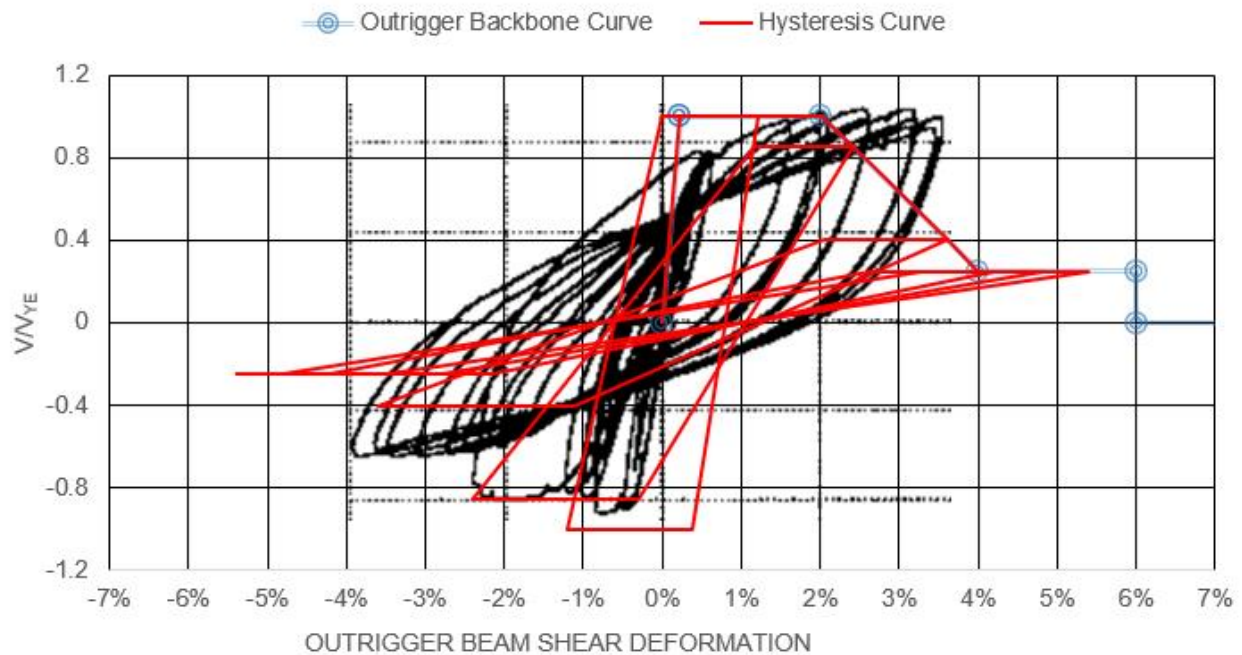


Figure 1-15 – Degrading Hysteretic Model for Outrigger Coupling Beams

1.2.2.4 Embedded Steel Coupling Beams

We modeled the embedded steel coupling beams spanning core shear wall segments in the Tower’s longitudinal direction on gridlines 4 and 9 as nonlinear shear-controlled beams. We confirmed this behavior through preliminary analysis results. We used the Shear Hinge, Displacement Type element in Perform and assigned it to the beam mid-span. Outside the shear hinge, we used a steel beam cross section per structural drawings with elastic material properties and a reduction factor of 0.6 applied to the strong-axis bending inertia. We modeled embedded beams with zero mass and increased flexural stiffness in the model to simulate the continuity of coupling beams at wall supports.

We matched the coupling beam nonlinear shear behavior, including element stiffness, yield, and degradation characteristics, to coupling beam testing performed by Dr. John Wallace at UCLA. We defined the limiting shear hinge displacement corresponding to the Collapse Prevention level as the shear displacement at initiation of strength loss, between 2.6% and 3.0% depending on the beam aspect ratio. Test results indicate that beams can maintain a significant portion of their strength under rotations on the order of 7% to 13%.

Figure 1-16 shows the shear hinge force-displacement relationships used for the different steel coupling beams in the tower.

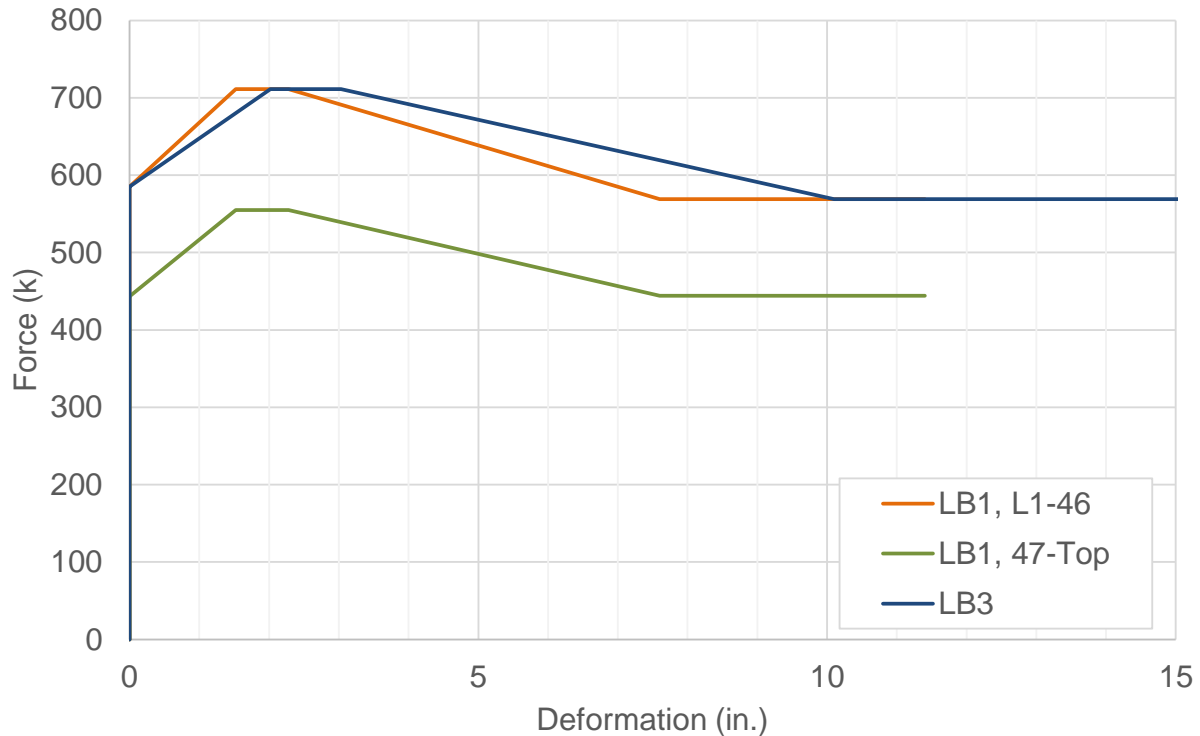


Figure 1-16 – Shear Hinge Model for Steel Coupling Beams

1.2.3 Reinforced Concrete Columns

We modeled the reinforced concrete moment frame columns using the FEMA Columns, Concrete Type with symmetric elastic-perfectly-plastic behavior, strength loss, deformation capacities, and no cyclic degradation. We defined flexural plastic hinges at both ends of the columns, assuming an inflection point at mid-span. We used Table 10-8 of ASCE 41-13 to define the parameters of the nonlinear hinge model considering ACI 318-14 conforming details with 135 deg hooks, high axial and shear demands as computed in preliminary analysis results, and high transverse reinforcement ratio as shown in structural drawings.

For each column type we determined if the behavior is shear-controlled or flexural-controlled by comparing the plastic shear capacity (i.e. shear demand at flexural yielding of plastic hinges) to the nominal shear capacity based on transverse reinforcement detailing. At lower levels, due to relatively high longitudinal reinforcement ratios, columns were determined to be shear-controlled (condition iii).

We used the program spColumn v6.00 to determine the flexural capacity and axial load - moment interaction diagram for each column in the weak- and strong-axis directions.

We used effective cross section properties to define the elastic behavior of the columns by applying a 0.5 multiplier to the strong-and weak-axis bending inertias of each column, and a 0.7 multiplier to the axial area to account for expected cracking at the bottom 20 stories. Above the 20th-story we applied a 0.6 multiplier to the axial area.

The resulting ASCE 41-13 Table 10-8 parameters defining the nonlinear behavior of these column hinges are $a=0\%$ rad, $b=0.8\%$ rad, $c=0\%$ corresponding in Perform to DL, DX, and FR/FU, respectively.

Figure 1-17 shows column locations in plan. Figure 1-18, Figure 1-19, and Figure 1-20 show sample P-M interaction diagrams, moment-rotation curves, and axial-shear curves for D Columns from Levels 3 to 14. Sample calculations for the backbone curves are provided. Table 1-3 details equivalent key parameters for all columns.

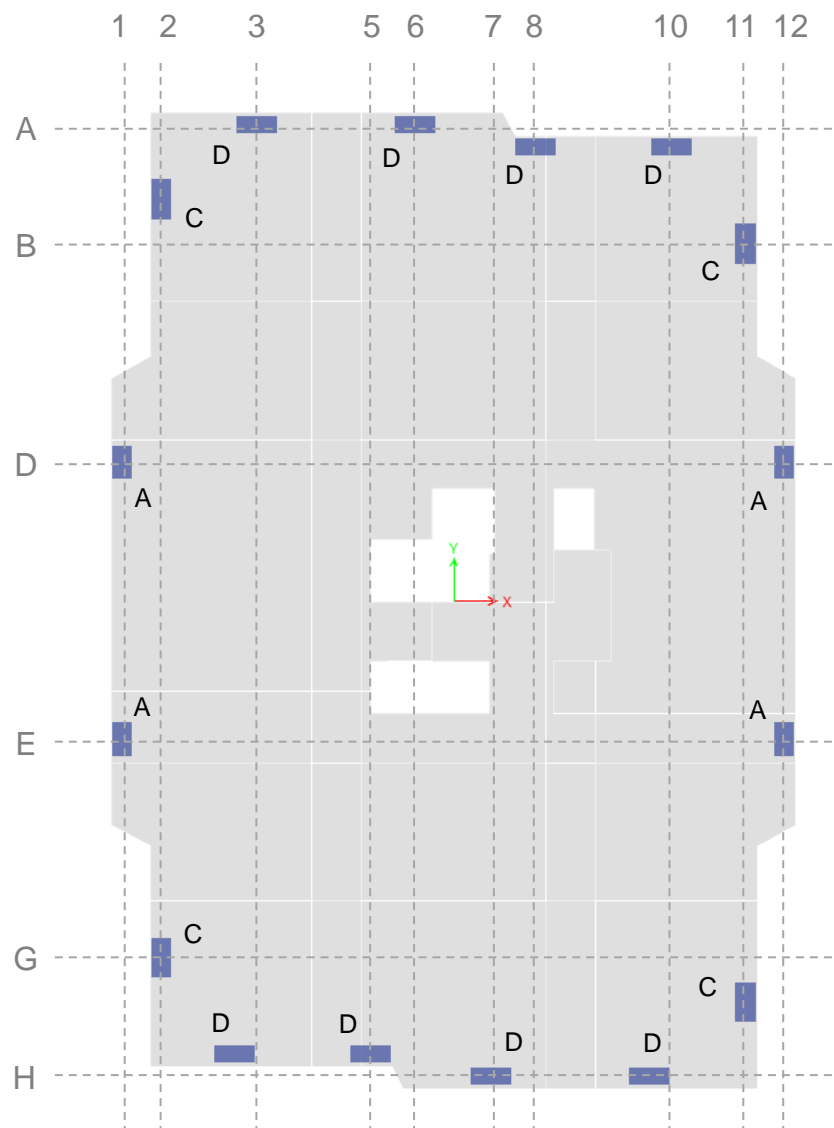


Figure 1-17 – Column Labels

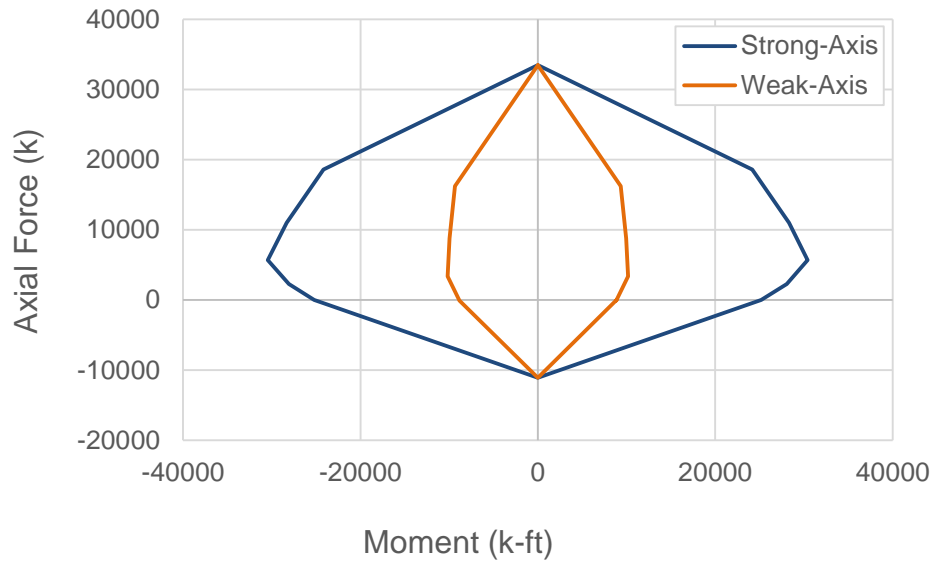


Figure 1-18 – PM Interaction (Yield Surface) Curves for D Columns from L3-14

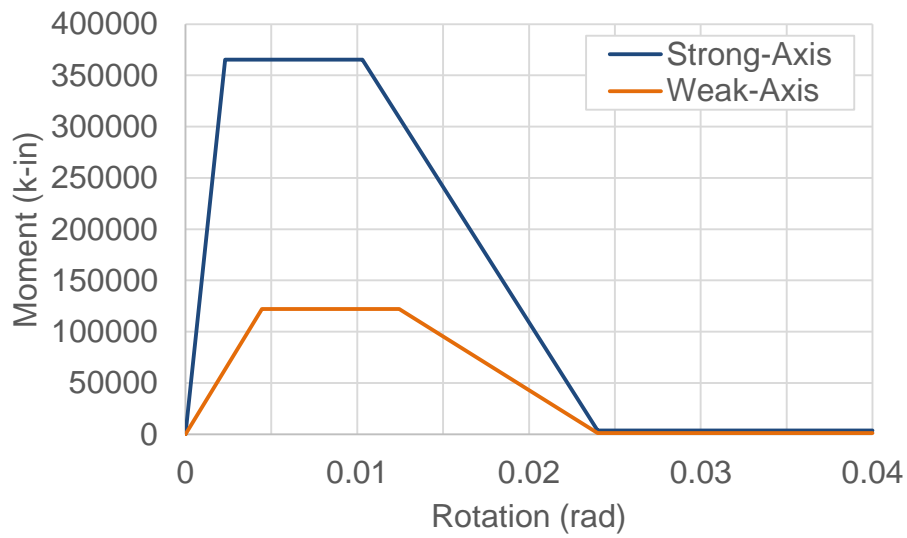


Figure 1-19 – Moment-Rotation Curves for D Columns from L3-14

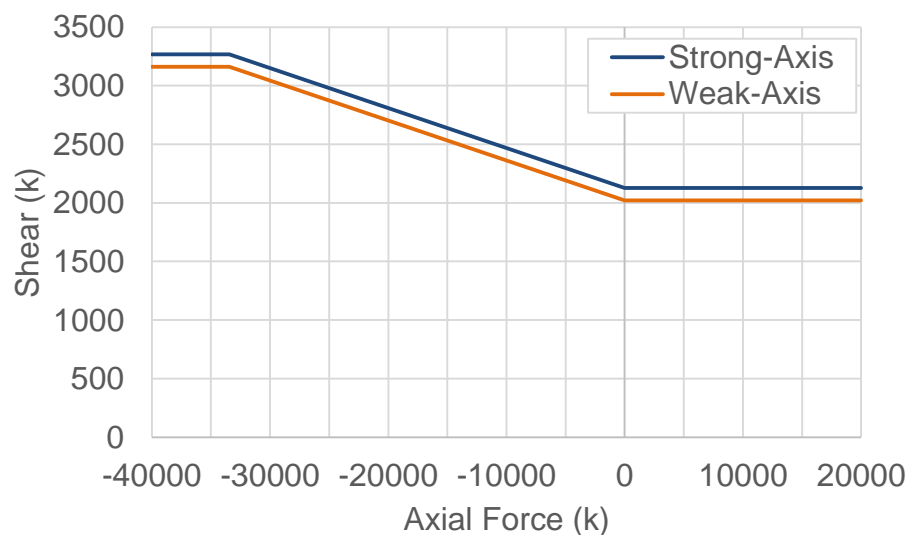


Figure 1-20 – Axial-Shear Curves for D Columns from L3-14

Flexural Backbone Curve for D Columns from L3-14

Elastic modulus $E := 57000 \sqrt{13 \frac{\text{ksi}}{\text{psi}}} \cdot \text{psi} = 6499 \text{ ksi}$

Column width $b := 30 \text{ in}$

Column depth $h := 72 \text{ in}$

Flexural cracking modification factor $f_b := 0.5$

Effective moment of inertia $I_{cr} := \frac{f_b}{12} \cdot b \cdot h^3 = 4.666 \times 10^5 \text{ in}^4$

Column length $L := 115 \text{ in}$

Flexural stiffness $k_f := \frac{6 \cdot E \cdot I_{cr}}{L} = 1.582 \times 10^8 \text{ kip} \cdot \text{in}$

Plastic rotation at strength loss $a := 0.008$ ASCE 41-13 Table 10-8

Moment capacity $M_{ne} := 30433 \text{ kip} \cdot \text{ft}$ spColumn

Rotation at yield $\theta_y := \frac{M_{ne}}{k_f} = 2.308 \times 10^{-3}$

Rotation at strength loss $\theta_{sl} := \theta_y + a = 0.01$

Shear Backbone Curve for D Columns from L3-14

Compression capacity $P_c := 33438 \text{ kip}$ spColumn

Tension capacity $P_t := 11056 \text{ kip}$ spColumn

Column width $b := 30 \text{ in}$

Column height $h := 72 \text{ in}$

Column depth $d := 67.3 \text{ in}$

Concrete strength $f_c := 13 \text{ ksi}$

Steel yield $f_y := 87.75 \text{ ksi}$

Shear reinforcement bar area $A_s := .31 \text{ in}^2$

Number of stirrups $n_l := 4$

Stirrup spacing $s := 4 \text{ in}$

Ratio of moment to shear $r_{mv} := 4$ conservative value

$$V_c := \frac{A_s \cdot f_y \cdot n_l \cdot d}{s} + 6 \cdot \sqrt{\frac{f_c}{\text{psi}}} \cdot \text{psi} \cdot \frac{0.8 \cdot b \cdot h}{r_{mv}} \cdot \sqrt{1 + \frac{P_c}{6 \cdot \sqrt{\frac{f_c}{\text{psi}}} \cdot \text{psi} \cdot b \cdot h}}$$

$$V_c = 3.267 \times 10^3 \cdot \text{kip}$$

$$V_t := \frac{A_s \cdot f_y \cdot n_l \cdot d}{s} + 6 \cdot \sqrt{\frac{f_c}{\text{psi}}} \cdot \text{psi} \cdot \frac{0.8 \cdot b \cdot h}{r_{mv}} \cdot \sqrt{1 + \frac{\max(-P_t, 0)}{6 \cdot \sqrt{\frac{f_c}{\text{psi}}} \cdot \text{psi} \cdot b \cdot h}}$$

$$V_t = 2.126 \times 10^3 \cdot \text{kip}$$

Table 1-3 – Column Capacities

Column	Max Moment (k-ft)	Max Comp (k)	Max Tension (k)	Shear at Max Comp (k)	Shear at Max Tension (k)
ColA_LB1-4	20,477	28,607	5,476	3,230	2,192
ColA_L4-14	19,204	27,726	4,458	3,217	2,199
ColA_L14-20	12,607	20,988	3,566	2,349	1,581
ColA_L20-30	10,993	17,497	3,566	2,216	1,558
ColA_L30-40	7,730	14,762	2,282	1,944	1,378
ColA_L40-47	5,478	10,496	1,755	1,467	1,056
ColA_L47-Top	3,293	8,268	1,755	1,096	779
ColB_L47-Top	3,293	8,268	1,755	1,096	779
ColC_LB1-4	31,656	36,224	8,761	3,946	2,659
ColC_L4-14	30,102	34,329	6,571	3,904	2,659
ColC_L14-20	15,254	22,977	3,566	2,614	1,769
ColC_L20-30	13,245	19,088	3,566	2,466	1,743
ColC_L30-40	7,730	14,762	2,282	1,944	1,378
ColC_L40-47	5,478	10,496	1,755	1,467	1,056
ColC_L47-Top	3,293	8,268	1,755	1,096	779
ColD_LB1-3	36,859	39,578	12,636	4,002	2,644
ColD_L3-14	30,433	33,438	11,057	3,268	2,127
ColD_L14-20	21,348	27,751	9,082	2,700	1,752
ColD_L20-30	19,454	24,002	9,082	2,557	1,726
ColD_L30-40	11,588	18,357	6,318	2,002	1,355
ColD_L40-47	7,370	12,126	3,559	1,473	1,025
ColD_L47-Top	3,293	8,268	1,755	1,096	779

1.2.4 Reinforced Concrete Beams

We modeled reinforced concrete moment frame beams using the FEMA Beam, Concrete Type with symmetric elastic-perfectly-plastic behavior, strength loss, deformation capacities, and no cyclic degradation. We defined flexural plastic hinges at both ends of the beams, assuming an inflection point at mid-span. We used Table 10-7 of ASCE 41-13 to define the parameters of the nonlinear hinge model conservatively assuming high shear demands, as well as similar negative and positive reinforcement ratios and conforming transverse reinforcement, as shown in structural drawings. The resulting parameters are $a=2.0\%$ rad, $b=4.0\%$ rad, $c=20\%$ corresponding in Perform to DL, DX, and FR/FU, respectively. We checked the performance of the beams using a limiting plastic hinge rotation of 4.0% corresponding to the Collapse Prevention level per ASCE 41-13 for primary elements modeled with strength degradation.

We used effective cross section properties to define the elastic behavior of the beams by applying a 0.5 multiplier to the strong- and weak-axis bending inertias of each beam to account for expected cracking.

Figure 1-21 shows reinforced concrete perimeter moment frame beam locations in plan. Figure 1-22 shows a sample flexural backbone curve for B1 and B2 beams from Levels 1 to 14. Sample calculations for the backbone curve are provided. Table 1-4 details flexural capacities for all beams.

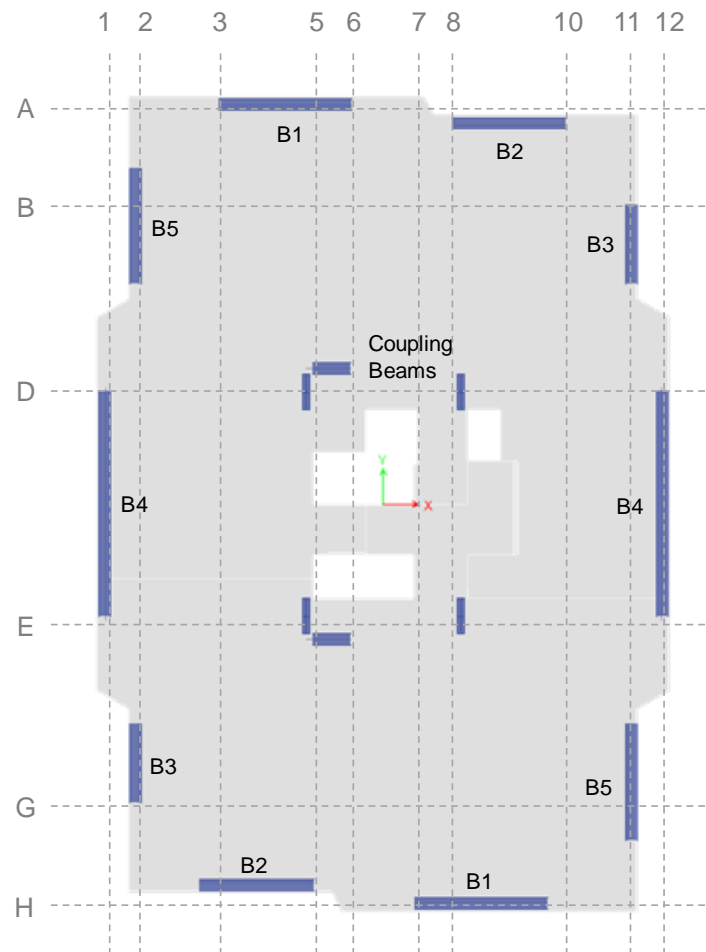


Figure 1-21 – Beam Labels

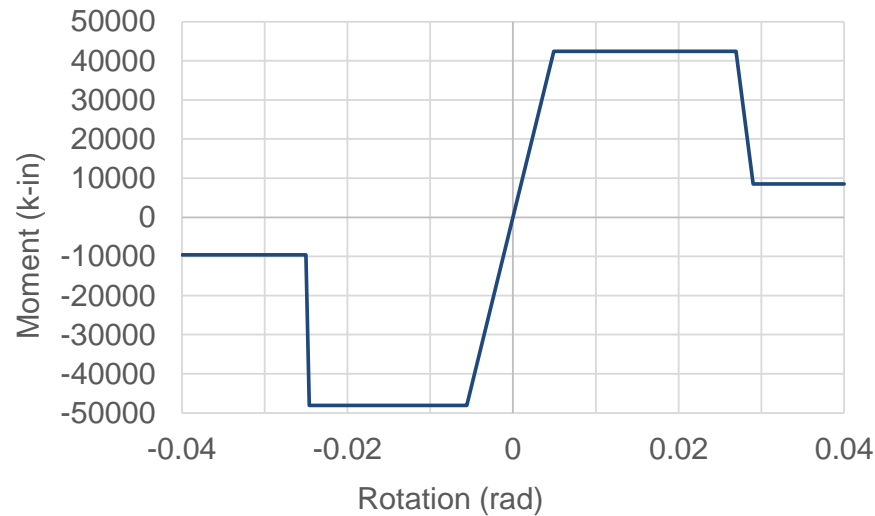


Figure 1-22 – Moment-Rotation Curve for B1 and B2 Beams from L1-14

Flexural Backbone Curve for B1 and B2 Beams from L1-14

Elastic modulus	$E := 57000 \sqrt{13 \frac{\text{ksi}}{\text{psi}}} \cdot \text{psi} = 6499 \text{ ksi}$	
Beam width	$b := 24 \text{ in}$	
Beam depth	$h := 38 \text{ in}$	
Flexural cracking modification factor	$f_b := 0.5$	
Effective moment of inertia	$I_{cr} := \frac{f_b}{12} \cdot b \cdot h^3 = 5.487 \times 10^4 \text{ in}^4$	
Beam length	$L := 249 \text{ in}$	
Flexural stiffness	$k_f := \frac{6 \cdot E \cdot I_{cr}}{L} = 8.593 \times 10^6 \text{ kip} \cdot \text{in}$	
Plastic rotation at strength loss	$a := 0.02$	ASCE 41-13 Table 10-7
Plastic rotation at failure	$b := 0.04$	ASCE 41-13 Table 10-7
Residual strength ratio	$c := 0.2$	ASCE 41-13 Table 10-7
Moment capacity	$M_{ne} := 42431 \text{ kip} \cdot \text{in}$	
Rotation at yield	$\theta_y := \frac{M_{ne}}{k_f} = 4.938 \times 10^{-3}$	
Rotation at strength loss	$\theta_{sl} := \theta_y + a = 0.025$	
Rotation at failure	$\theta_f := \theta_y + b = 0.045$	
Residual moment	$M_r := M_{ne} \cdot c = 8.486 \times 10^3 \text{ kip} \cdot \text{in}$	

Table 1-4 – Beam Capacities

Beam	Level	Positive Moment Capacity (k-in)	Negative Moment Capacity (k-in)
B1	1-14	48,095	42,431
B1	15-20	41,854	37,082
B1	21-30	34,466	30,890
B1	41-47	23,931	19,981
B1	48-58	19,981	19,981
B1	59	20,872	20,872
B2	1-14	48,095	42,431
B2	15-20	41,854	37,082
B2	21-30	34,466	30,890
B2	48-57	19,981	15,763
B2	58	22,655	17,769
B3	1-14	39,756	39,756
B3	15-20	37,082	31,621
B3	21-40	30,890	26,577
B3	41-47	19,403	16,091
B3	48-57	16,091	12,613
B3	58	18,197	14,193
B4	1-14	28,800	18,102
B4	15-20	25,290	15,996
B4	21-40	21,417	13,760
B4	41-58	19,403	12,613
B4	59	20,280	13,140
B5	1-14	42,431	42,431
B5	15-20	29,763	29,763
B5	21-40	25,028	21,417
B5	41-47	19,403	16,091
B5	48-58	16,091	12,613
B5	59	16,793	13,140
B6	1	117,557	117,557
B6	2	152,990	152,990
B6	3	69,414	69,414

1.2.5 Pile Cap

The tower is supported on a single, continuous 10 ft thick cast-in-place reinforced concrete pile cap connecting precast concrete piles spaced at 4ft-8 in. on center. The 10 ft portion of the tower foundation extends from gridline A-J.1 in the North-South direction and gridlines 1-12 in the East-West directions. On the South, a PG&E vault is supported on a 3 ft thick slab cantilevered off of the pile cap from gridline J.1 and extending to gridline K. This portion of the mat is directly supported on soil.

We developed a nonlinear grillage model of the entire foundation system. We used a relatively regular and orthogonal layout of beam elements representing segments of the pile cap at an approximate spacing of 5 ft on center in both longitudinal (North-South) and transverse (East-West) directions of the mat. This spacing corresponds to the spacing of precast piles throughout the mat North of line J.1. As shown in Figure 4, we slightly distorted the regular beam layout in some locations to match shear wall and column layouts and to provide nodal points at the 31 points at which settlement measurements are available.

The selected grillage beam spacing results in deep rectangular beams measuring 5 ft wide by 10 ft deep. We evaluated the validity of this modeling approach by comparing the flexural and shear force-deformation relationship of simple elastic beam models in Perform to a thick mat foundation modeled using finite element analysis (FEA) in Abaqus v6.13.1. We assessed two different beam lengths: 60 in. (5 ft beam spacing in orthogonal direction) and 240 in. (4 beams in series arbitrarily selected to represent a longer beam span). In the Abaqus model we used solid 3D deformable elements with 8 integration points and a mesh size of 5x5x5 in., as shown in Figure 1-23. The elastic material properties matched those used in Perform.

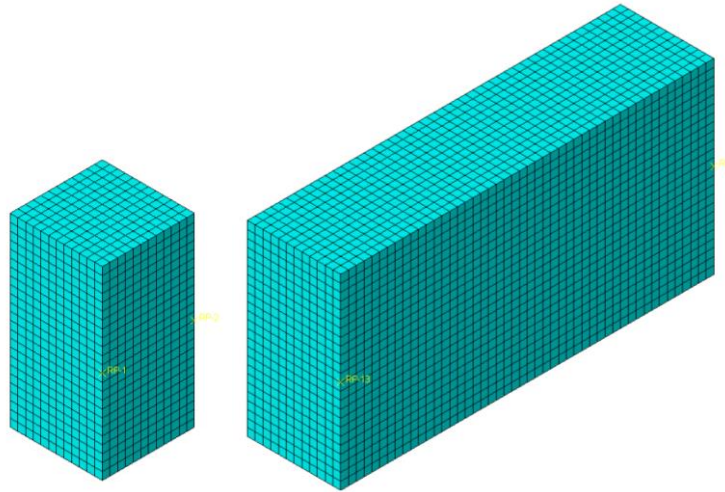
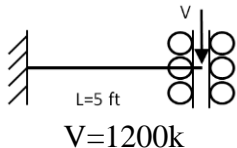
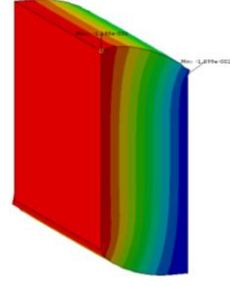
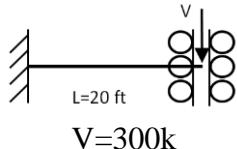
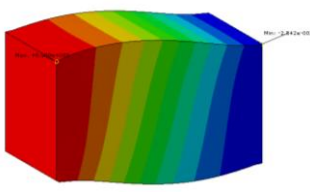
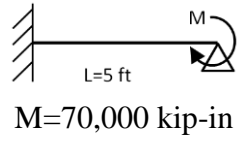
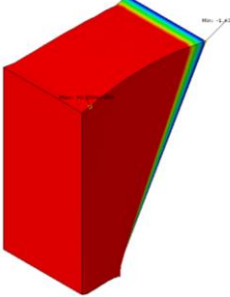
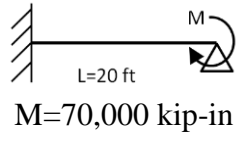
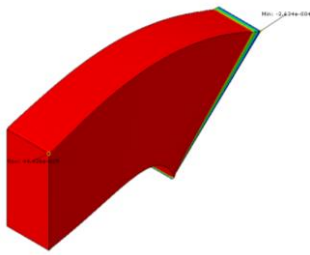


Figure 1-23 – Rendering of Abaqus models of short and long beam/slab segments

We defined the boundary conditions with one fixed support in all 6 degrees of freedom while the other beam end had an applied shear load, V , or bending moment, M . Under shear load we allowed the beam end to move vertically (with all other degrees of freedom restrained). Under bending moment we allowed the beam end to rotate (with all other degrees of freedom restrained). Table 1-5 compares the results obtained from the Perform and Abaqus models, indicating close agreement and suggesting that the beam elements used in the Perform model are able to adequately capture the pile cap behavior.

Table 1-5 – Comparison of Perform and Abaqus Results

Model	Deformation Results		
	FEA (Abaqus)	Perform-CSI	Difference
 $L=5\text{ ft}$ $V=1200\text{ k}$	 $\square_{\text{vertical}}=1.099\text{e-2 in.}$	$\square_{\text{vertical}}=1.18\text{e-2 in.}$	7%
 $L=20\text{ ft}$ $V=300\text{ k}$	 $\square_{\text{vertical}}=2.542\text{e-2 in.}$	$\square_{\text{vertical}}=2.60\text{e-2 in.}$	2%
 $L=5\text{ ft}$ $M=70,000\text{ kip-in}$	 $\theta = 1.432\text{e-4 rad}$	$\theta = 1.477\text{e-4 rad}$	3%
 $L=20\text{ ft}$ $M=70,000\text{ kip-in}$	 $\theta = 2.634\text{e-4 rad}$	$\theta = 2.673\text{e-4 rad}$	1%

We applied a 0.45 multiplier to the concrete elastic modulus to represent that state of cracking expected.

We used inelastic concrete type FEMA beams with shear hinges at the ends to model the grillage beams. We defined both flexural and shear hinges as trilinear curves with no strength loss or

cyclic degradation. We calculated all the hinge backbone curve properties per Table 10-7 of ASCE 41-13.

Figure 1-24 and Figure 1-25 show moment capacity throughout the cap about each horizontal axis. Figure 1-26 shows shear capacity throughout the cap. Figure 1-27 shows a sample flexural backbone curve for Section 1 of the cap. Flexural and shear sample calculations are provided.

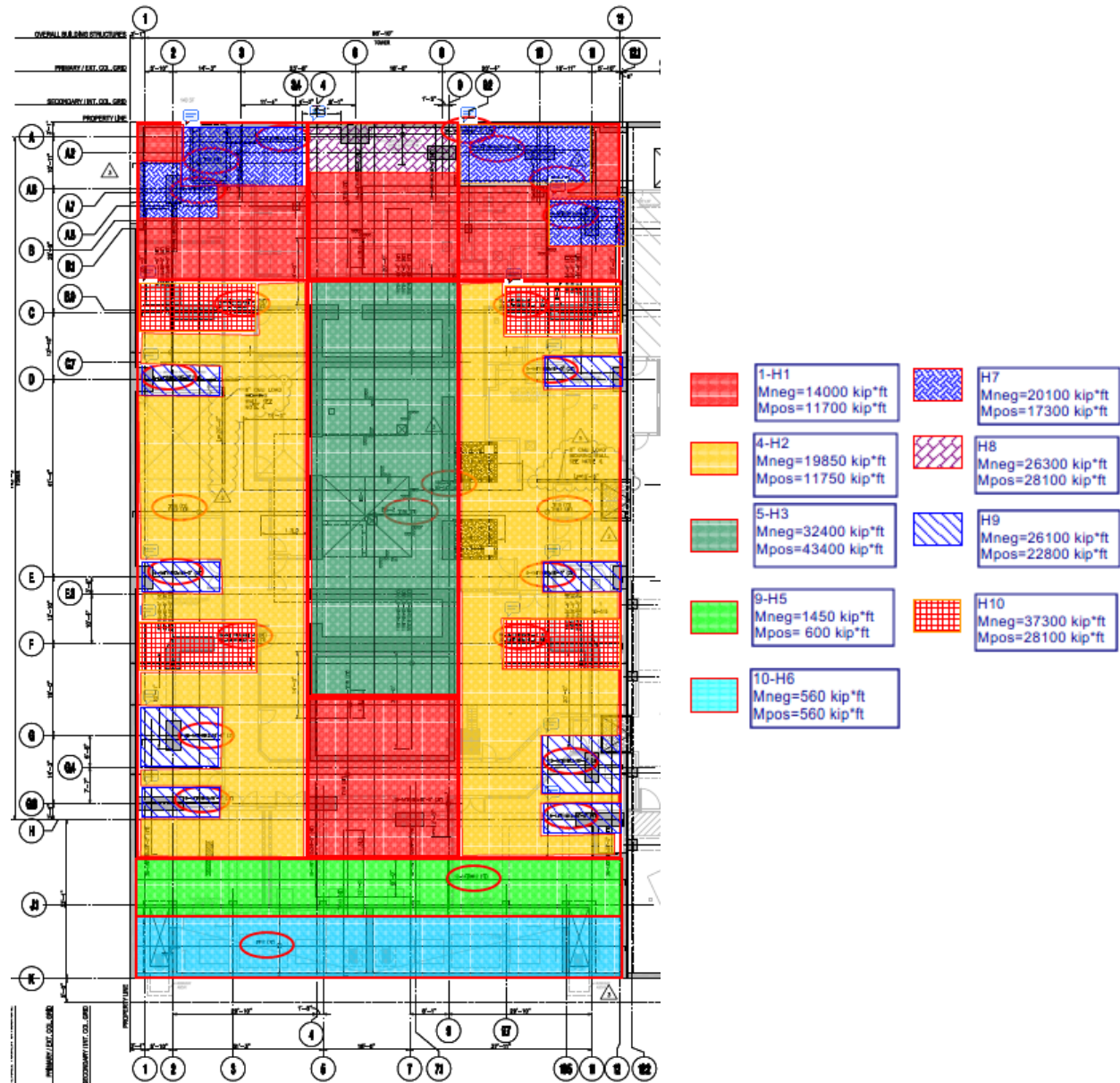


Figure 1-24 – Pile Cap Moment Capacity about N-S Axis

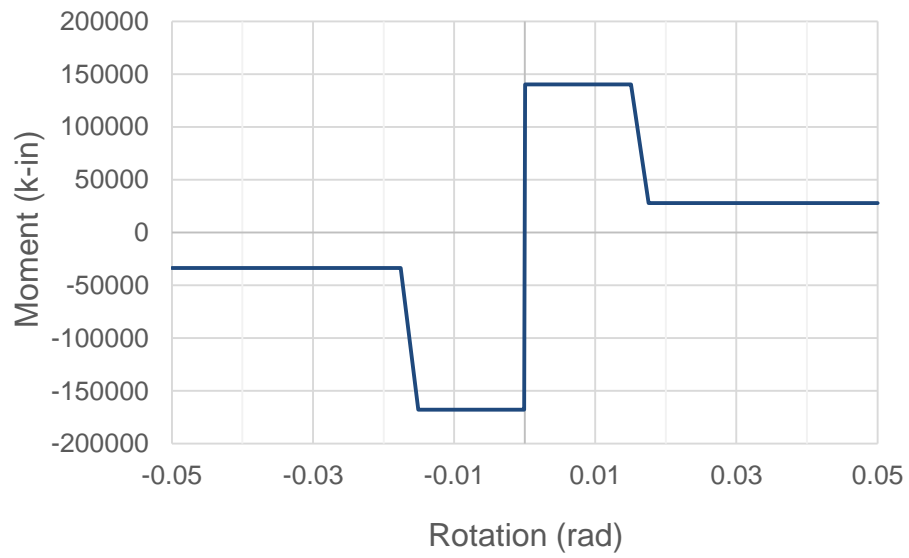


Figure 1-27 – Moment-Rotation Curve for Pile Cap Section 1

Flexural Backbone Curve for Section 1 Grillage Beams

Concrete strength	$f_c := 7.8 \text{ ksi}$	
Elastic modulus	$E := 57000 \sqrt{\frac{f_c}{\text{psi}}} \cdot \text{psi} = 5034 \cdot \text{ksi}$	
Column width	$b := 5 \text{ ft}$	
Column depth	$h := 10 \text{ ft}$	
Flexural cracking modification factor	$f_b := 0.5$	
Effective moment of inertia	$I_{cr} := \frac{f_b}{12} \cdot b \cdot h^3 = 4.32 \times 10^6 \cdot \text{in}^4$	
Effective length	$L := 5 \text{ ft}$	
Flexural stiffness	$k_f := \frac{6 \cdot E \cdot I_{cr}}{L} = 2.175 \times 10^9 \cdot \text{kip} \cdot \text{in}$	
Plastic rotation at strength loss	$a := 0.015$	
Mat positive moment capacity	$M_{mp} := 2338 \frac{\text{kip} \cdot \text{ft}}{\text{ft}}$	spColumn
Grillage beam positive moment	$M_{bp} := M_{mp} \cdot b = 1.403 \times 10^5 \cdot \text{kip} \cdot \text{in}$	
Rotation at yield	$\theta_y := \frac{M_{bp}}{k_f} = 6.45 \times 10^{-5}$	
Rotation at strength loss	$\theta_{sl} := \theta_y + a = 0.015$	

Shear Capacity for Section 1 Grillage Beams

Concrete strength	$f_c := 7.8 \text{ ksi}$	
Steel yield	$f_y = 87.75 \text{ ksi}$	
Shear reinf bar area	$A_s := \frac{2.25 \text{ in}^2}{24 \text{ in}} = 0.094 \frac{\text{in}^2}{\text{in}}$	#14@24in
Beam width	$b := 5 \text{ ft}$	
Beam depth	$d := 9 \text{ ft}$	
Shear capacity	$V_e := 2 \sqrt{\frac{f_c}{\text{psi}}} \cdot \text{psi} \cdot b \cdot d + A_s \cdot f_y \cdot d \cdot \frac{b}{\text{ft}} = 5.587 \times 10^3 \cdot \text{kip}$	

1.2.6 Pile and Soil Springs

1.2.6.1 ENGEO Properties

We used springs to represent the vertical support beneath the pile cap, as shown in Figure 1-28. The model does not explicitly include each of the 942 piles. To facilitate meshing, we used a total of 853 pile/soil springs (738 springs representing piles and 115 representing soil) distributed throughout the foundation plan and located at the nodes connecting the grillage beams that represent the pile cap. The 115 soil springs are all located at the 3 ft thick soil-supported region along the south edge of the mat.

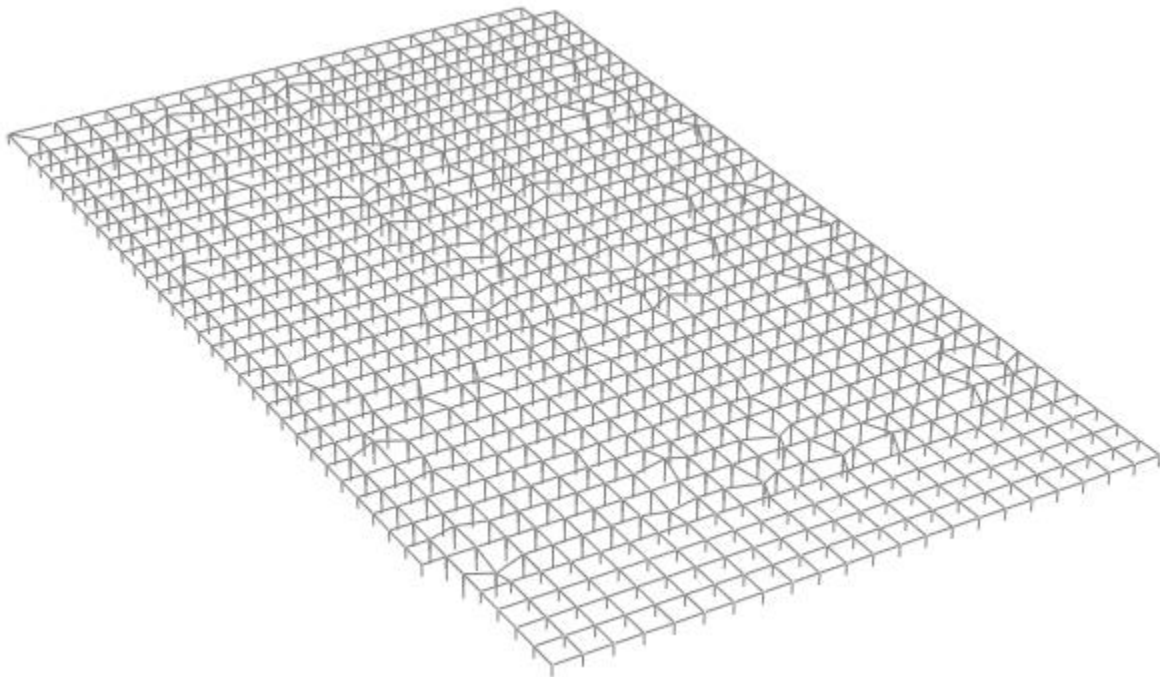


Figure 1-28 – Pile and Soil Springs Supporting Pile Cap

We calculated the stiffness of these springs by geographic interpolation between the data provided by ENGEO, shown in Figure 1-29 and then factoring these properties by the tributary area for each spring. We used the Kriging Method available in the Surfer 8 computer program to perform the 2-dimensional interpolation.

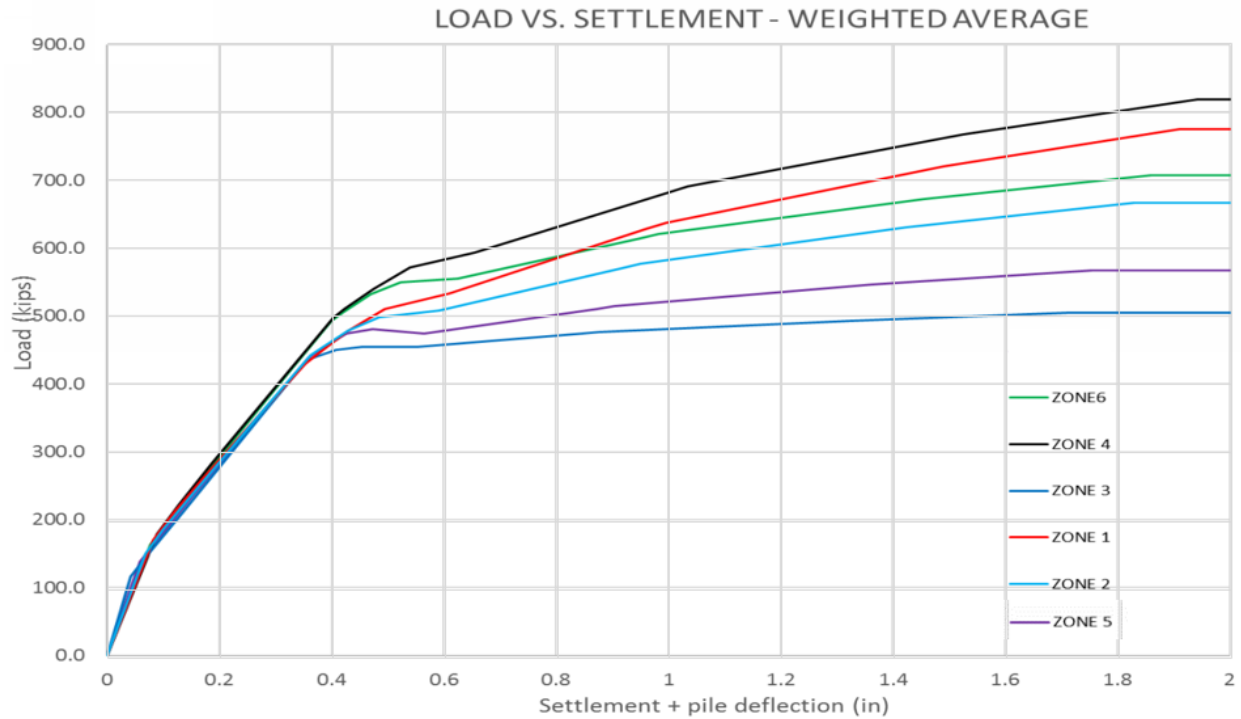


Figure 1-29 – ENGEO Pile Properties

1.2.6.2 Alternate Pile Properties

We also analyzed the model using pile spring properties provided by John Egan, Slate Geotechnical Consultants and Shannon & Wilson, Inc on 31 October 2018.

We applied non-linear, compression only springs representing the soil/pile stiffness under long-term loading. The soil springs use the force-deformation relationship provided factored by the spring tributary area. We obtained spring force-deformation relationship for the pile springs by interpolating between the data provided for the piles nearest to the grid point at which we applied a spring, and then factoring these properties by the tributary area for each spring. We used the Kriging Method available in the Surfer 8 computer program to perform the 2-dimensional interpolation.

We then applied gravity loads (dead and live) to the structure, resulting in downward displacement of the pile springs and deformation of the mat. We iteratively applied thermal loading to the individual piles to produce a deformed shape of the mat that reasonably represented the surface we obtained from the 2 June 2017 Arup settlement data.

We then applied an additional set of springs at each of the support nodes. One compression-only spring added at each node represents the incremental pile strength and stiffness provided for seismic response. We also added a tension-only spring to represent the dynamic strength and stiffness of the piles in uplift. We connected the tension only springs to the mat using a combination of gap and hook elements, such that the springs are effective only when the piles actually experience uplift forces. We determined the strength and stiffness values for each of these spring elements using the normalized relationships shown in Figure 1-30 and the long term compressive capacities obtained using the geographic interpolation approach described previously.

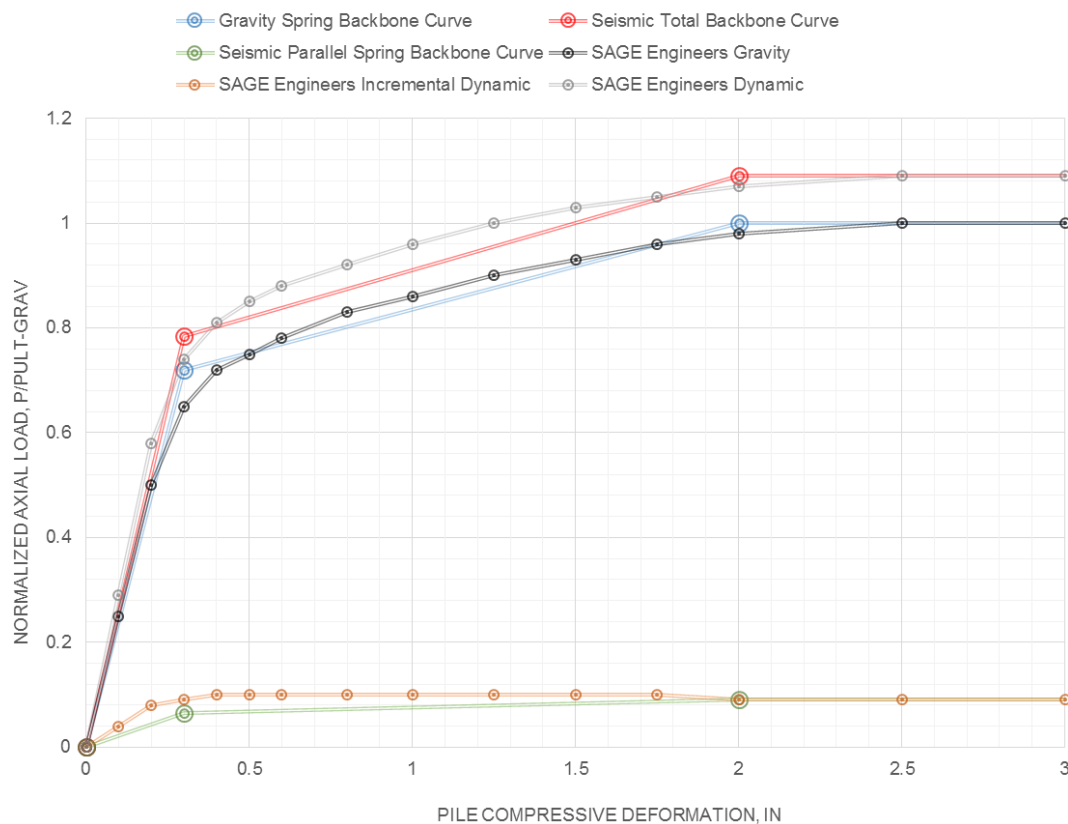


Figure 1-30 – Implementation of Pile Load-Deformation Curves

1.3 Loading

After applying gravity loads as described in Section 1.1.2 and applying pile and soil springs to achieve the measured displacement profile as described in Section 1.2.6, we applied jacking loads to simulate the addition of the retrofit piles. The retrofit pile locations are described in

Section **Error! Reference source not found.** We applied an 800k upward load at each retrofit pile location simultaneously.

We combined the unfactored dead, settlement, and jacking loads with 25% of the live loads in accordance with PEER TBI recommendations.

1.4 Substructure Results

1.4.1 Results for ENGEO Pile Properties

We checked the flexural behavior of the mat using the pile properties and loading described in Section 1.2.6.1. Figure 1-31 shows demand-to-capacity ratios for allowable plastic hinge rotation of the mat grillage elements relative to 1%. The mat performance is adequate as it does not form a hinge across the gross section at any locations.

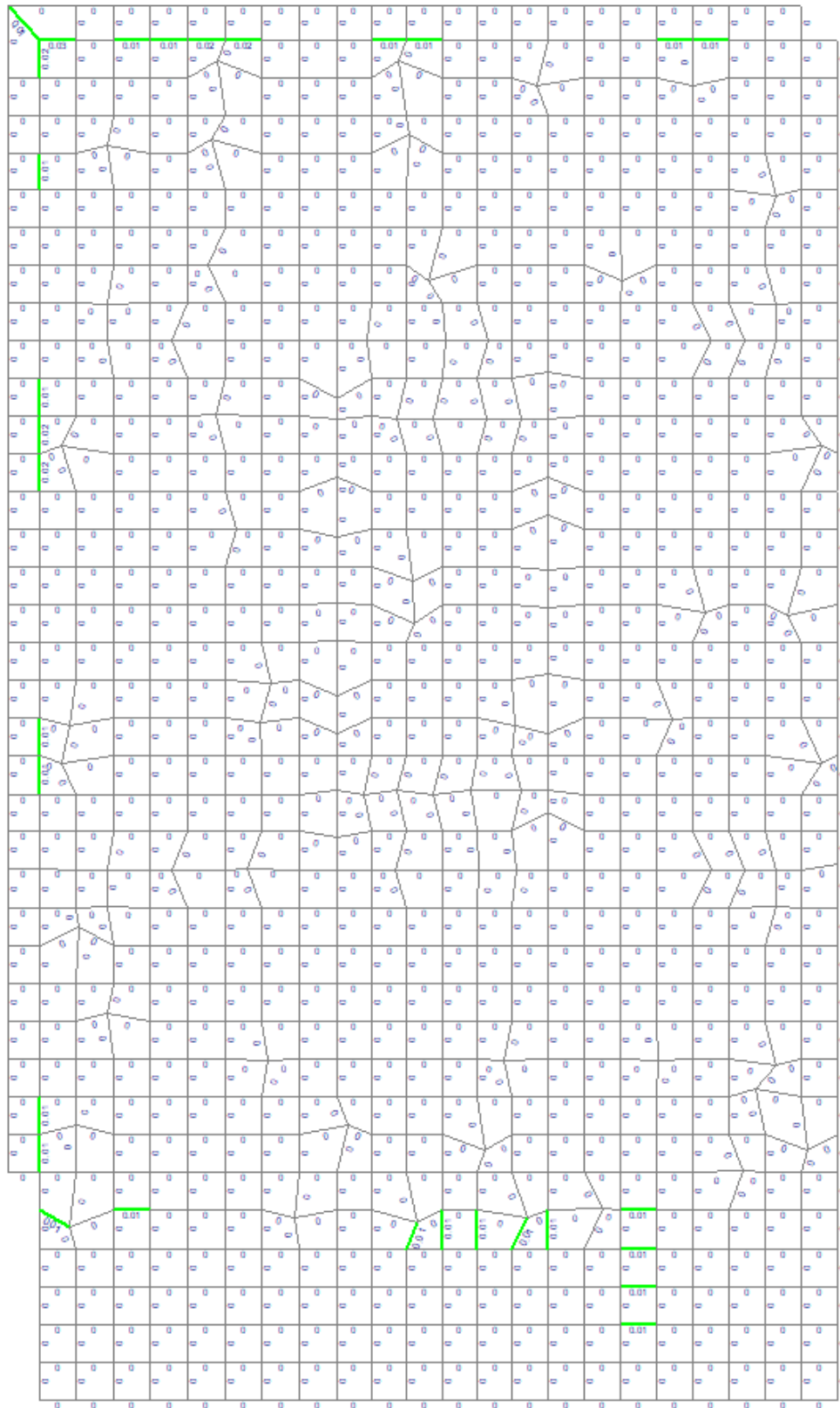
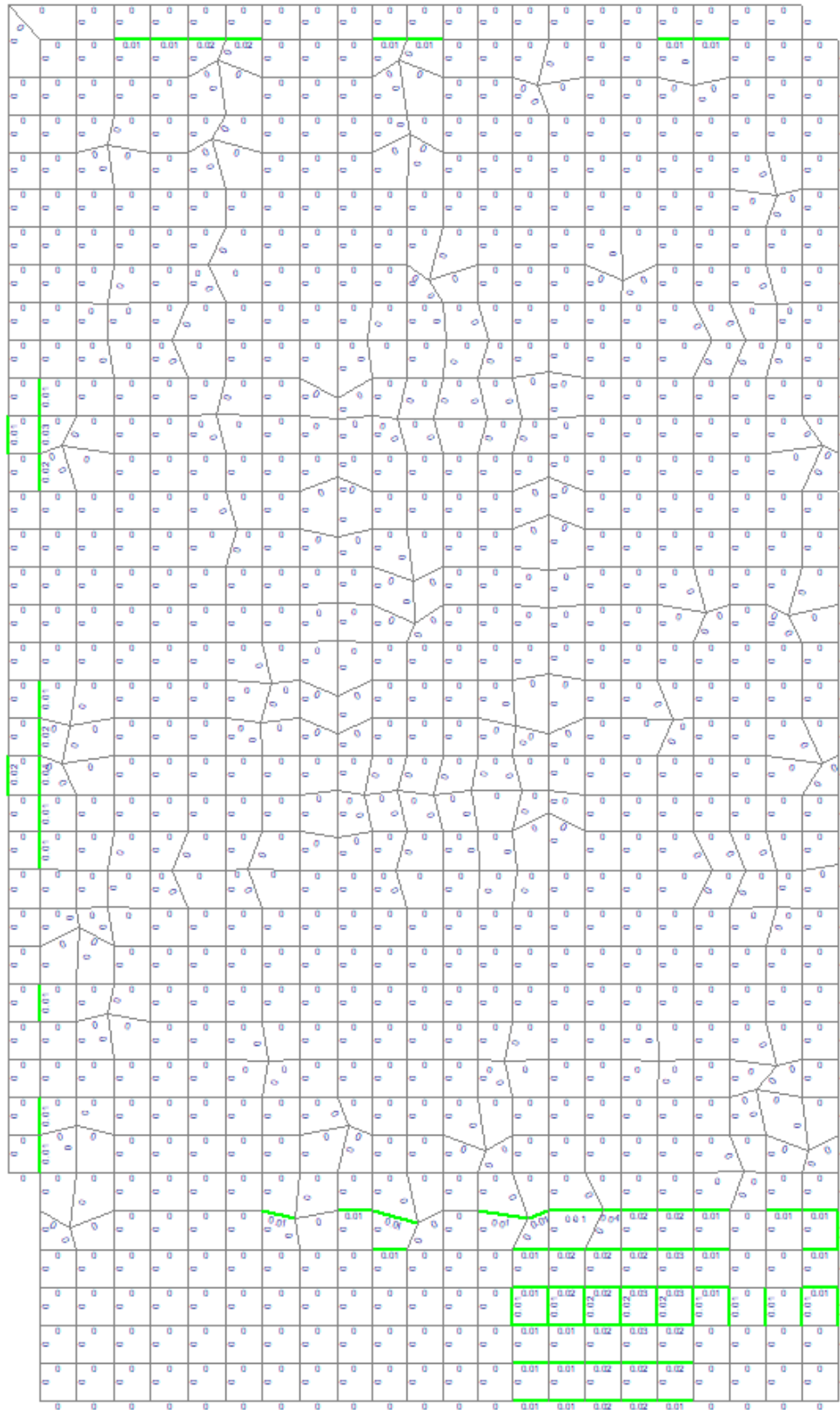


Figure 1-31 – Mat Flexural Hinge DCRs, Gravity + Jacking, ENGEO Pile Properties

1.4.2 Results for Alternate Pile Properties

We checked the flexural behavior of the mat using the pile properties and loading described in Section 1.2.6.2. Figure 1-32 and Figure 1-33 show demand-to-capacity ratios for allowable plastic hinge rotation of the mat grillage elements relative to 1%. The results show minor local yielding ($DCR > 0$). Results are similar to the analyses with ENGEO pile properties. Figure 1-32 shows mat flexural hinge DCRs for the existing settled condition without retrofit. Figure 1-33 shows mat flexural hinge DCRs for the retrofit condition after jacking the new piles.



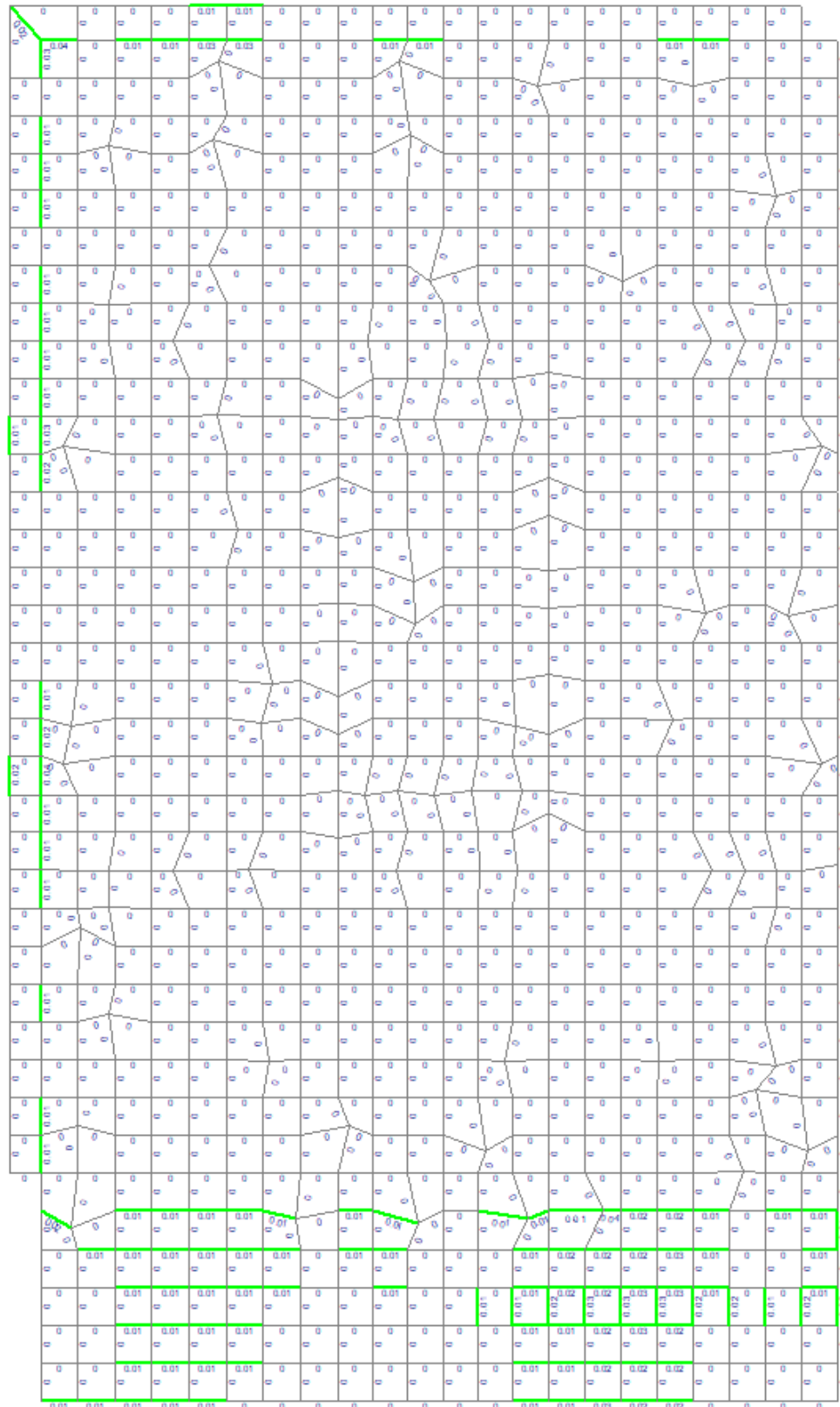


Figure 1-33 – Mat Flexural Hinge DCRs, Gravity + Settlement + Retrofit Pile Jacking, Alternate Pile Properties

2. ANALYTICAL MODEL: SAFE V2016

2.1 Description and Screenshots

2.1.1 SAFE Model

We also checked the mat slab foundation flexural capacity for jacking of the proposed retrofit piles using SAFE v2016. Figure 2-1 shows a plan of the retrofit piles. Figure 2-2 features a reinforcing plan of the mat slab foundation under the tower issued by DeSimone. Figure 2-4 highlights the elements of the SAFE foundation model. The model consists of shell elements that represent the slab, core walls, and foundation walls and elasto-plastic springs that represent the pile supports.

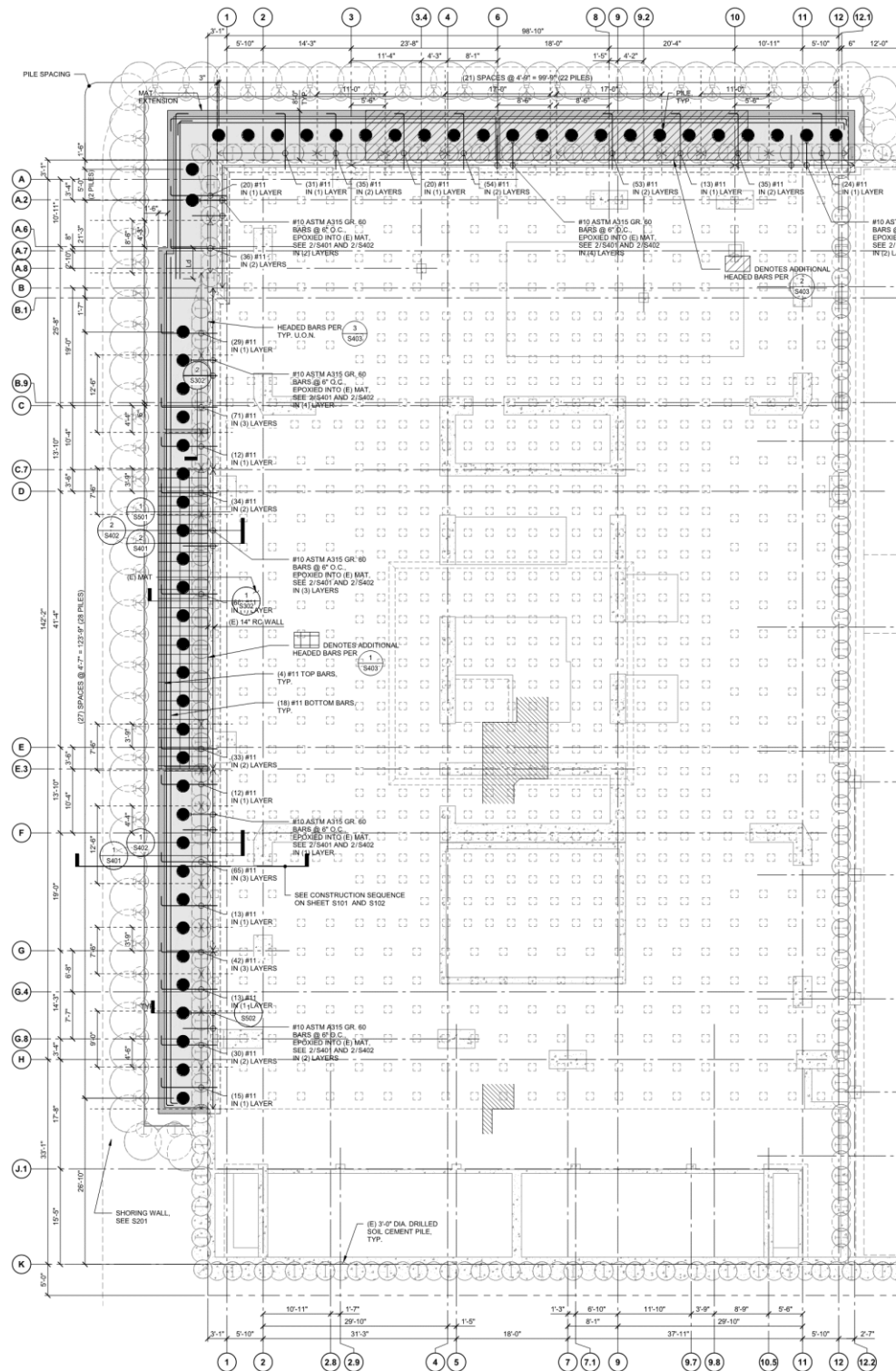
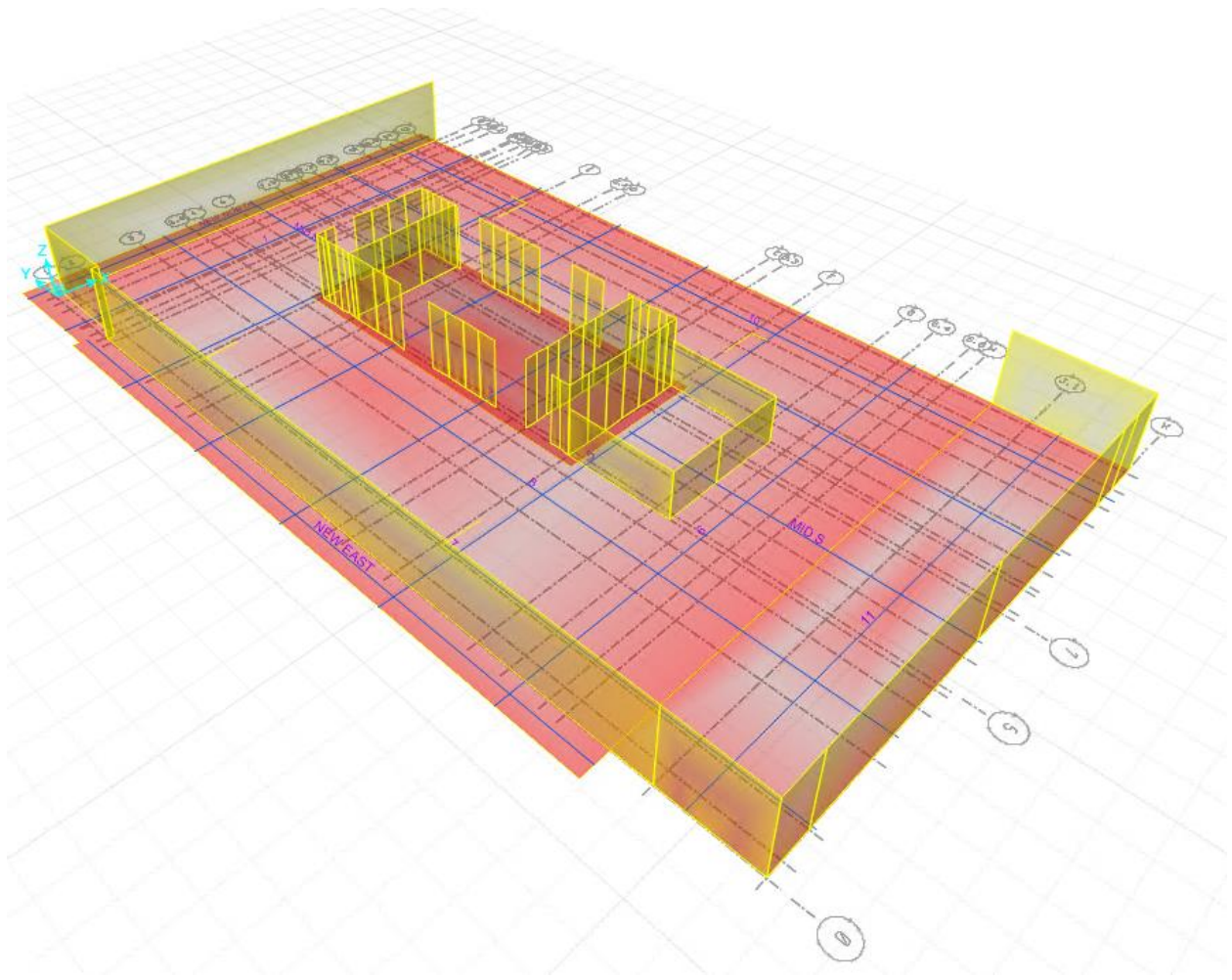


Figure 2-1: Retrofit Pile Layout





**Figure 2-3: SAFE v2016 Model of Foundation Slab with Foundation and Core Walls
Isometric View**

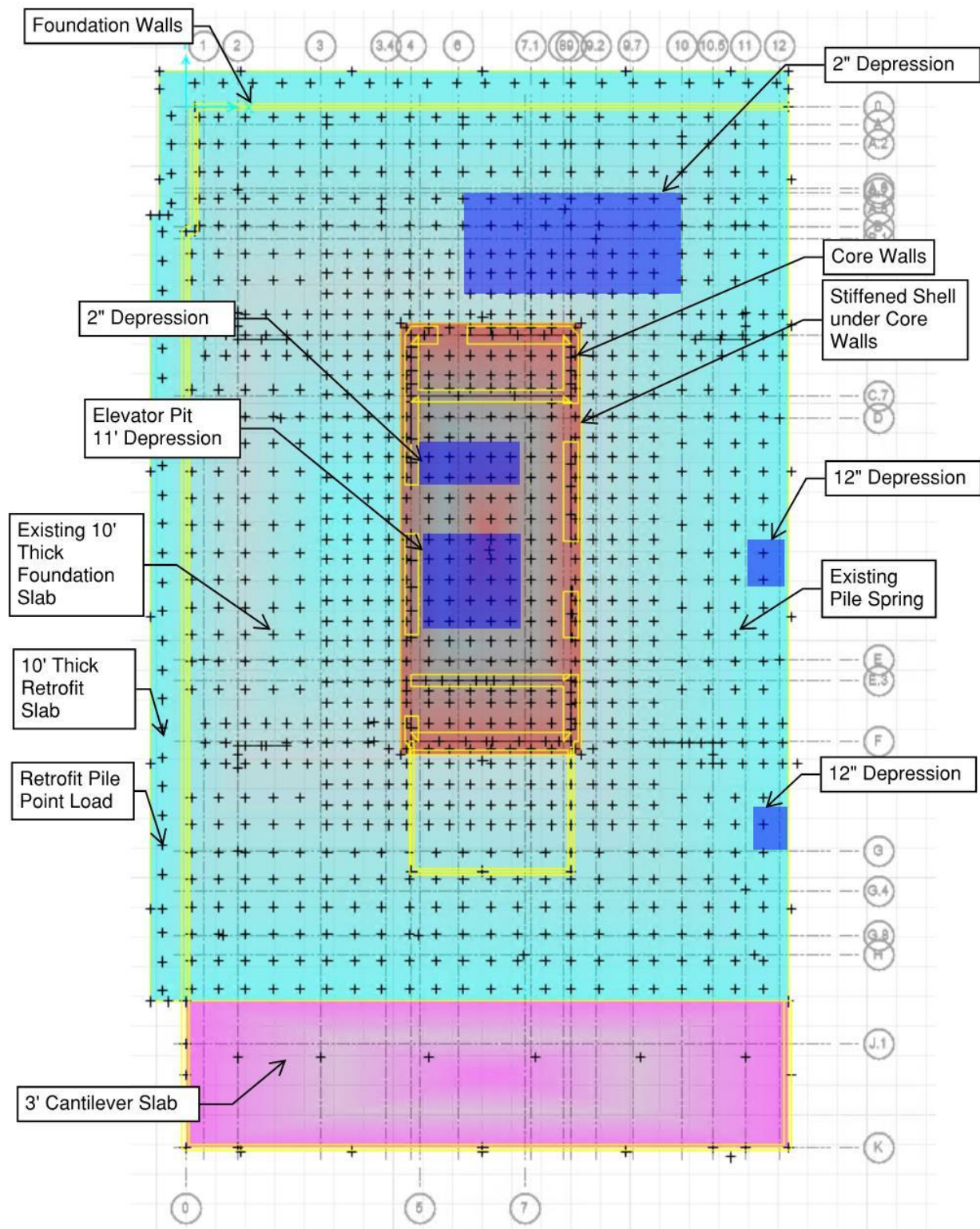


Figure 2-4: Mat Slab Foundation Plan View

2.1.2 Mat Slab

We modeled the slab with a 10 ft. thick shell element for the pile supported slab and a 3 ft. thick shell for the cantilever portion. We used the “Thick Plate” element formation to consider the transverse shear deformations from the column and core wall loading for the pile supported mat slab. Using the orthotropic slab feature, the slab redistributes twisting moments to the principle moments. The thickness considered for torsional stiffness for the pile supported and cantilever slabs are set to zero and therefore causes the entire bending load to be resisted in the X and Y directions and results in zero twisting moments. The depressions were not modeled in the

The SAFE model contains the existing slab reinforcement which is used by the program to perform the cracked section nonlinear analysis computation. According to the design drawings by DeSimone existing reinforcement larger than #9 bars is ASTM A615 Grade 75. The existing reinforcement reflects design drawings as well as the reinforcement shop drawings dated February 13, 2006 with revisions dated July 7, 2006.

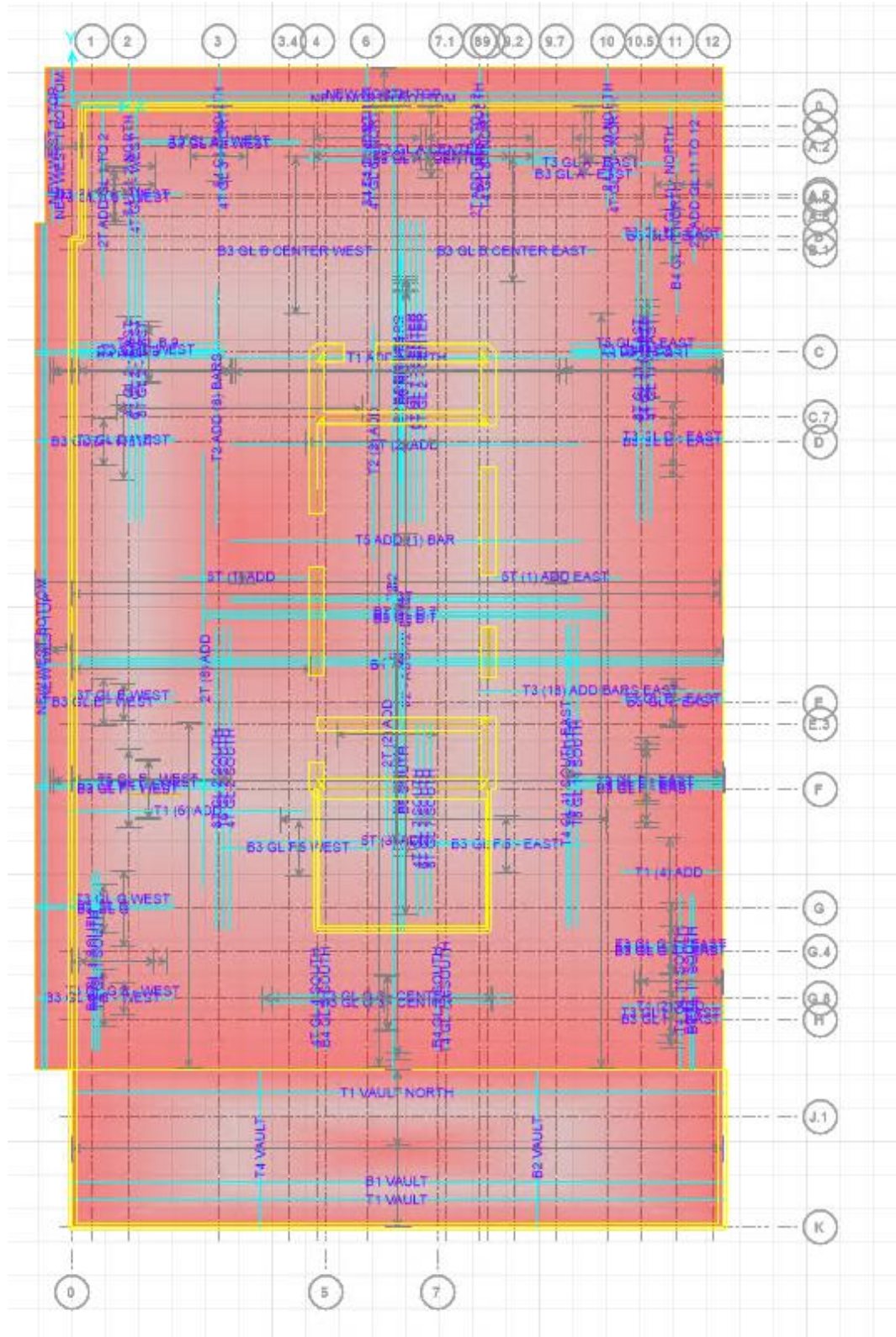


Figure 2-7: Steel Reinforcement Definition Layout in SAFE

We determined the compressive strength of the concrete used in the 10 ft. thick mat slab using the required average compressive strength equation from ACI 301-16, which is the standard concrete specification used for most new buildings in the United States. The required average compressive strength (f_{cr}) is the average strength of the sets of concrete cores samples taken at 91 days, dated 8/25/2006 and 9/20/2006. Using this method we demonstrate that the concrete breaks of the mat are adequate for a specified concrete compressive strength of 7,000 psi.

The transformer vault cantilever slab has a compressive strength of 5,000 psi, as specified on the original design drawings.

Title: Minimum Required Compressive Strength from Core Strength Tests

References: ACI 318-14, ACI 301-16, Mat Slab Core Strength Tests (08/25/2006, 09/20/2006)

Statistics of Core Samples

Sample Standard Deviation $\sigma := 989.1 \text{ psi}$
Average Compressive Strength of
Core Samples $X_{\text{bar}} := 8747.5 \text{ psi}$

ACI Calculations

k Factor for 30 or more samples $k := 1$

Table 4.2.3.3(a)2—k-factor for increasing sample standard deviation for number of tests considered in calculating standard deviation

Total number of tests considered	k-factor for increasing sample standard deviation
15	1.16
20	1.08
25	1.03
30 or more	1.00

To determine the minimum specified concrete compressive strength, we set the average equal to the required average compressive strength for both equations in Table 4.2.3.3(a).

Table 4.2.3.3(a)1—Required average compressive strength f_{cr}' when data are available to establish a sample standard deviation, psi

f_c' , psi	f_{cr}' , psi
	Use the larger of:
5000 or less	$f_{cr}' = f_c' + 1.34ks_s$
	$f_{cr}' = f_c' + 2.33ks_s - 500$
Over 5000	$f_{cr}' = f_c' + 1.34ks_s$
	$f_{cr}' = 0.90f_c' + 2.33ks_s$

Notes: f_{cr}' is required average compressive strength; f_c' is specified concrete strength; k is factor from Table 4.2.3.3(a)2; and s_s is standard deviation calculated in accordance with 4.2.3.2.

$$f_c' := 7155 \text{ psi}$$

$$f_{c1}' := X_{\text{bar}} - 1.34 \cdot k \cdot \sigma = 7.422 \times 10^3 \text{ psi}$$

$$f_{c2}' := \frac{(X_{\text{bar}} - 2.33 \cdot k \cdot \sigma)}{0.9} = 7.159 \times 10^3 \text{ psi}$$

Therefore model uses 7000 psi for the mat slab concrete compressive strength.

2.1.3 Walls

2.1.3.1 Core Walls

Core walls vary from 24 to 36 inches at the foundation slab level. The figure below illustrates the size and location of the shear walls. The compressive strength of the shear walls between Level B1 and 1 is 10,000 psi as specified in the design drawings.

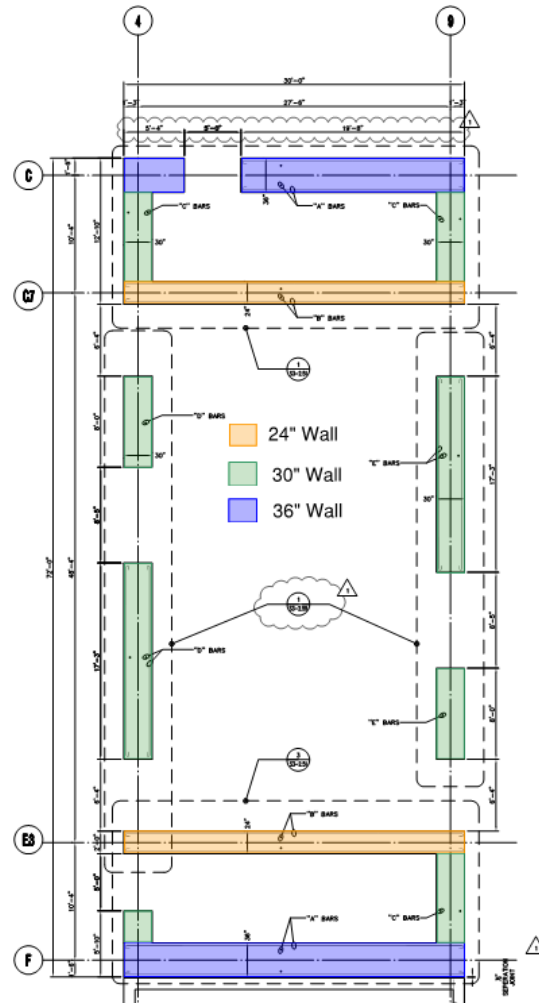


Figure 2-8: Core Wall Thickness and Geometry

SAFE v16 automatically considers the connection between walls and slab elements as a rigid slab zone, as explained in SAFE Knowledge Base under Modeling Techniques on the CSI website. The program therefore prevents deformation of the slab at the wall or column location which will cause the maximum design moments to be at the face of the walls instead of at the center line, which is appropriate.

A weightless shell with cracked properties connects the core walls at the top. We place a “stiff” shell under the shear walls so that the core remains rigid in relation to the mat slab. The “stiff” shell property will ignore the overlapping slab properties and the program will not perform design checks on this shell. Core walls have a stiffness modifier of 0.7 in-plane and 0.25 out-of-plane to represent the cracked moment of inertia.

2.1.3.2 - Foundation Walls

We modeled the foundation walls with a 14-inch-thick shell element extending to the north, south, and west edges of the foundation slab. The program connects the walls to the slab automatically with a rigid connection, as described for the core walls. We modeled Level 1 with a shell element that connects the top of the walls. This shell has cracked properties similar to the core walls and has no weight assigned. To represent the 1” gap between Level 1 slab and the core walls, the Level 1 shell does not connect to the core walls. The foundation walls have a concrete compressive strength of 5000 psi. We use this value from the original design drawings by DeSimone. Foundation walls also have a modified cracked stiffness of 0.7 in-plane and 0.25 out-of-plane to represent the cracked moment of inertia.

2.1.4 Piles

2.1.4.1 Existing Piles

2.1.4.1.1. ENGEO Spring Definition

Elasto-plastic point springs represent the existing vertical pile stiffness. The graph below shows the idealized elasto-plastic curve defined in SAFE with the tri-linear backbone curve provided in the draft Geotechnical Memorandum – 301 Mission Retrofit Design by ENGEO dated April 24, 2018. We determined the SAFE point spring load-deformation response by reducing our best-fit bilinear curve to 80% of its original strength value in accordance with the provisions of ASCE 7-16 Section 12.13.5.2.

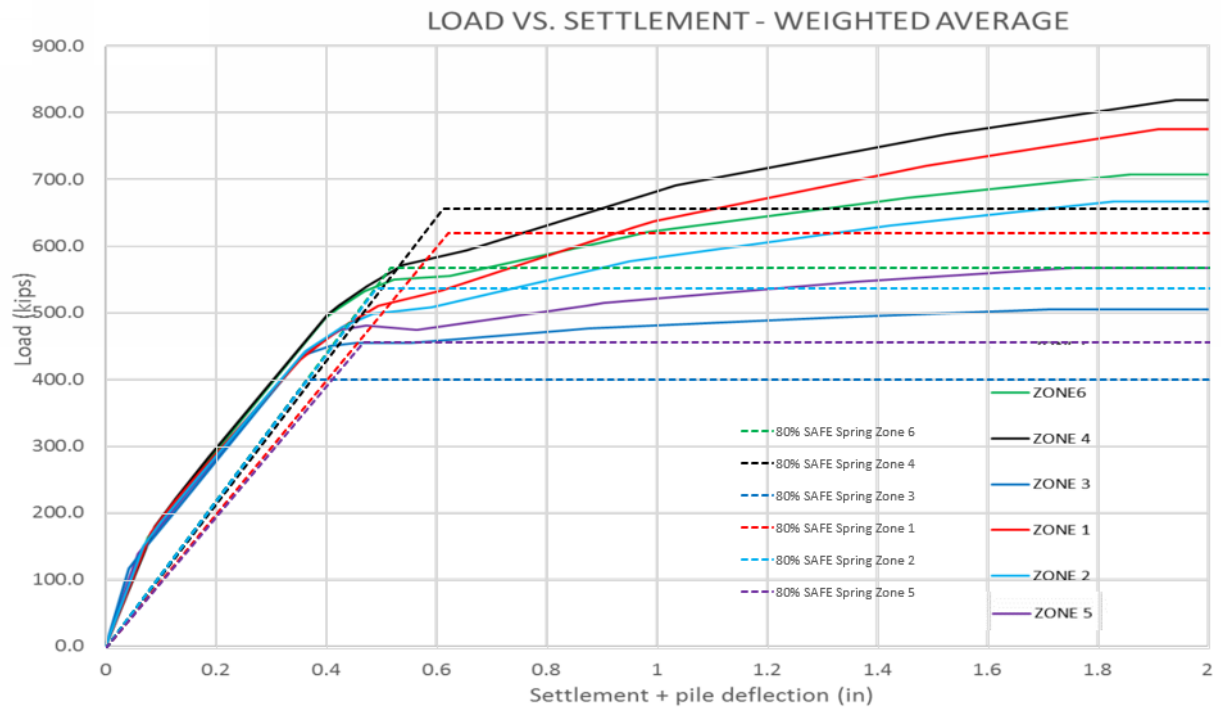


Figure 2-9: Pile Vertical Spring Definition

Figure 2-10 shows the pile spring definition within the SAFE model. Table 6 below shows the vertical nonlinear spring properties for all pile zones. The existing pile capacities vary from 500 kips to 820 kips across the site. Figure 2-11 illustrates the pile strength variation throughout the foundation.

Figure 2-10: Pile Point Spring Definition in SAFE

Table 6: Pile Spring Definition

ENGEO Ultimate Compressive Strength (kips)	Reduced Compressive Strength (kips)	Compression Stiffness (kip/in)
500	400	1100
570	456	980
670	536	1093
710	568	1104
775	620	1000
820	656	1076

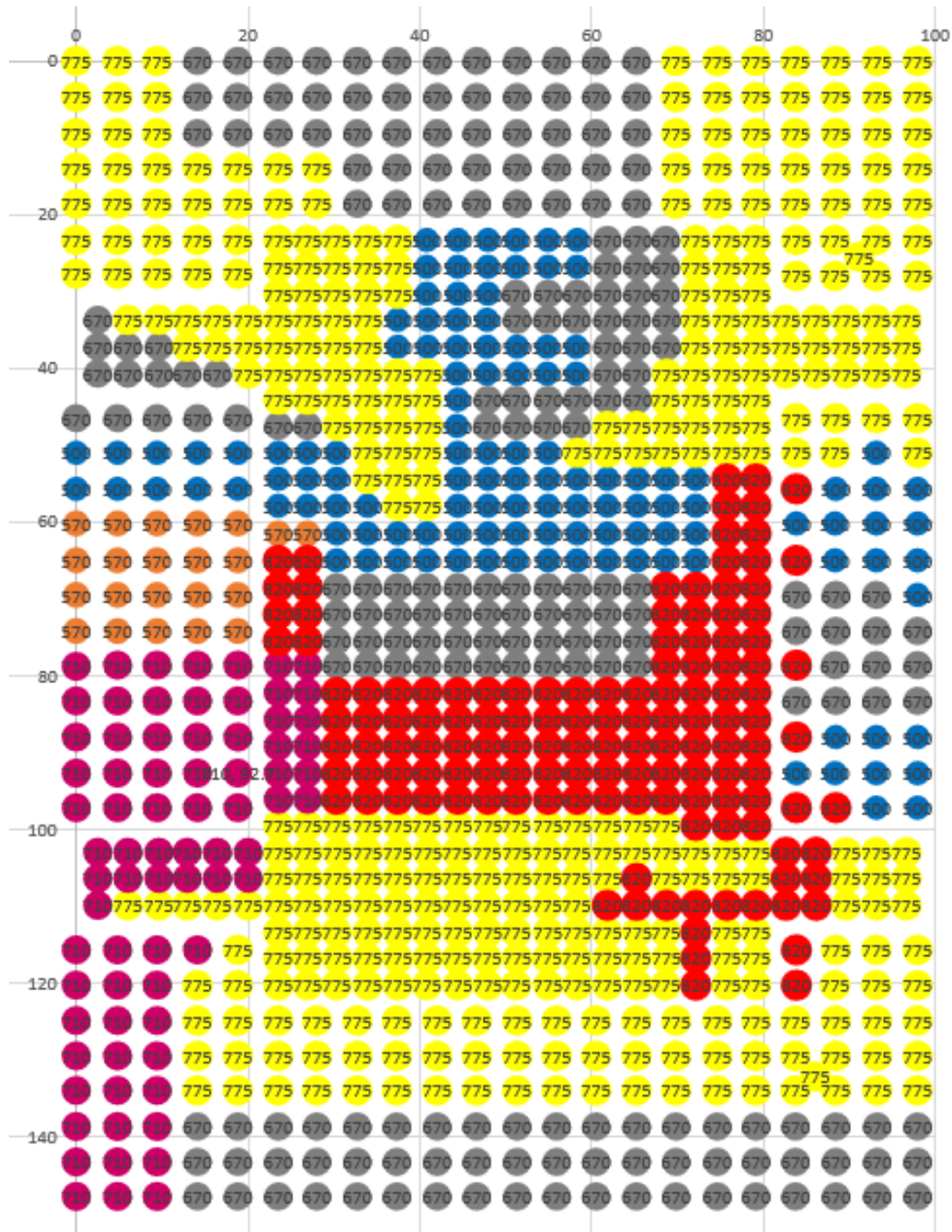


Figure 2-11: Spring Strength Diagram

2.1.4.1.2. Alternative Pile Spring Definition

In addition, we analyzed the model with pile spring definitions from the report titled Geotechnical Evaluation for the Perimeter Pile Upgrade, Millennium Tower, City and County of San Francisco, CA, by John Egan, GE, Slate Geotechnical Consultants, Inc., and Shannon & Wilson, Inc., dated 10/31/18. The graph below shows the idealized elasto-plastic curve defined in SAFE based on a normalized pile stiffness curve for compression and tension. Dynamic pile springs are plotted on the same graph and have additional strength and stiffness as seen in Table 7. The geotechnical tension spring strength was capped at 280.6 kips to represent the yielding of the longitudinal dowels in the pile.

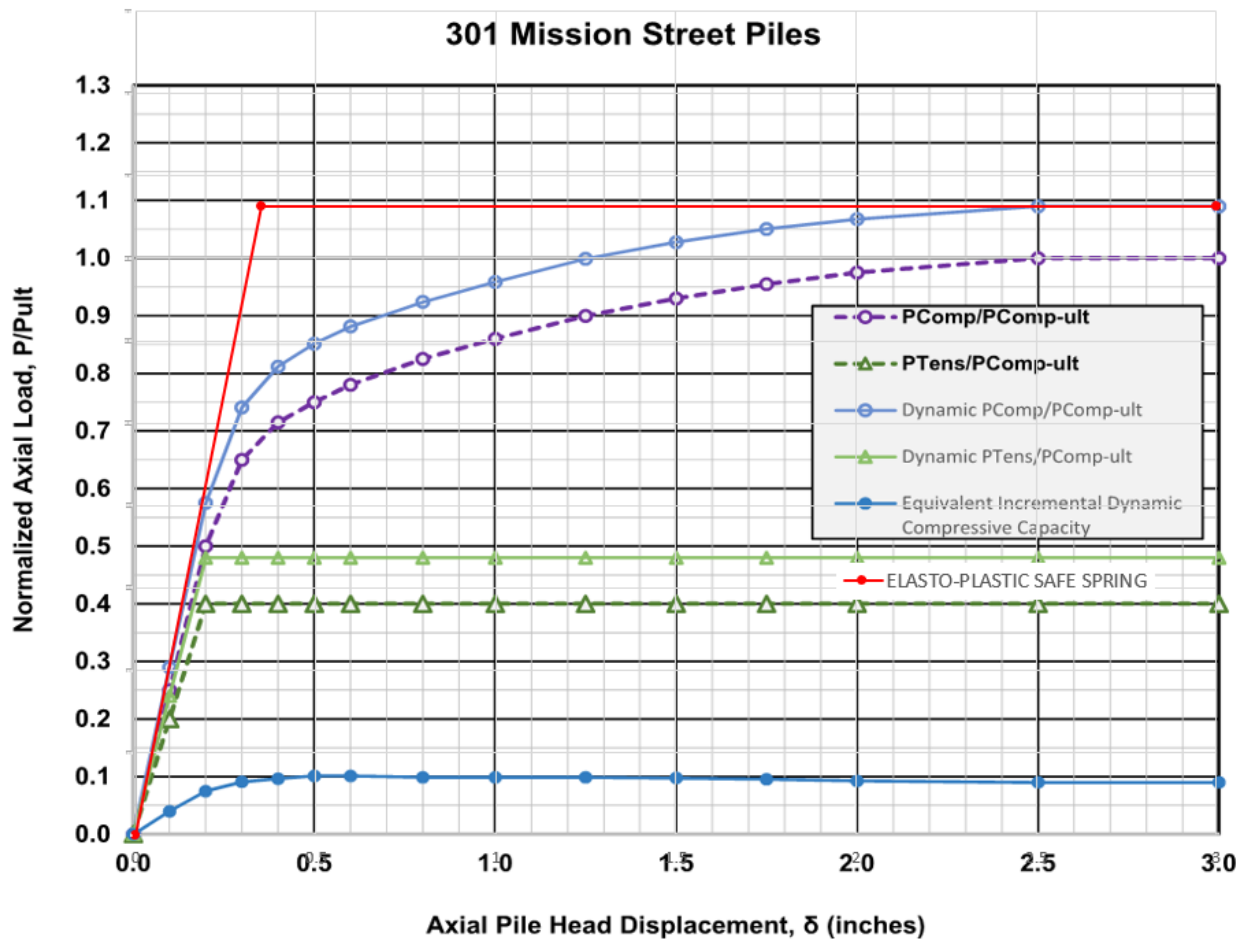


Figure 2-12: Pile Vertical Spring Definition

Table 7: Normalized Compression and Tension Pile Stiffness Curve Values

δ (inches)	$P_{Comp}/P_{Comp-ult}$	Dynamic $P_{Comp}/P_{Comp-ult}$	$P_{Tens}/P_{Comp-ult}$	Dynamic $P_{Tens}/P_{Comp-ult}$	Equivalent Incremental Dynamic Compressive Capacity
0.00	0.00	0.00	0.00	0.00	0.00
0.10	0.25	0.29	0.20	0.24	0.04
0.20	0.50	0.58	0.40	0.48	0.08
0.30	0.65	0.74	0.40	0.48	0.09
0.40	0.72	0.81	0.40	0.48	0.10
0.50	0.75	0.85	0.40	0.48	0.10
0.60	0.78	0.88	0.40	0.48	0.10
0.80	0.83	0.92	0.40	0.48	0.10
1.00	0.86	0.96	0.40	0.48	0.10
1.25	0.90	1.00	0.40	0.48	0.10
1.50	0.93	1.03	0.40	0.48	0.10
1.75	0.96	1.05	0.40	0.48	0.10
2.00	0.98	1.07	0.40	0.48	0.09
2.50	1.00	1.09	0.40	0.48	0.09
3.00	1.00	1.09	0.40	0.48	0.09

Notes:

$P_{Comp-ult}$	Ultimate Compressive Axial Pile Capacity
P_{Comp}	Axial Compressive Pile Load
P_{Tens}	Axial Tensile (Uplift) Pile Load

Figure 2-13 shows the pile spring definition within the SAFE model. Table 8 below shows the vertical dynamic compression and tension nonlinear spring properties. The existing pile capacities vary from 175 kips to 1400 kips across the site. Figure 2-14 illustrates the pile strength variation throughout the foundation.

General Data	
Property Name	1400
Display Color	[Green Square] Change...
Property Notes	Modify/Show Notes...

Spring Stiffness in Global Directions	
Translation X	0 kip/in
Translation Y	0 kip/in
Translation Z (Effective Linear)	4360 kip/in
Rotation about X-Axis	0 kip-in/rad
Rotation about Y-Axis	0 kip-in/rad
Rotation about Z-Axis	0 kip-in/rad

Nonlinear Option (Translation Z Only) (Nonlinear Cases Only)	
<input type="radio"/> None (Linear) <input type="radio"/> Tension Only <input type="radio"/> Compression Only <input checked="" type="radio"/> Elasto-Plastic	
Compression Stiffness	4360 kip/in
Compression Strength	1526 kip
Tension Stiffness	1403 kip/in
Tension Strength	280.6 kip

OK Cancel

Figure 2-13: Pile Point Spring Definition in SAFE

Table 8: Dynamic Pile Spring Definition

SAGE Ultimate Compressive Strength	Compression Stiffness	Compression Strength	Tension Stiffness	Tension Strength
175	545.0	190.75	420.00	84.00
250	778.6	272.5	600.00	120.00
275	856.4	299.75	660.00	132.00
300	934.3	327	720.00	144.00
325	1012.1	354.25	780.00	156.00
350	1090.0	381.5	840.00	168.00
375	1167.9	408.75	900.00	180.00
400	1245.7	436	960.00	192.00
425	1323.6	463.25	1020.00	204.00
450	1401.4	490.5	1080.00	216.00
475	1479.3	517.75	1140.00	228.00
500	1557.1	545	1200.00	240.00
525	1635.0	572.25	1260.00	252.00
550	1712.9	599.5	1320.00	264.00
575	1790.7	626.75	1380.00	276.00
600	1868.6	654	1403.00	280.60
625	1946.4	681.25	1403.00	280.60
650	2024.3	708.5	1403.00	280.60
675	2102.1	735.75	1403.00	280.60
700	2180.0	763	1403.00	280.60
725	2257.9	790.25	1403.00	280.60
750	2335.7	817.5	1403.00	280.60
775	2413.6	844.75	1403.00	280.60
800	2491.4	872	1403.00	280.60
825	2569.3	899.25	1403.00	280.60
850	2647.1	926.5	1403.00	280.60
875	2725.0	953.75	1403.00	280.60
900	2802.9	981	1403.00	280.60
925	2880.7	1008.25	1403.00	280.60
950	2958.6	1035.5	1403.00	280.60
975	3036.4	1062.75	1403.00	280.60
1000	3114.3	1090	1403.00	280.60
1025	3192.1	1117.25	1403.00	280.60
1050	3270.0	1144.5	1403.00	280.60
1150	3581.4	1253.5	1403.00	280.60
1175	3659.3	1280.75	1403.00	280.60
1200	3737.1	1308	1403.00	280.60
1225	3815.0	1335.25	1403.00	280.60
1250	3892.9	1362.5	1403.00	280.60
1275	3970.7	1389.75	1403.00	280.60
1300	4048.6	1417	1403.00	280.60
1325	4126.4	1444.25	1403.00	280.60
1350	4204.3	1471.5	1403.00	280.60
1400	4360.0	1526	1403.00	280.60

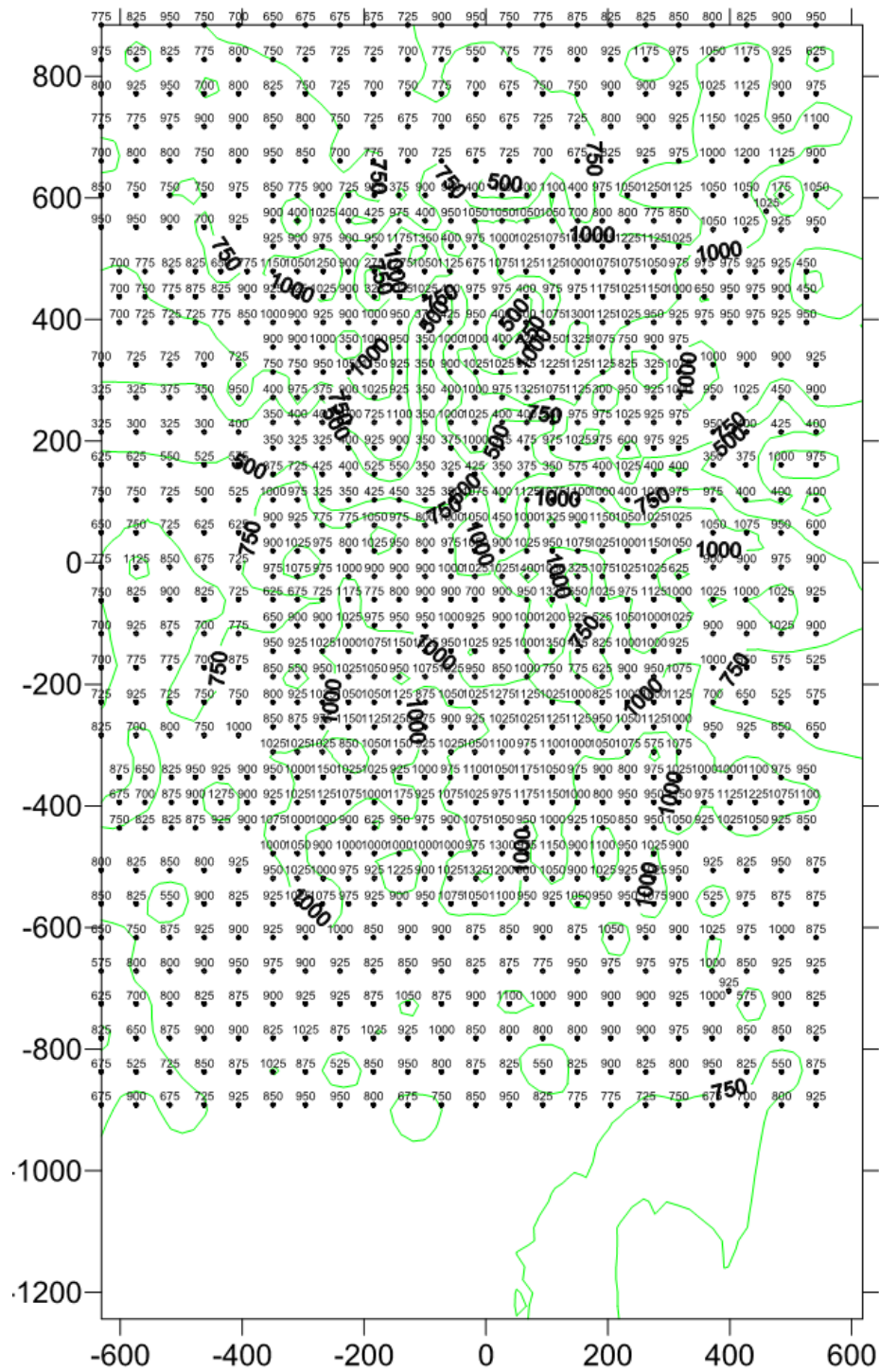


Figure 2-14: Spring Strength Diagram

2.1.4.2 Retrofit Piles

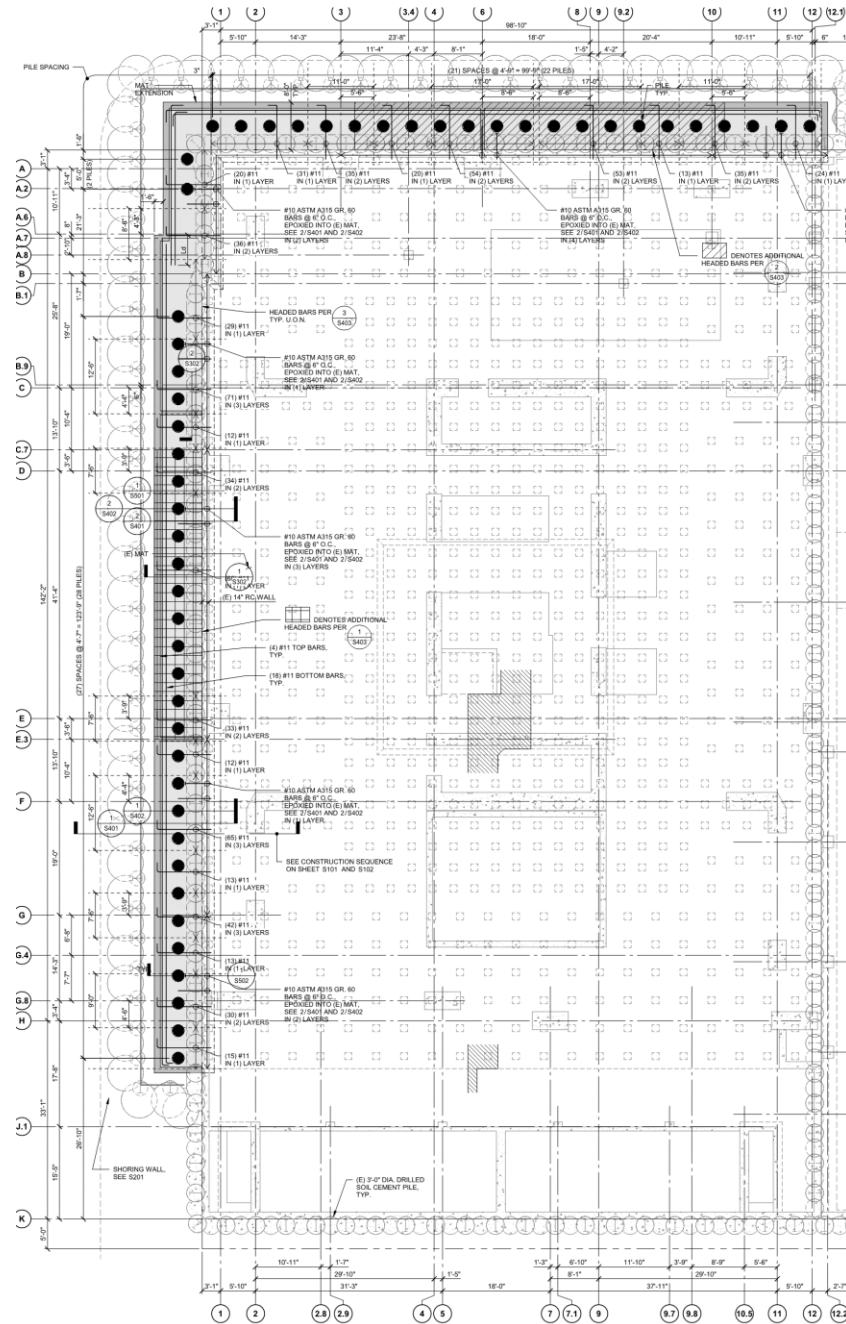


Figure 2-15: Retrofit Pile Plan

Figure 2-15: Retrofit Pile Plan Figure 2-15 illustrates the locations of the retrofit slab and piles. Point loads represent the jacking force the retrofit piles exert on the foundation. The perimeter retrofit slab is the same thickness as the existing mat slab and serves to connect the new retrofit

piles to the existing mat slab. In SAFE, we apply the jacking forces of 800 kips at each pile location simultaneously.

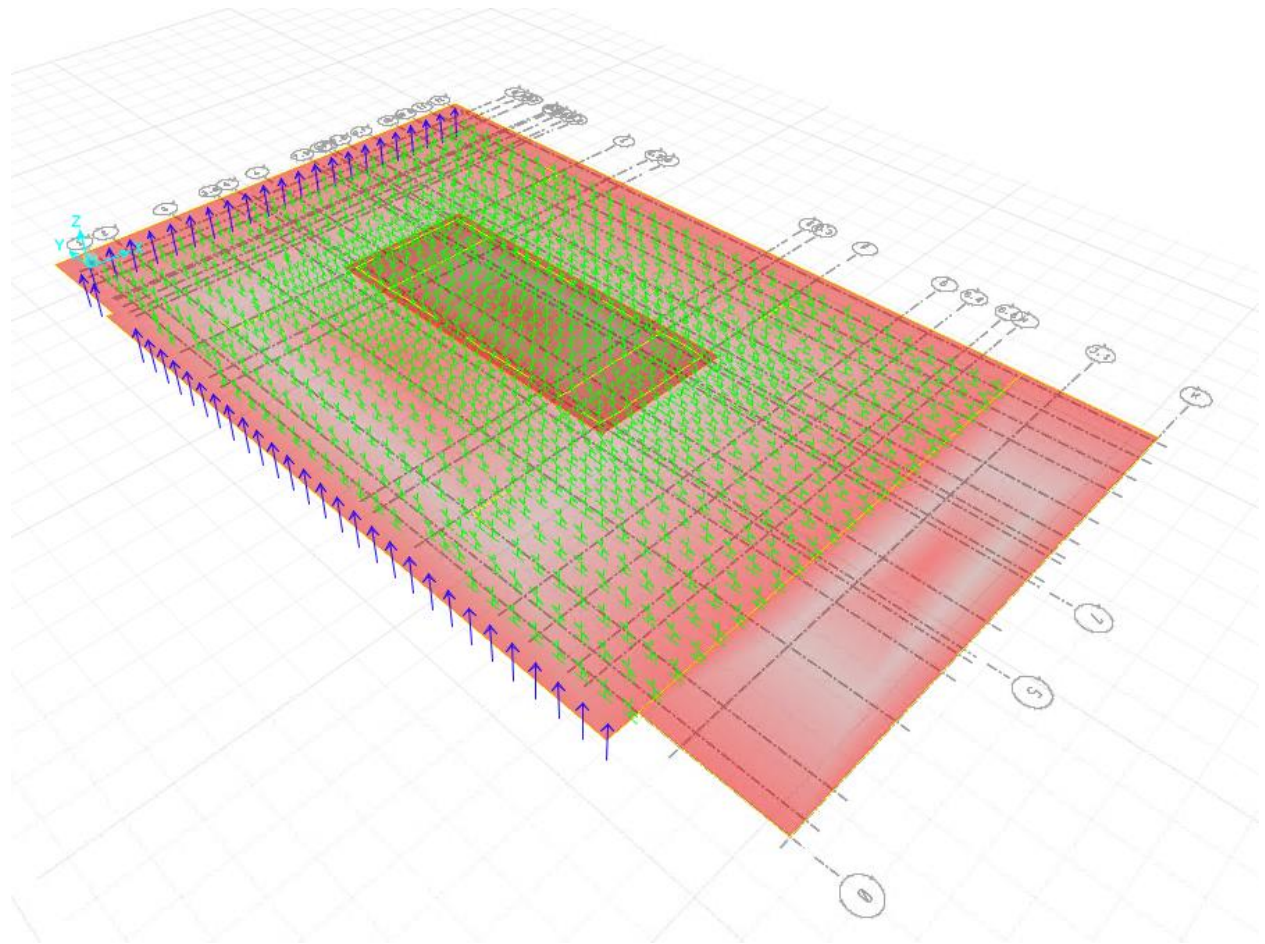


Figure 2-16: SAFE Model Layout with Existing Pile Springs and Retrofit Pile Perimeter Point Loads

2.1.5 Mesh and Analysis Options

To capture the point loads, line loads, and point springs within the model, we use a localized standard mesh of 5 ft. by 5 ft. In addition, we use the “merge points” option to consolidate mesh points where two points are located close to each other.

2.2 Weight and Assigned Loads Summary

2.2.1 Load Combinations

The load combinations of ASCE 7-16 are used for this analysis to determine the greatest anticipated loads. We use each load case listed below with and without retrofit pile jacking

forces to determine foundation slab load demands. Each load is described more thoroughly in their respective sections below.

ASCE 7-16 : Section 2.3

- | | |
|---|-----------------------------|
| 1. $1.4D$ | |
| 2. $1.2D + 1.6L + 0.5(L_r \text{ or } S \text{ or } R)$ | 5. $1.2D + 1.0E + L + 0.2S$ |
| 3. $1.2D + 1.6(L_r \text{ or } S \text{ or } R) + (L \text{ or } 0.5W)$ | 6. $0.9D + 1.0W$ |
| 4. $1.2D + 1.0W + L + 0.5(L_r \text{ or } S \text{ or } R)$ | 7. $0.9D + 1.0E$ |

ASCE 7-16: Section 2.3.6

$$\begin{aligned} &1.2D + E_v + E_h + L + 0.2S \\ &0.9D - E_v + E_h \end{aligned}$$

Per ASCE 7-16 Section 12.4.2.2, we calculate E_v with the following equation

$$E_v = 0.2S_{DS}D \quad (12.4-4a)$$

Therefore, the seismic load combinations considering the vertical seismic component becomes:

$$\begin{aligned} &1.4 * D + L + E \\ &0.7 * D + E \end{aligned}$$

2.2.2 Dead Load

The dead load includes the self weight of the mat slab, the weight of the structural elements of the tower and supplemental dead load from architectural elements. The mat slab load pattern applies the foundation slab self weight as a uniform surface load on the shell element. We apply the tower structure dead load as point loads at the column and outrigger locations and as line loads along the core walls. We model the dead weight due to the perimeter foundation walls explicitly.

DL+SDL, kips

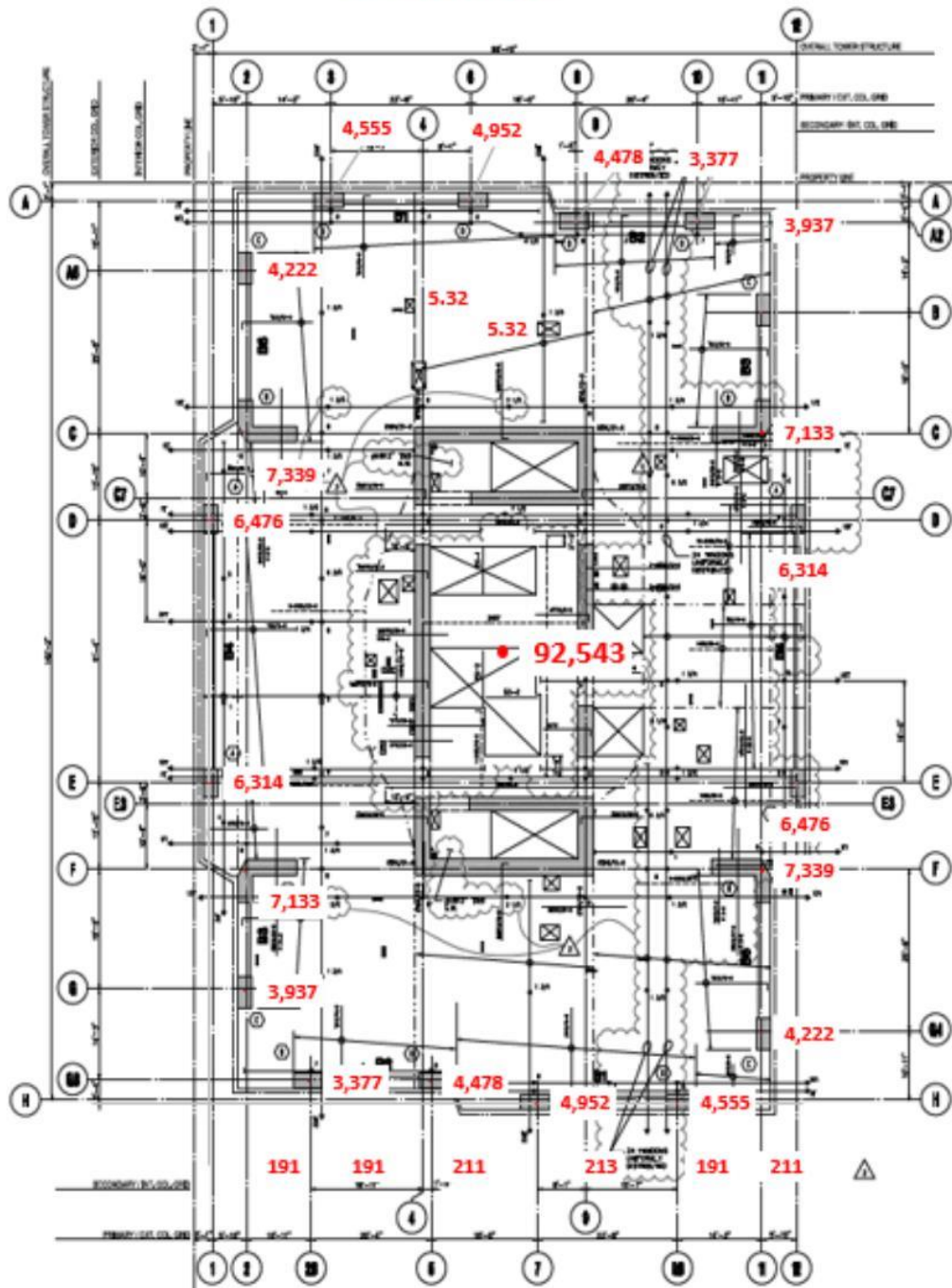


Figure 2-17: Dead Load Application at Columns and Core

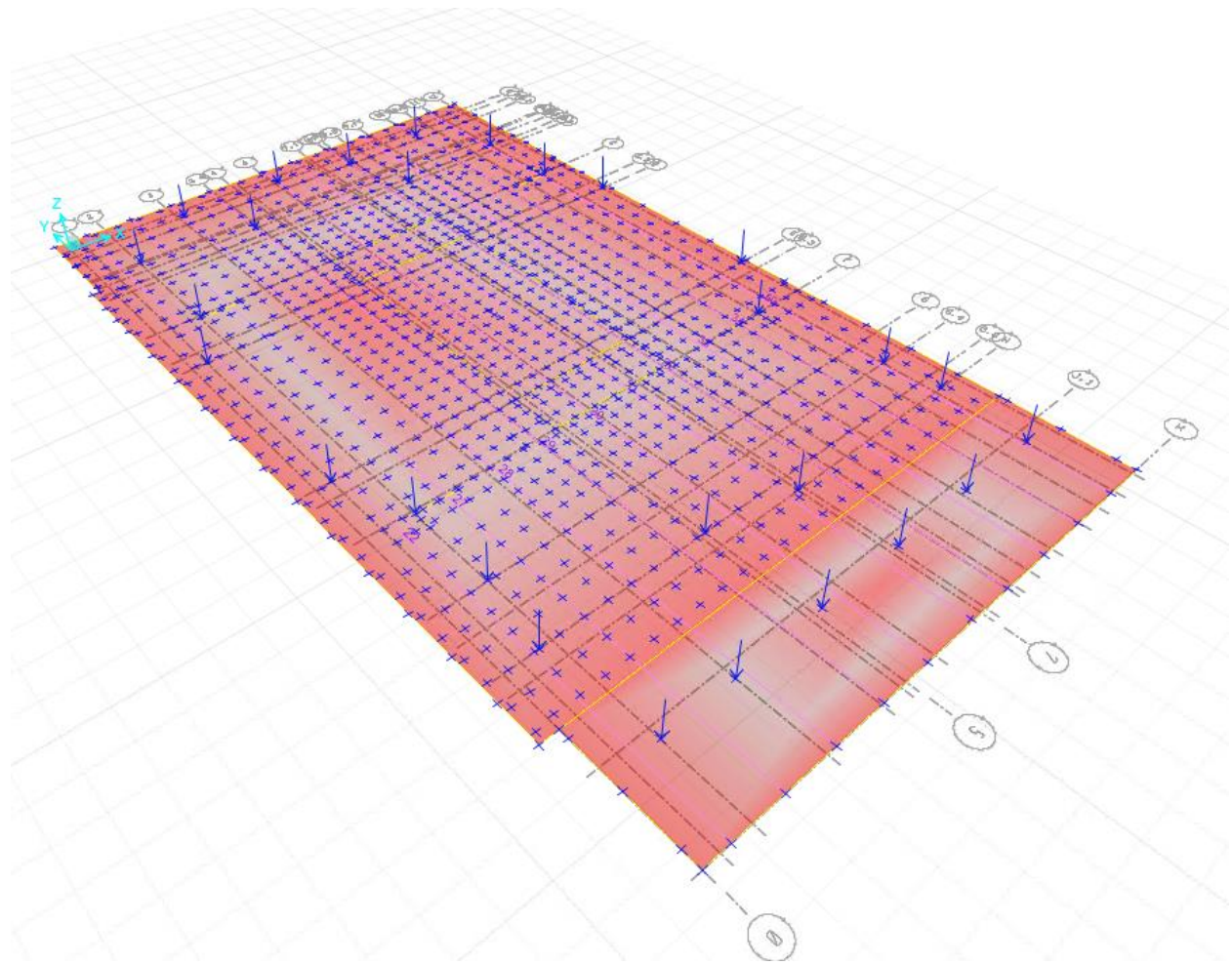


Figure 2-18: Point Load Application in SAFE Model for Dead Loads

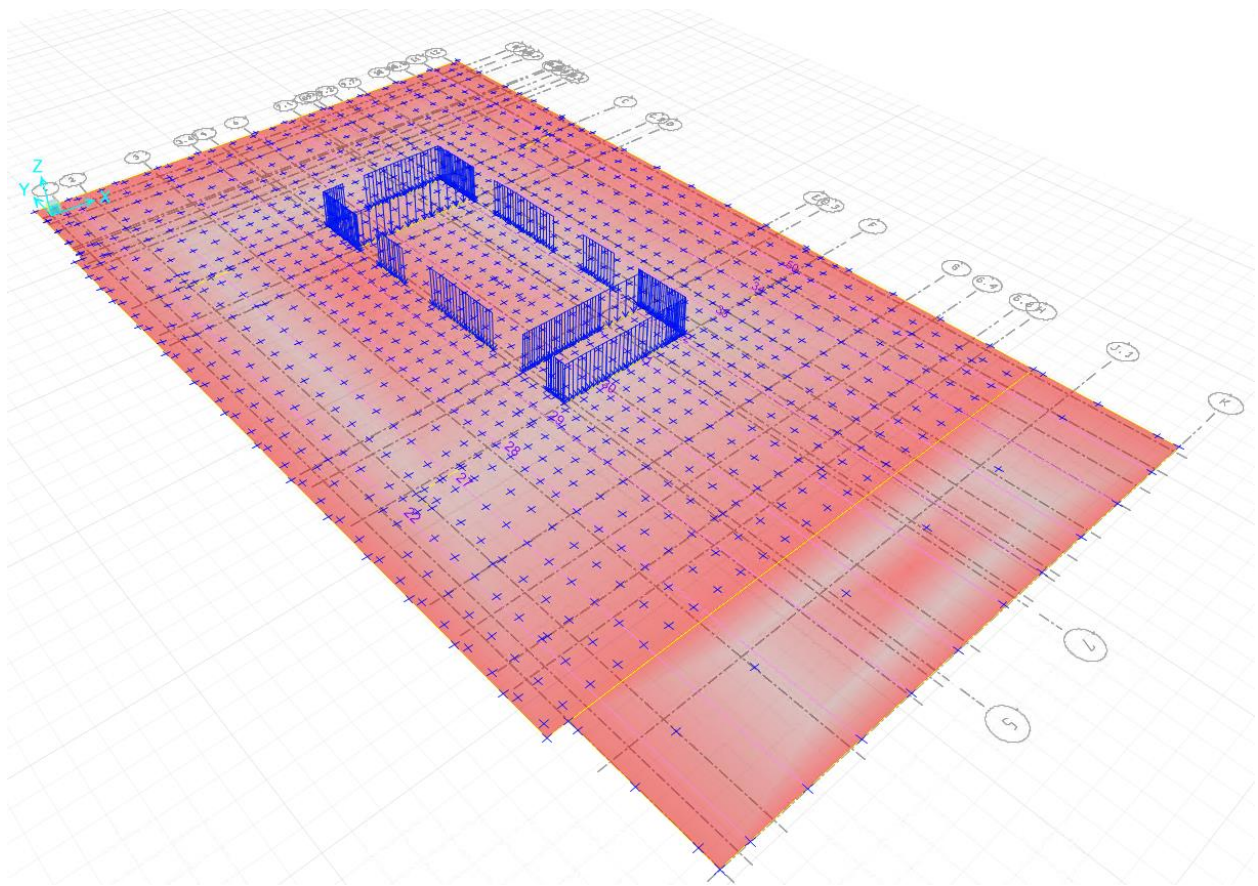


Figure 2-19: Line Load Application in SAFE Model for Dead Loads

2.2.3 Live Load

Live Load applied to the model consists of the total uniform live loading applied to all the floors depending on occupancy type. The table below summarizes the uniform load types and values.

Table 9: Uniform Live Load Occupancy Type and Value

Occupancy	Load (psf)
Residential	40
Mechanical	75
Lobby	100

We applied the live loads in a similar way to the dead loads applied above with point loads at columns or outriggers and line loads along the core walls. We reduced the live load with a factor of 0.4 in accordance with ASCE 7-16 Section 4.7.2. Per ASCE 7-16 Section 2.3.1, the Live Load in combinations 3, 4, and 5 can have a 0.5 factor for all occupancies for L_o less than or equal to 100 psf.

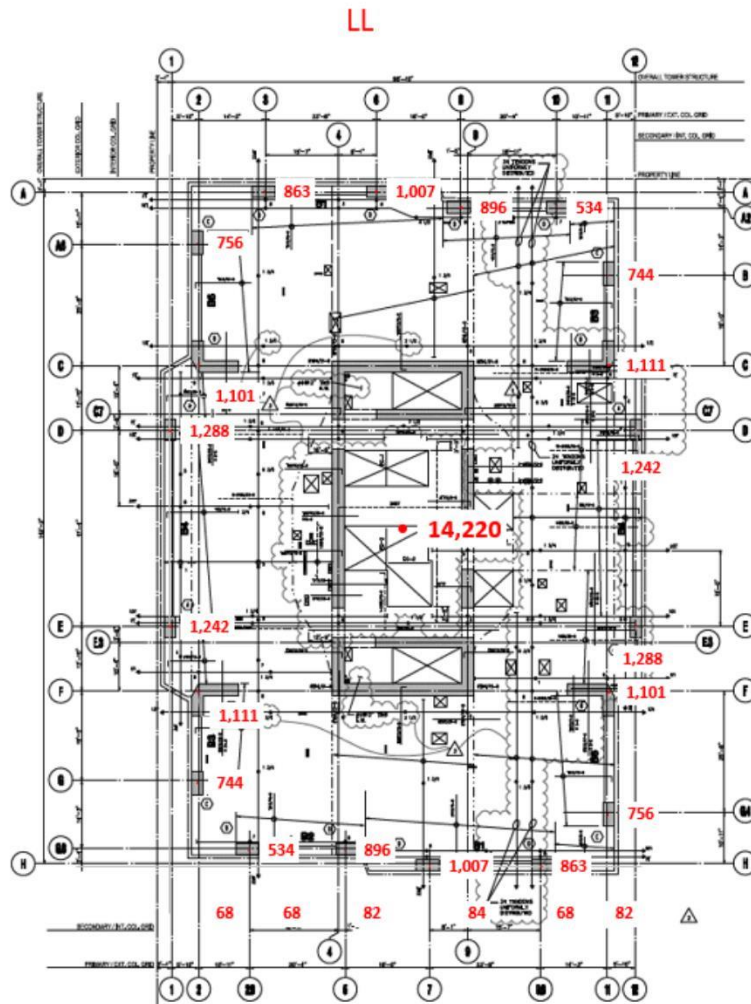


Figure 2-20: Reduced Live Load Application at Columns and Core

2.3 Design Strip Definitions

We defined the design strips in the north-south directions of the mat slab as 25 ft. wide and the east-west direction as 19 ft. wide at the exterior and 28 ft. at the interior. Figure 2-21 and Figure 2-22 illustrates the design strip definition in SAFE for the east-west and north-south directions respectively. The design strips use finite element analysis to determine the reinforcement required. Figure 2-23 and Figure 2-24 show the design preferences for each strip including preferred design code, code reduction factors, and clear cover.

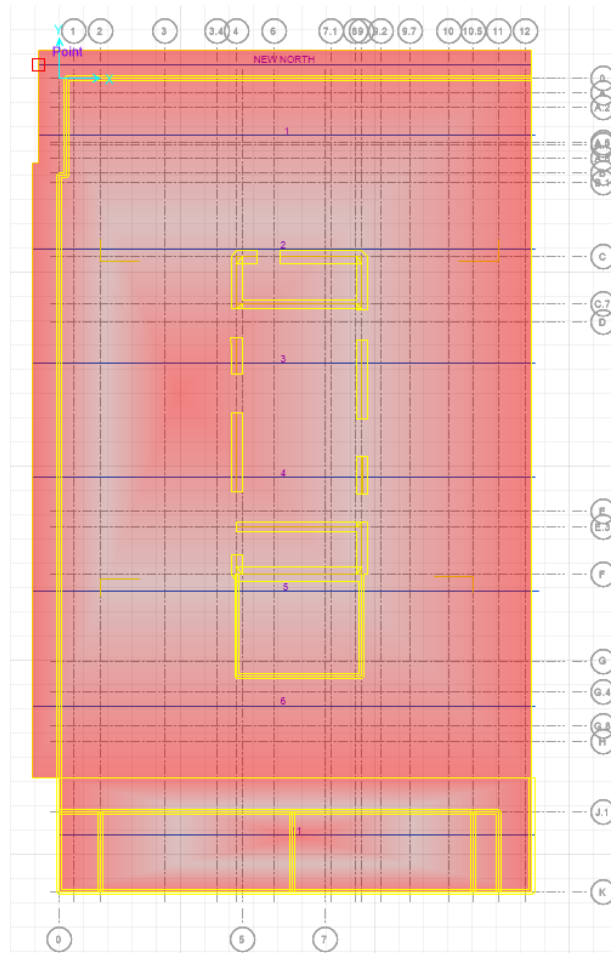


Figure 2-21: Rebar Design Strip in East-West Direction (Layer A)

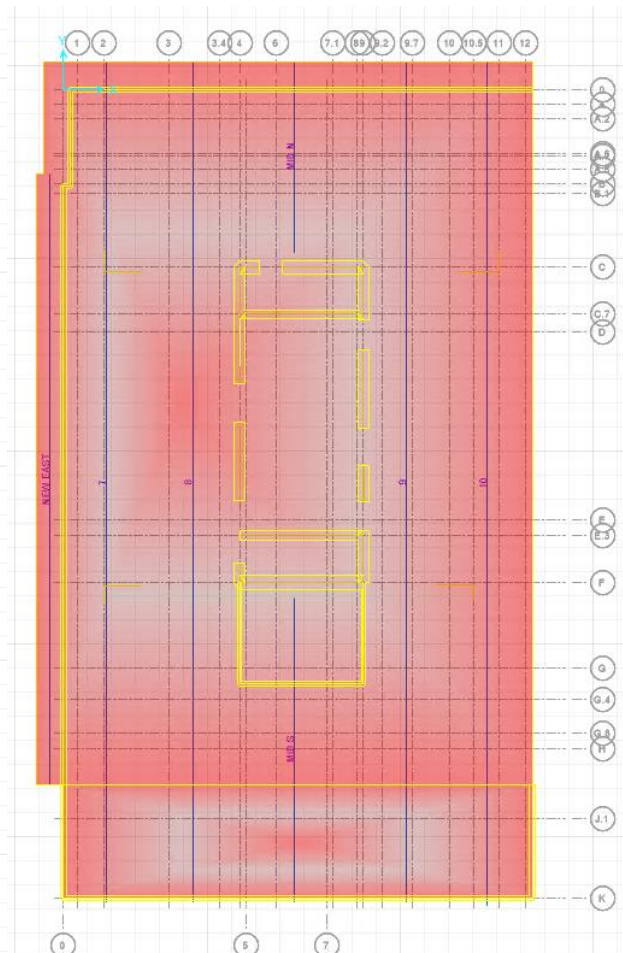


Figure 2-22: Rebar Design Strip in North-South Direction (Layer B)

Design Preferences

Code Min. Cover Slabs Min. Cover Beams P/T Stress Check

Design Code	ACI 318-14
Resistance Factors:	
Phi Tension Controlled	0.9000
Phi Compression Controlled	0.6500
Phi Shear	0.7500

Reset Tab Defaults

OK Cancel

Figure 2-23: Design Preferences for Design Strips

Design Preferences

Code Min. Cover Slabs Min. Cover Beams P/T Stress Check

Non-Prestressed Reinforcement	
Clear Cover Top (in)	4
Clear Cover Bottom (in)	12
Preferred Bar Size	#11
Inner Slab Rebar Layer	Layer B
Post-Tensioning	
CGS of Tendon Top (in)	1
CGS of Tendon for Bottom of Exterior Bay (in)	1.75
CGS of Tendon for Bottom of Interior Bay (in)	1
Minimum Reinforcing	
Slab Type for Minimum Reinforcing	Two Way

Reset Tab Defaults

OK Cancel

Figure 2-24: Design Preferences for Design Strips

2.4 Nonlinear Immediate Cracked Analysis

Nonlinear cracked analysis considers the immediate cracked moment of inertia using the existing reinforcement defined in the SAFE model. This analysis first runs a nonlinear analysis considering the elasto-plastic pile springs and gross moment of inertia. The program then iterates with the cracked section properties. Since results from a nonlinear analysis cannot be superimposed, the load case contains all loads with their respective load factors. Figure 2-25 shows an example nonlinear load definition in SAFE.

Load Case Data - Nonlinear Static

Load Case Name: 1.4D +L +100(X-eco) +30Y

Load Case Data Notes: Modify/Show Notes...

Load Case Type: Static Design...

Initial Conditions:

- ☒ Zero Initial Conditions - Start from Unstressed State
- ☐ Continue from State at End of Nonlinear Case

Important Note: Loads from this previous case are included in the current case

Analysis Type:

- ☐ Linear
- ☐ Nonlinear (Allow Uplift)
- ☒ Nonlinear (Cracked)
- ☐ Nonlinear (Long Term Cracked)

Creep Coefficient:

Shrinkage Strain:

Loads Applied:

	Load Name	Scale Factor
▶	DL	1.4000
	MAT	1.4000
	LL	0.2000
	ELF X-e	1.0000
	ELF Y	0.3000
*		

Uplift Solution Control:

Force Convergence Tolerance (Relative): 0.00001

OK Cancel

Figure 2-25: Example Nonlinear Analysis Load Case

2.5 Mat Slab Reinforcement Capacity

The mat slab flexural capacity is determined from the area of steel within the various segments of the design strip using the original design drawings from DeSimone and Shop Drawings.

Figure 2-26 and Figure 2-27 show the reinforcement area per foot of slab within the design strip definitions.

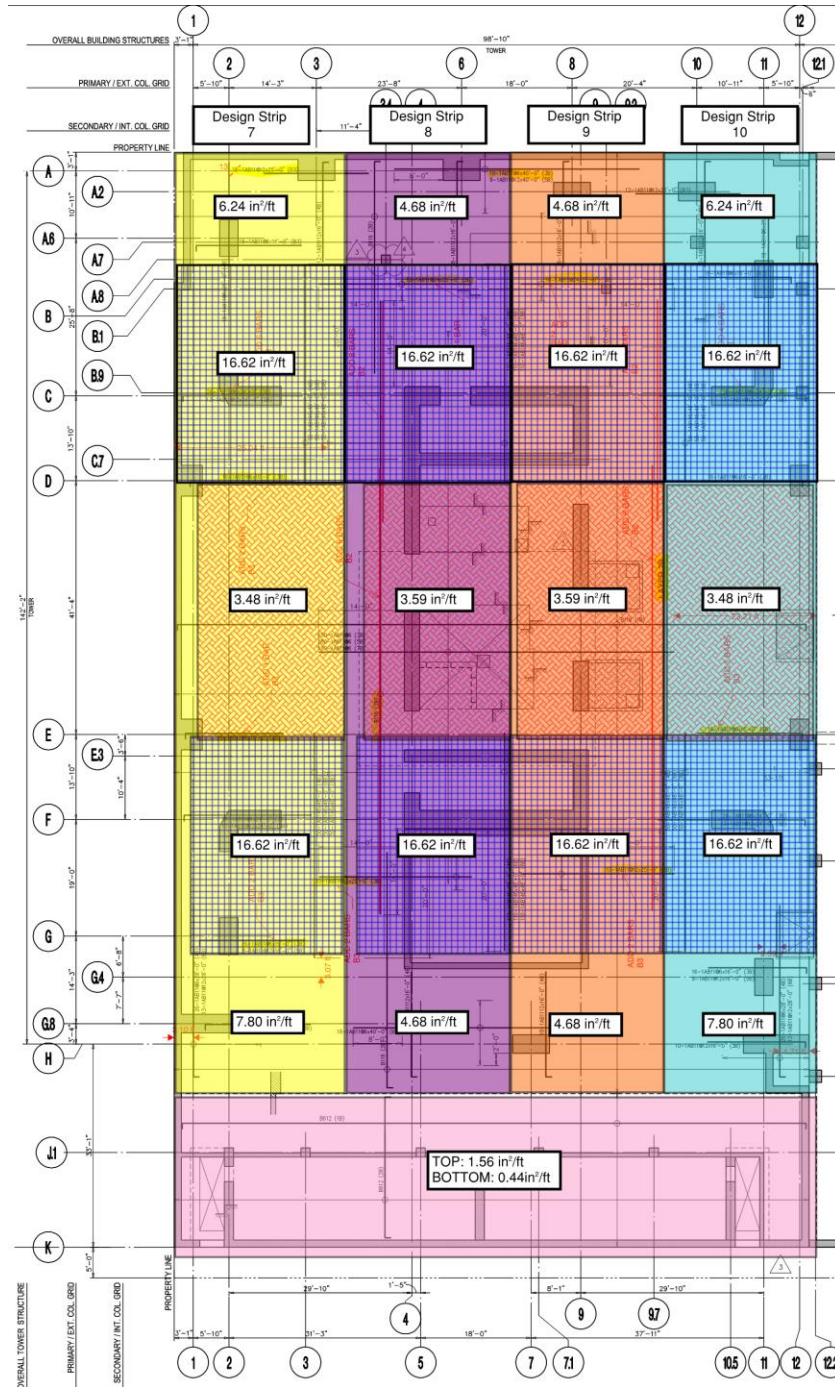


Figure 2-26: Top and Bottom North – South Reinforcement Area per Foot of Slab

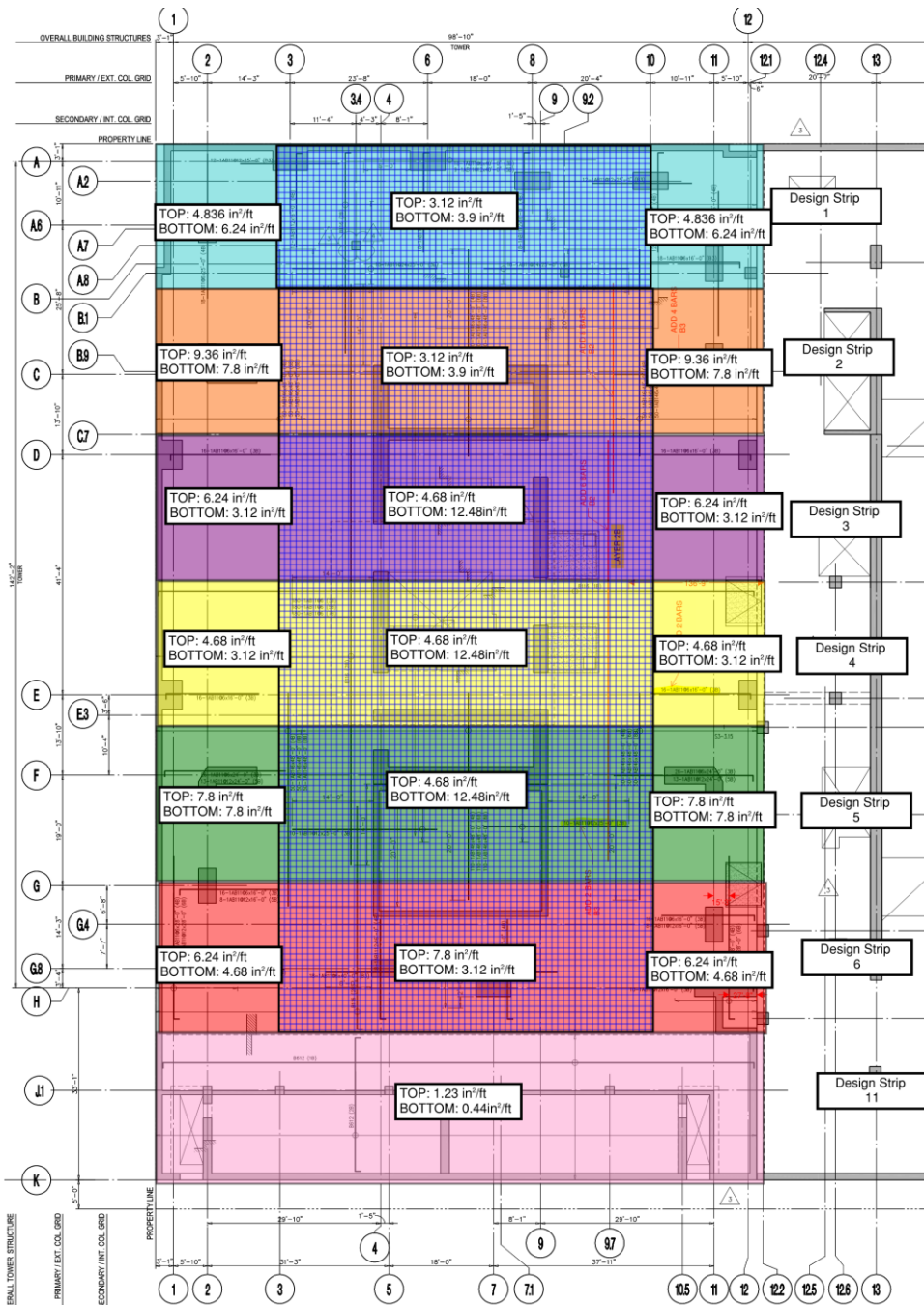


Figure 2-27: Top and Bottom North – South Reinforcement Area per Foot of Slab

2.6 Analysis Results

2.6.1 Flexural Design Checks with ENGEO Spring Definitions

For each load case presented in the sections above, SAFE calculates the moment demands along the defined strips in the east-west and north-south directions. The figures below present the design to capacity checks between the demands calculated at discrete points along the column strip with the calculated capacities. We use the ENGEO springs presented in Section 2.1.4.12.1.4.1.1 in the SAFE to produce the following results.

2.6.1.1 Gravity Loading

The results presented below include the maximum load envelope of the following gravity load combinations:

$$\textit{Envelope 1: } 1.4 * D \text{ and } 1.2 * D + 1.6 * L$$

The maximum DCR in each diagram is highlighted.

2.6.1.1.1. Gravity Loads Demands for Existing Condition

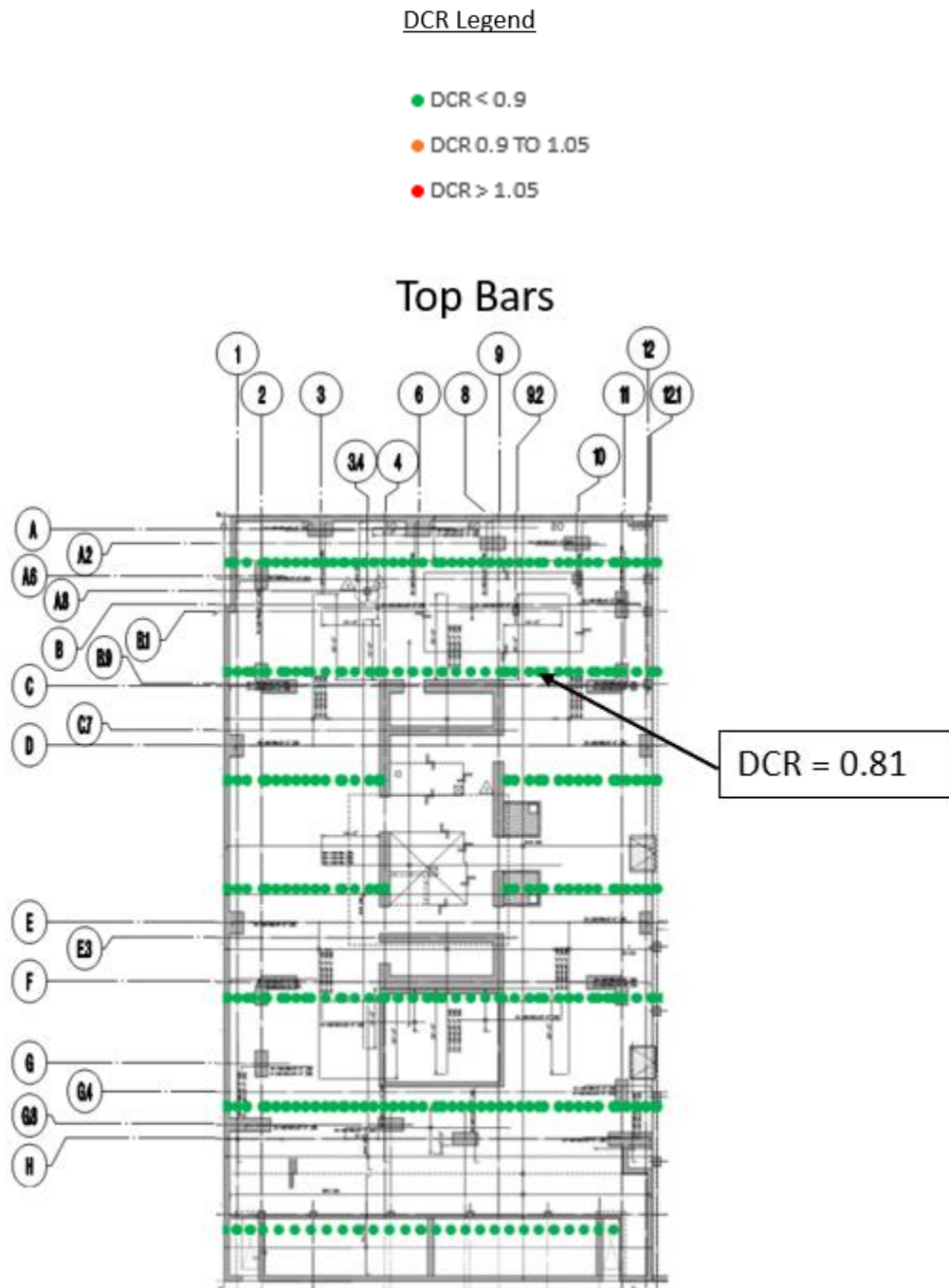


Figure 2-28: DCR Plot for East-West Top Reinforcement Design Strips for Gravity Load Envelope Existing Condition

DCR Legend

- DCR < 0.9
- DCR 0.9 TO 1.05
- DCR > 1.05

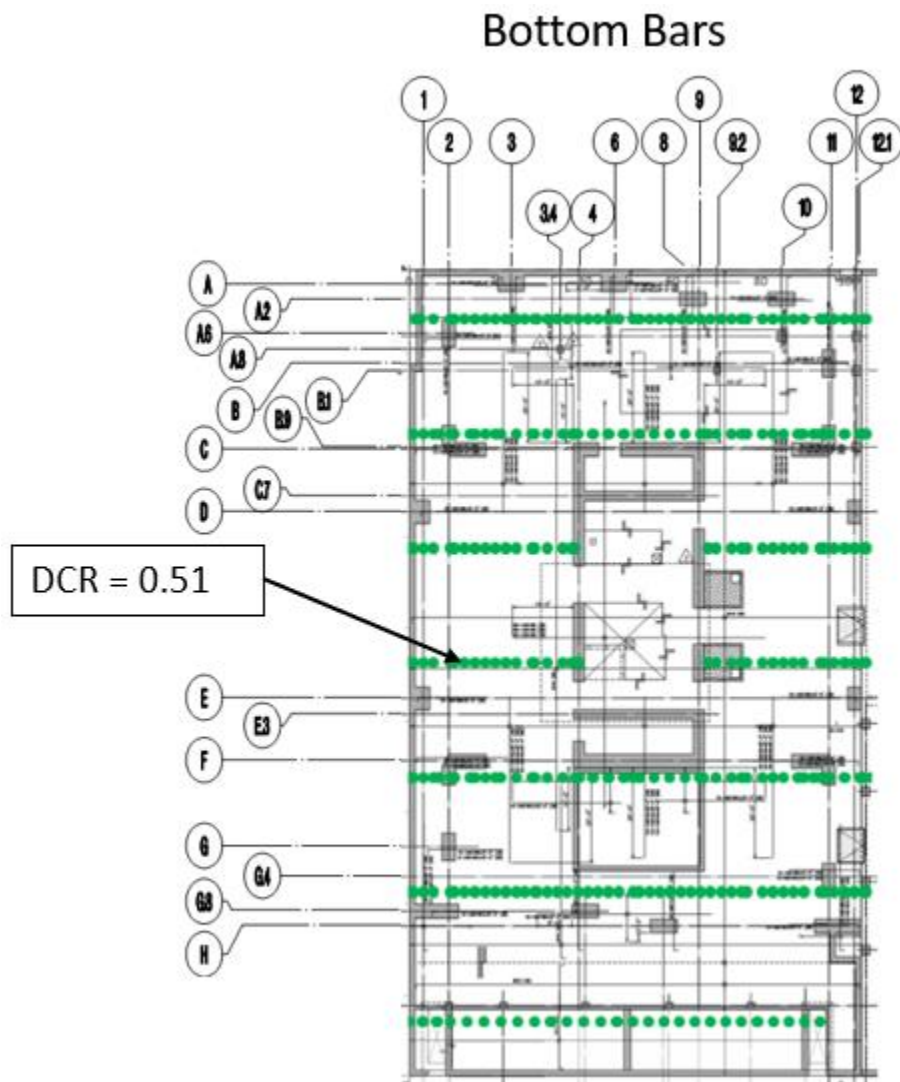


Figure 2-29: DCR Plot for East-West Bottom Reinforcement Design Strips for Gravity Load Envelope Existing Condition

DCR Legend

- DCR < 0.9
- DCR 0.9 TO 1.05
- DCR > 1.05

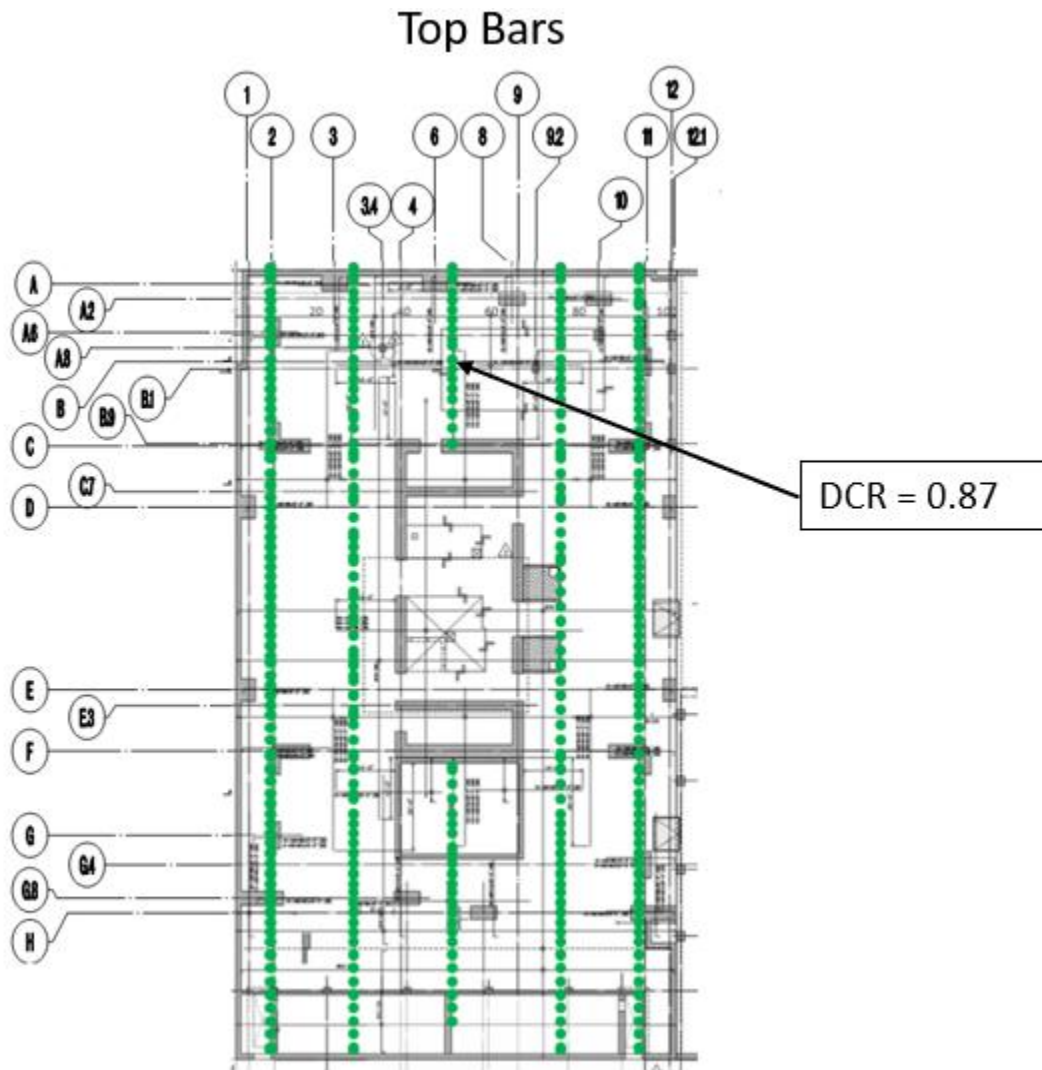


Figure 2-30: DCR Plot for North - South Top Reinforcement Design Strips for Gravity Load Envelope Existing Condition

DCR Legend

- DCR < 0.9
- DCR 0.9 TO 1.05
- DCR > 1.05

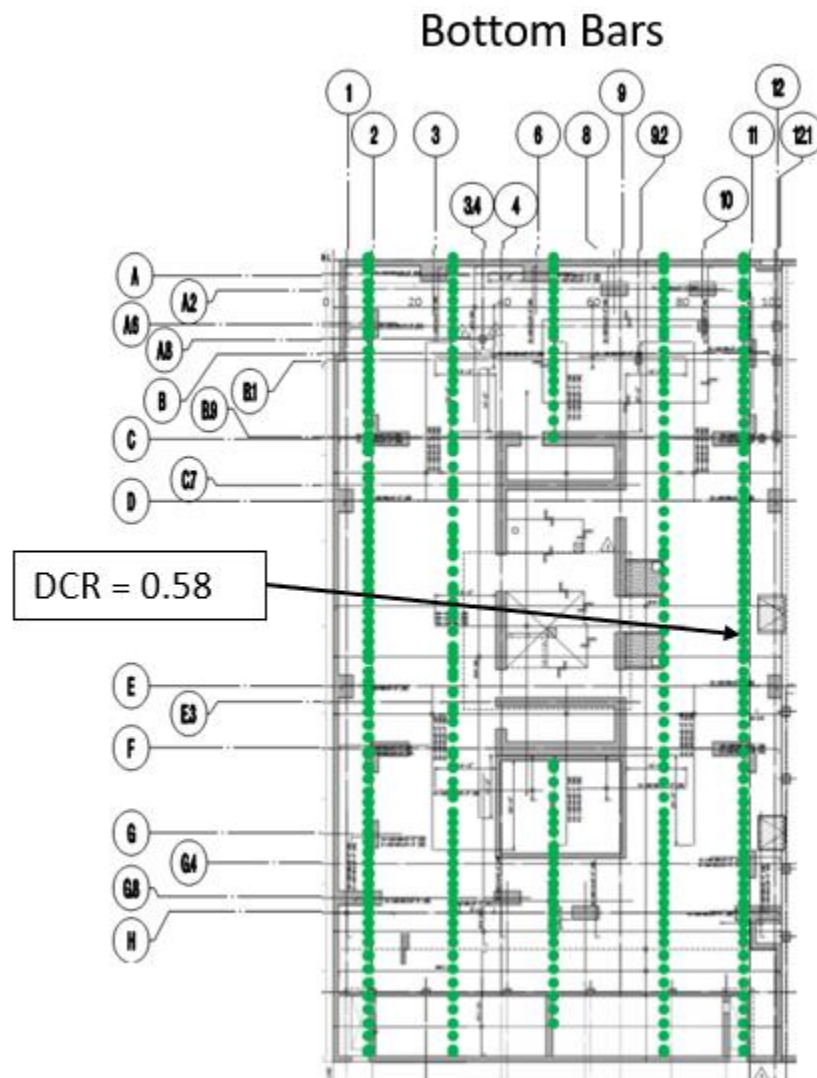


Figure 2-31: DCR Plot for North - South Bottom Reinforcement Design Strips for Gravity Load Envelope Existing Condition

2.6.1.1.2. Gravity Loads for Retrofit Condition

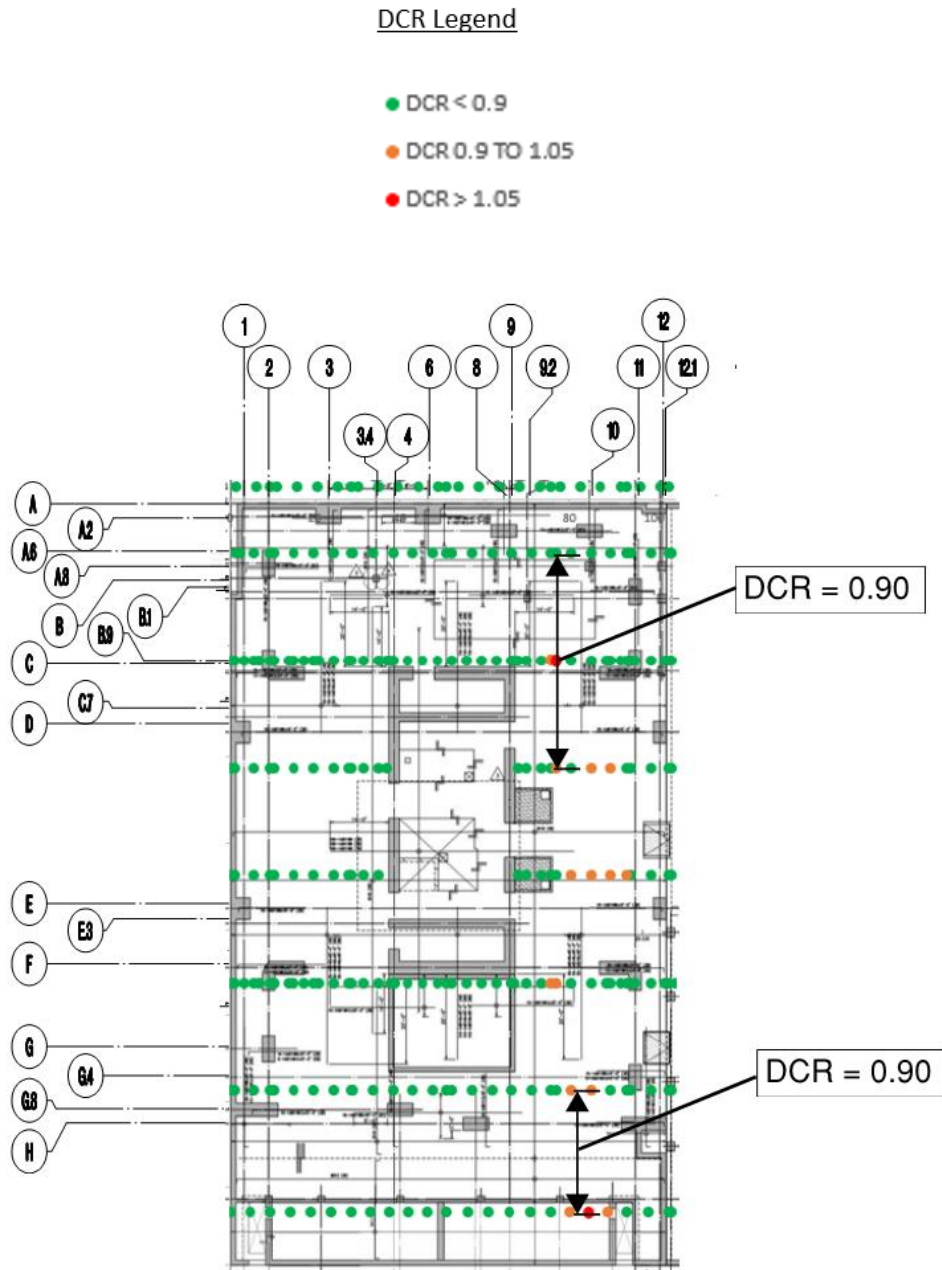


Figure 2-32: DCR Plot for East-West Top Reinforcement Design Strips for Gravity Load Envelope with Jacking Loads

DCR Legend

- DCR < 0.9
- DCR 0.9 TO 1.05
- DCR > 1.05

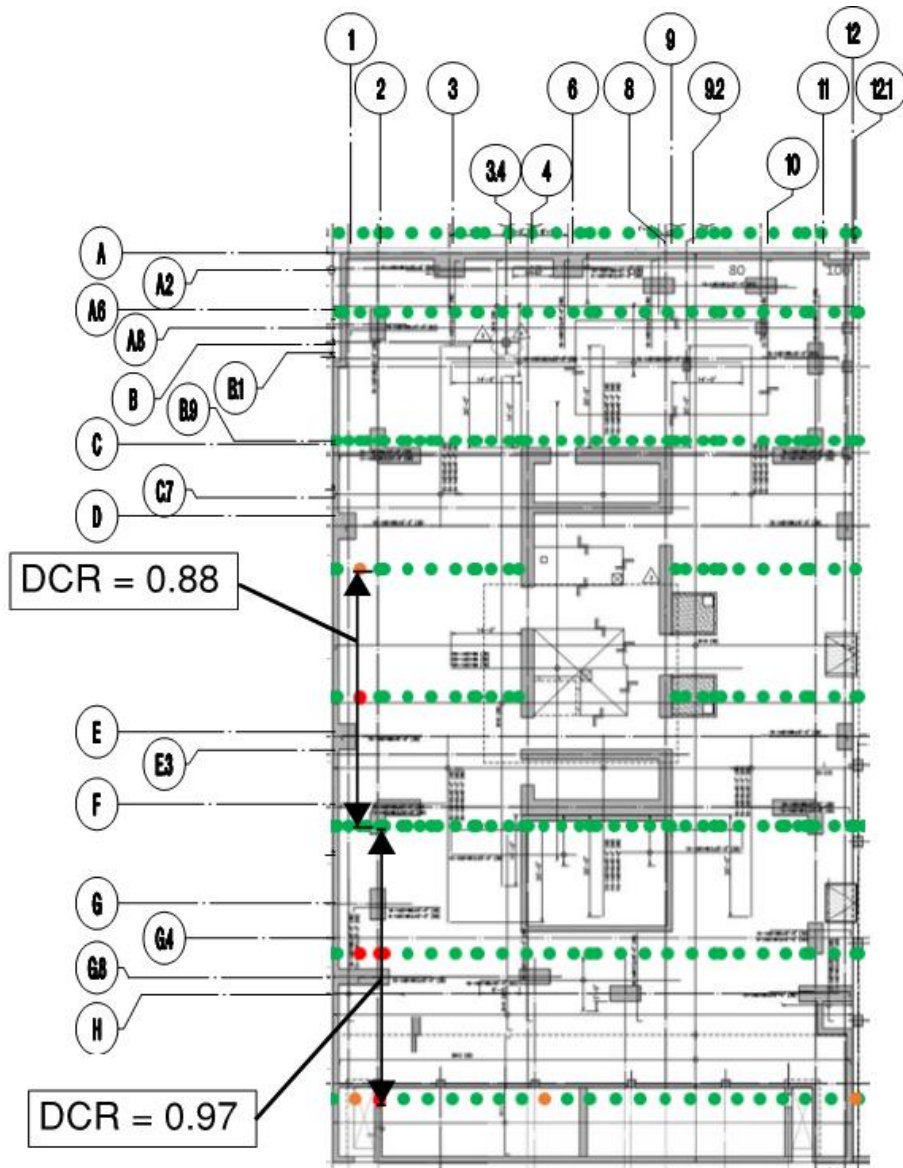


Figure 2-33: DCR Plot for East-West Bottom Reinforcement Design Strips for Gravity Load Envelope with Jacking Loads

DCR Legend

- DCR < 0.9
- DCR 0.9 TO 1.05
- DCR > 1.05

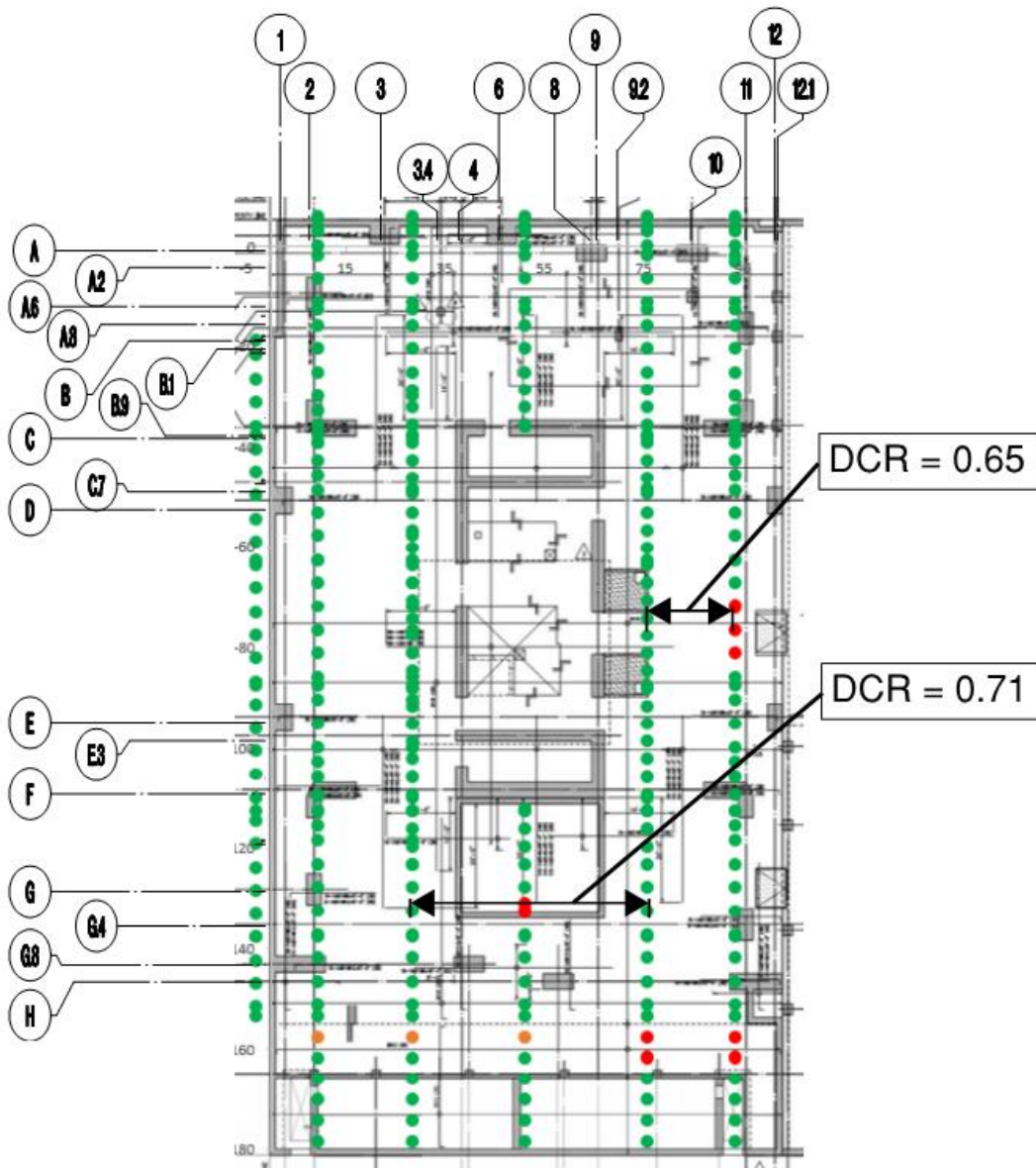


Figure 2-34: DCR Plot for North-South Top Reinforcement Design Strips for Gravity Load Envelope with Jacking Loads

DCR Legend

- DCR < 0.9
- DCR 0.9 TO 1.05
- DCR > 1.05

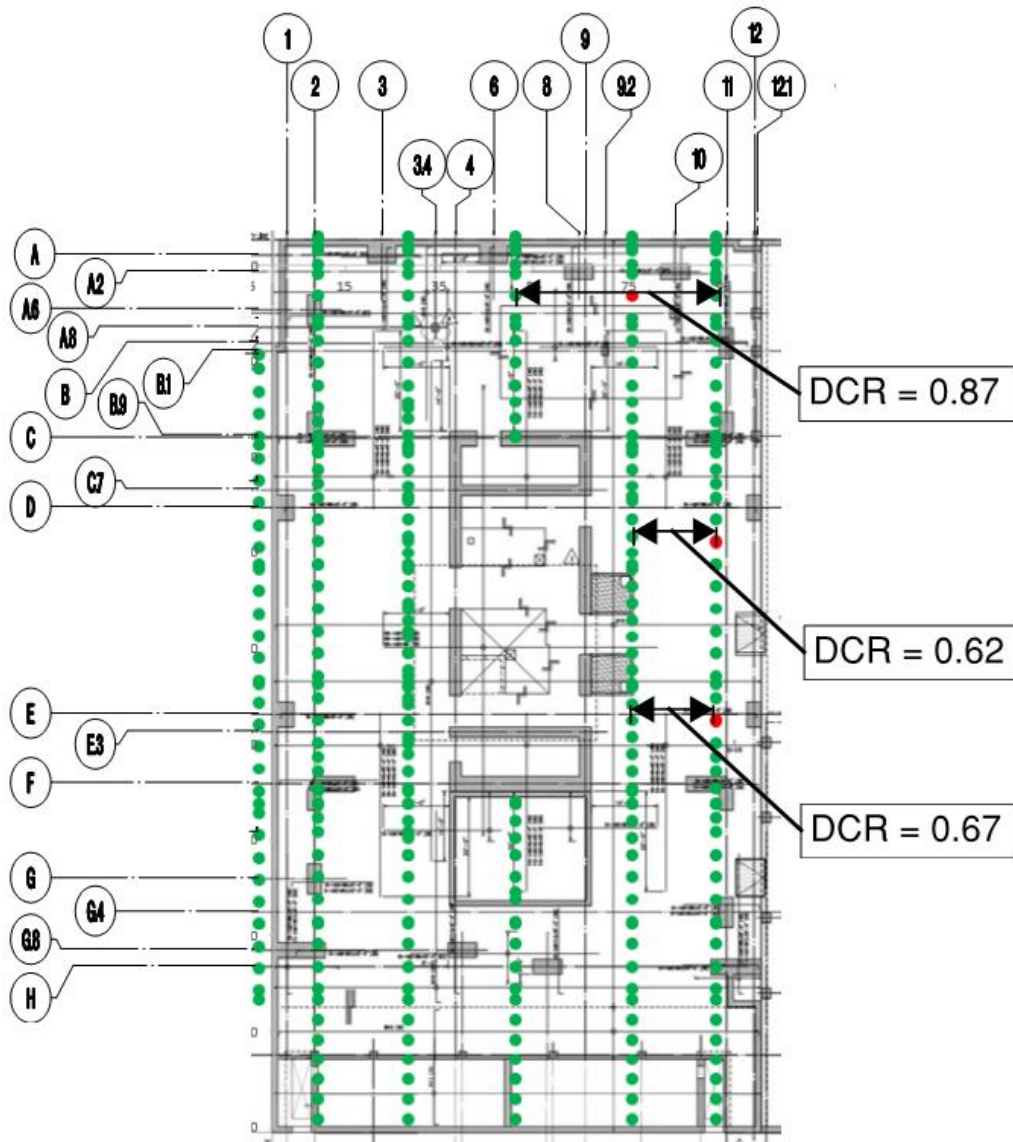


Figure 2-35: DCR Plot for North-South Top Reinforcement Design Strips for Gravity Load Envelope with Jacking Loads

2.6.2 Analysis Results with Alternative Spring Definitions

Alternatively, we perform similar analyses with soil springs provided by Slate Geotechnical Consultants, Inc. and Shannon & Wilson, Inc. as presented in Section 2.1.4.1.2.

2.6.2.1.1. Gravity Loads Demands for Existing Condition

DCR Legend

- DCR < 0.9
- DCR 0.9 TO 1.05
- DCR > 1.05

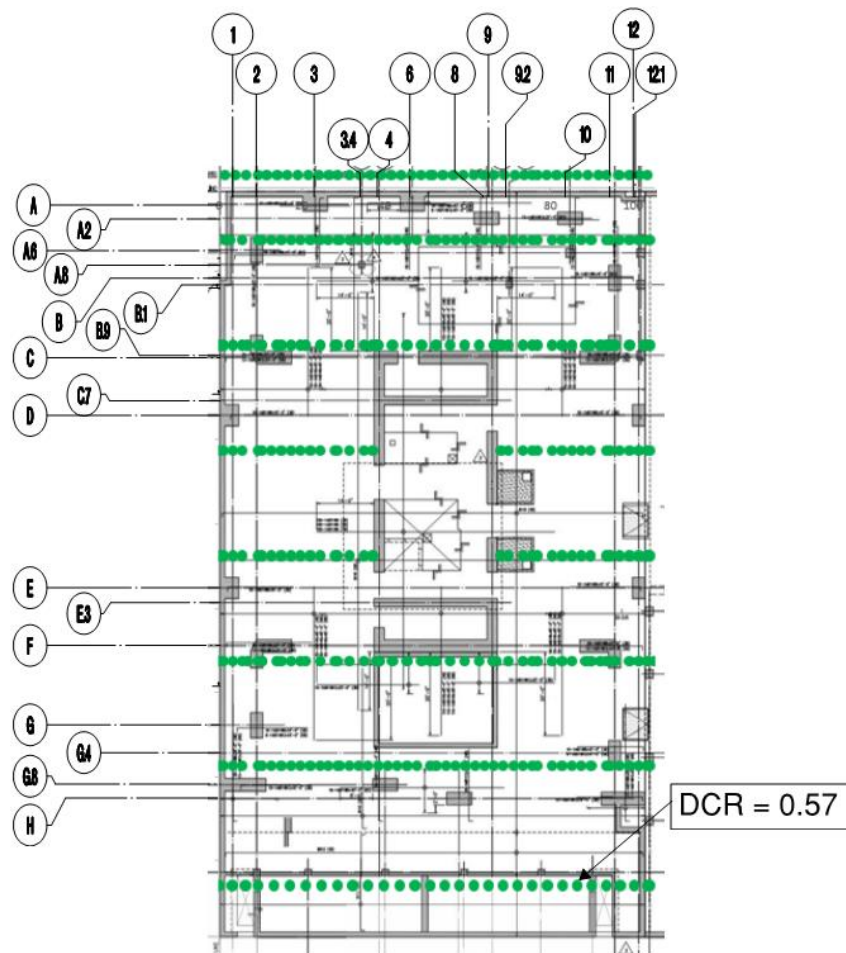


Figure 2-36: DCR Plot for East-West Top Reinforcement Design Strips for Gravity Load Envelope Existing Condition

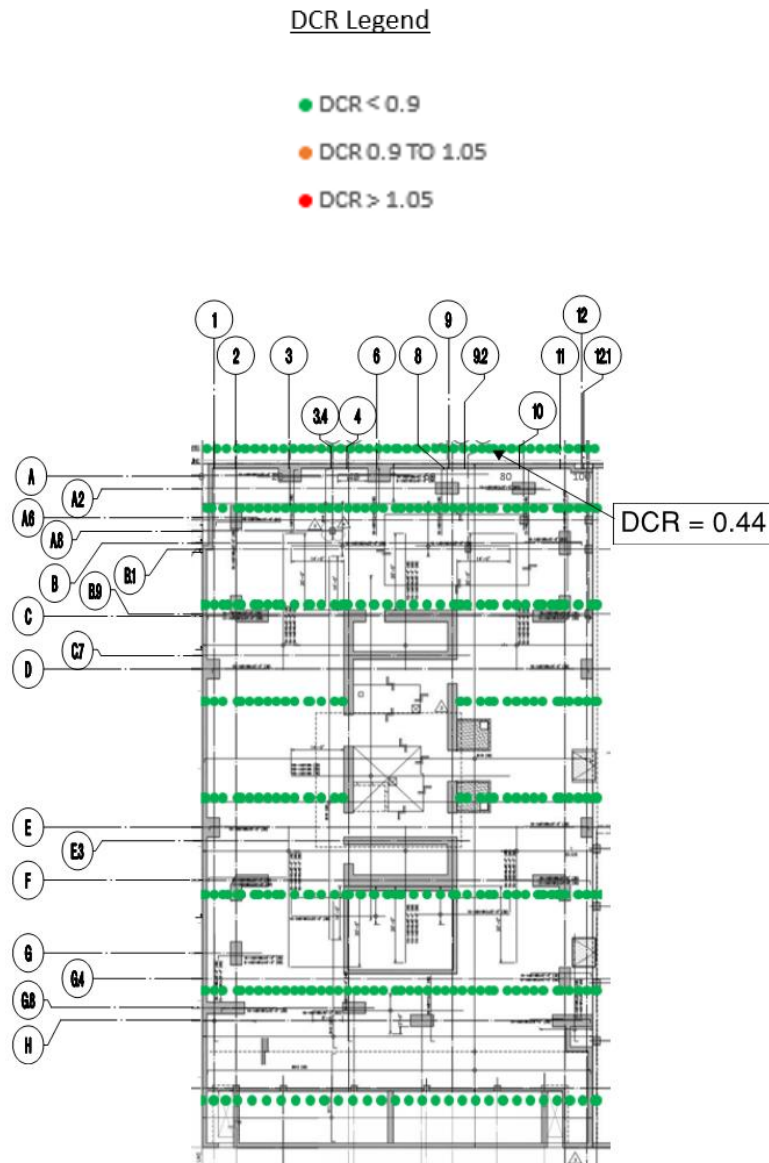


Figure 2-37: DCR Plot for East-West Bottom Reinforcement Design Strips for Gravity Load Envelope Existing Condition

DCR Legend

- DCR < 0.9
- DCR 0.9 TO 1.05
- DCR > 1.05

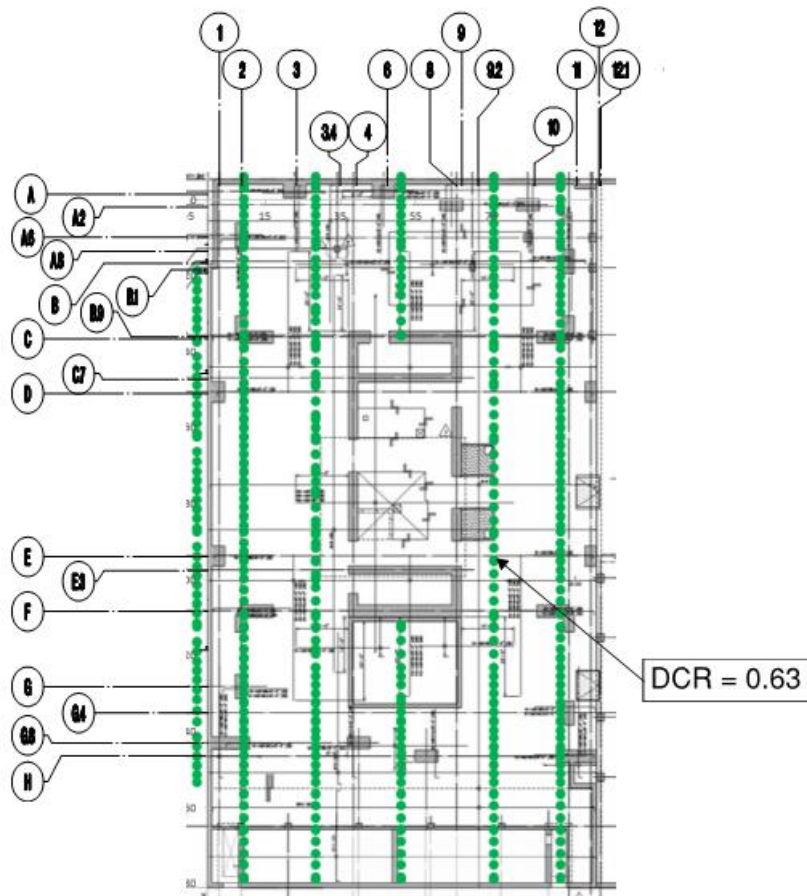


Figure 2-38: DCR Plot for North - South Top Reinforcement Design Strips for Gravity Load Envelope Existing Condition

DCR Legend

- DCR < 0.9
- DCR 0.9 TO 1.05
- DCR > 1.05

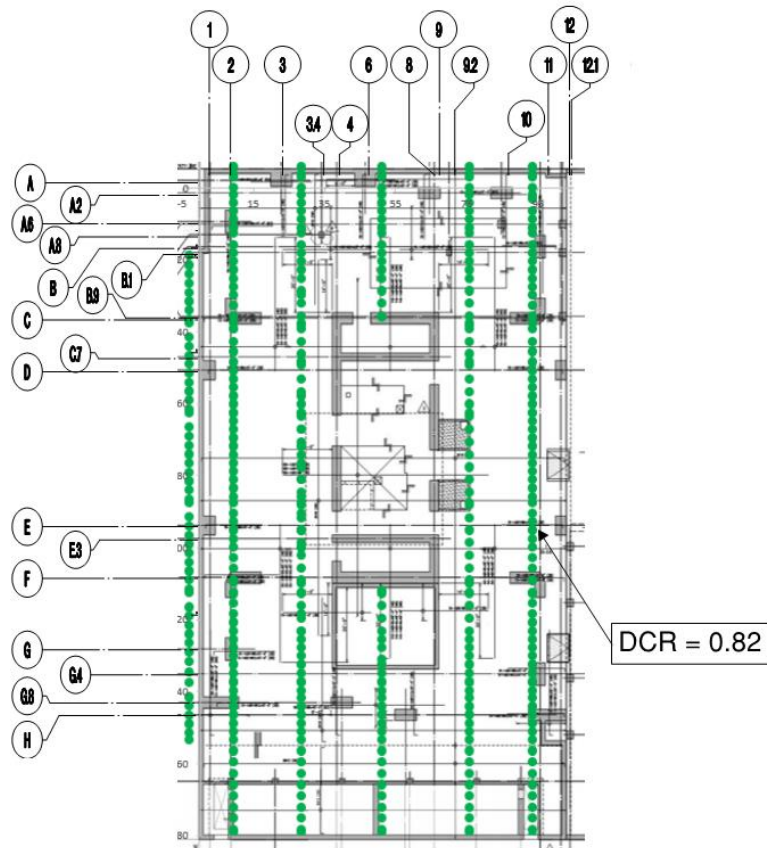


Figure 2-39: DCR Plot for North - South Bottom Reinforcement Design Strips for Gravity Load Envelope Existing Condition

2.6.2.1.2. Gravity Loads for Retrofit Condition

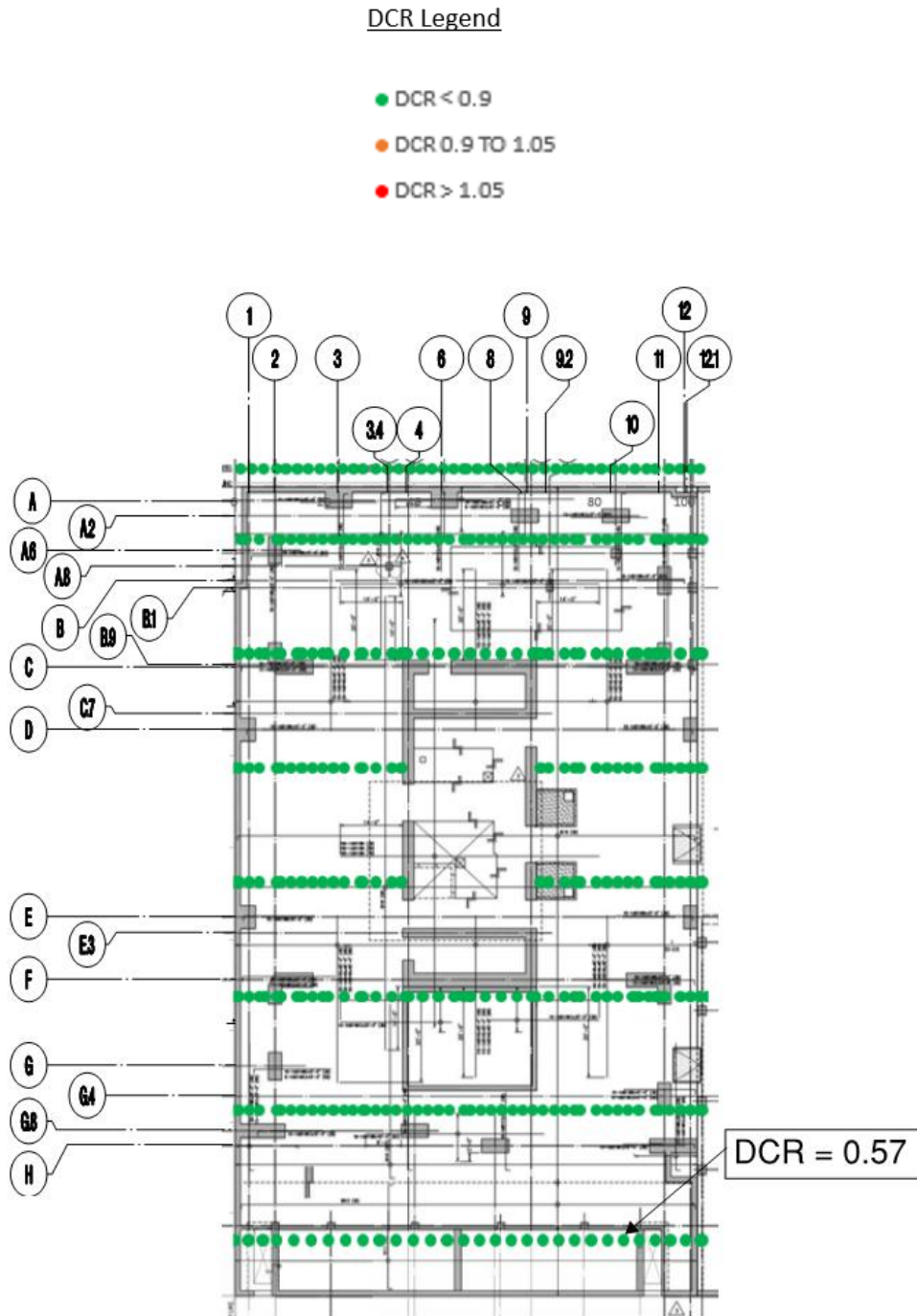


Figure 2-40: DCR Plot for East-West Top Reinforcement Design Strips for Gravity Load Envelope with Jacking Loads

DCR Legend

- DCR < 0.9
- DCR 0.9 TO 1.05
- DCR > 1.05

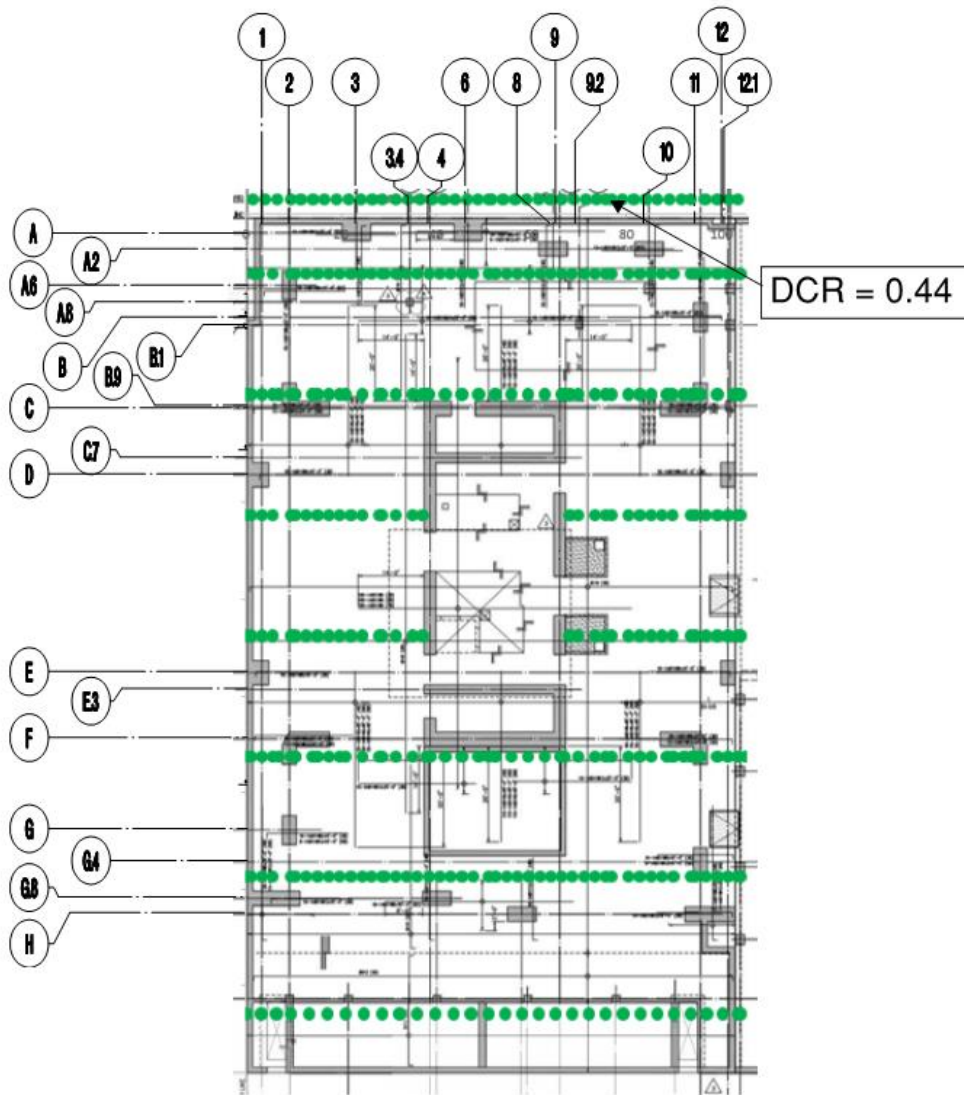


Figure 2-41: DCR Plot for East-West Bottom Reinforcement Design Strips for Gravity Load Envelope with Jacking Loads

DCR Legend

- DCR < 0.9
- DCR 0.9 TO 1.05
- DCR > 1.05

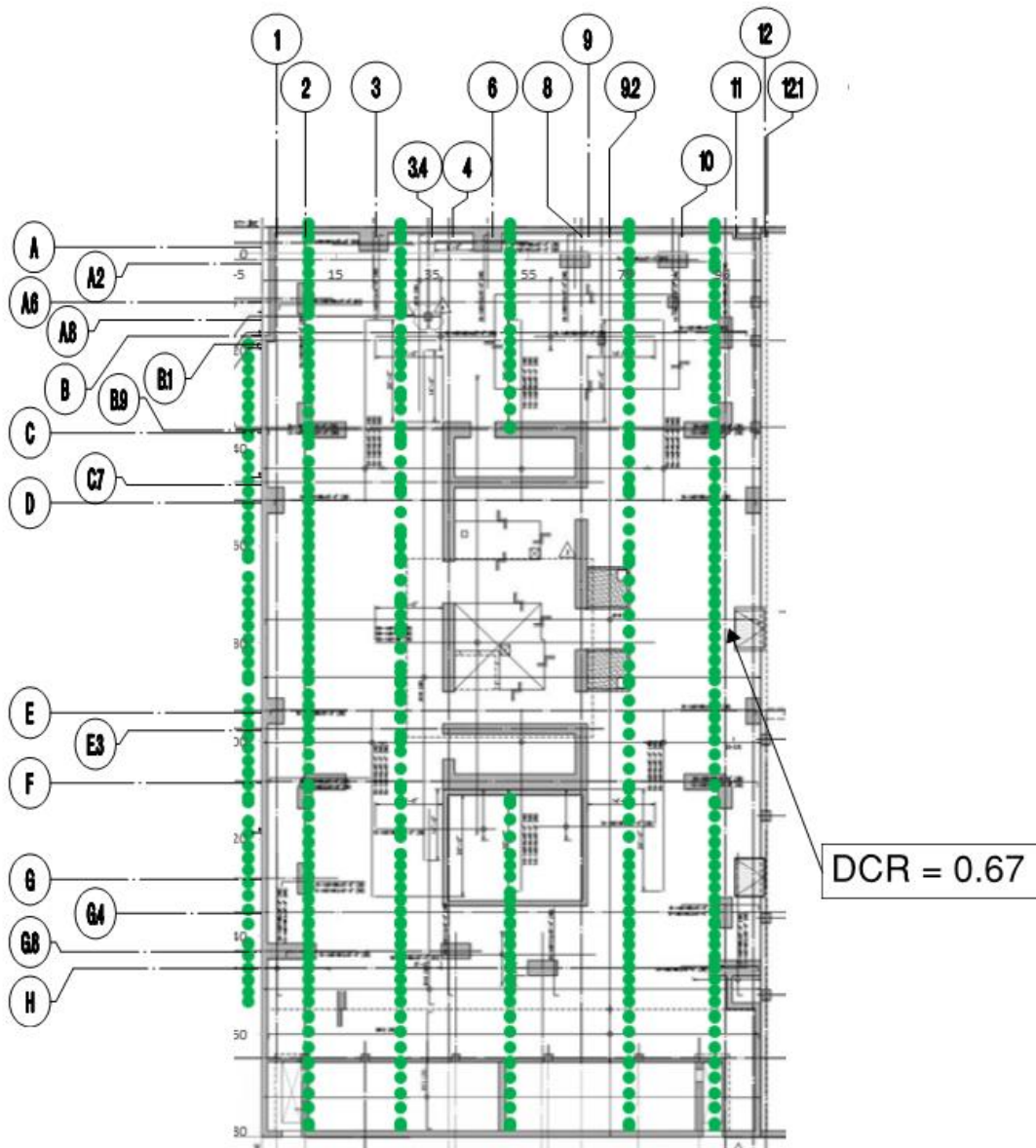


Figure 2-42: DCR Plot for North-South Top Reinforcement Design Strips for Gravity Load Envelope with Jacking Loads

DCR Legend

- DCR < 0.9
- DCR 0.9 TO 1.05
- DCR > 1.05

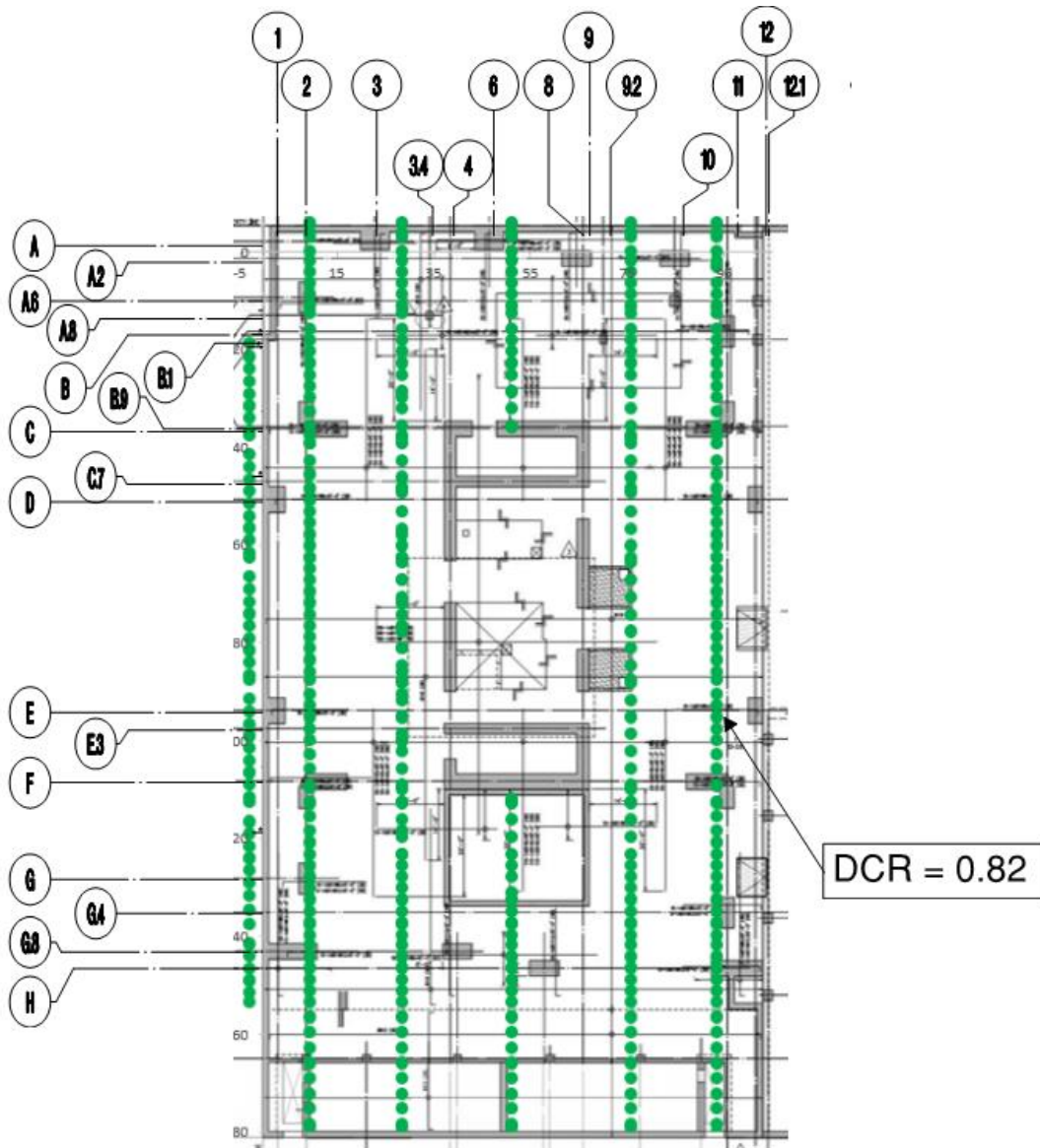


Figure 2-43: DCR Plot for North-South Bottom Reinforcement Design Strips for Gravity Load Envelope with Jacking Loads